

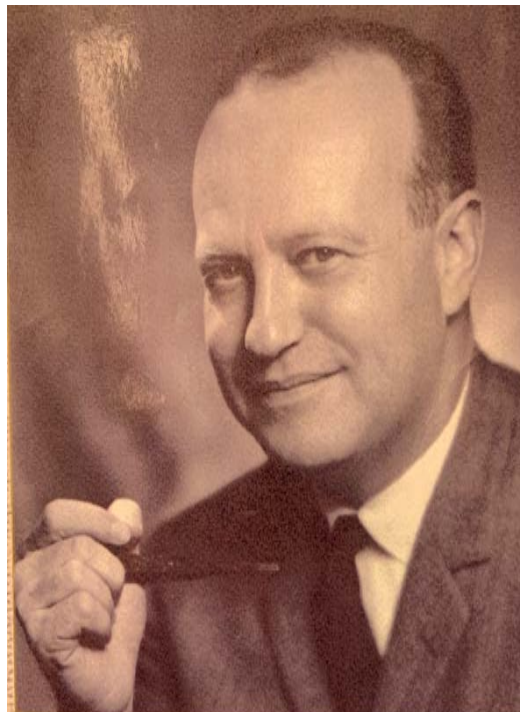
Garcia Center for Polymers at Engineered Interfaces



Summer Research Scholars 2022

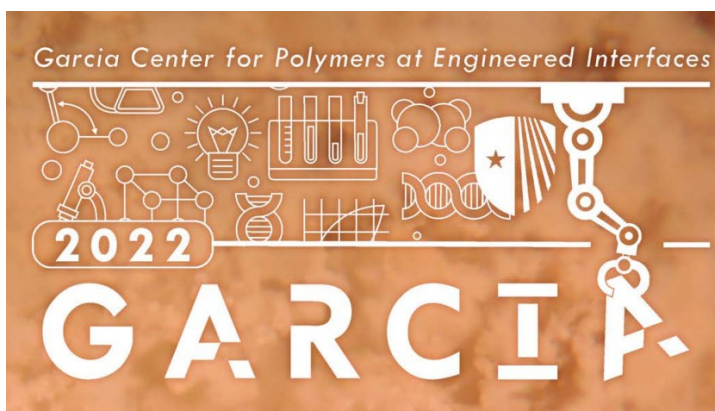
Commemorating Mr. Francis Kirschner (1923-2021)

Technical Consultant to the Morin
Charitable Trust, supporting our
students for over a decade



Mr. Kirschner was a valuable mentor, guiding new generations of students in STEM.

Mr. Kirschner emigrated to the United States from Hungary, after surviving the Holocaust. He was a sound engineer and founder of Soundcoat Co. Mr. Kirschner was passionate about enabling young people to excel in STEM and had a personal interest in research involving the science of music.



<https://you.stonybrook.edu/jesti>

Message to our students:

We were delighted to open our doors this year to high school students who were able to experience the excitement of research in person. Even though some students were still unable to participate, we were all able to work together for the first time in three years and accomplish significant advances in different areas of science and technology. This feeling was best expressed by Lee Ann Tai, whose design of the Garcia Logo, was selected again this year to represent the student cohort for 2022. " *The highlight of Garcia is undoubtedly the interdisciplinary experience. Though our projects varied from machine learning to DNA research to materials engineering, we are united by the goal to learn and the goal to discover. This unified diversity that pulls 'GARCIA' together is expressed in the design. The hands-on skills we gained from participating in exciting, cutting-edge research was truly irreplaceable. Thank you to Garcia 2022 for the forever-cherished memories and opening our eyes to life as a scientist.*"

The students this year went a step further in ensuring that science works for the benefit of society. With guidance from Professor Brooke Ellison, they took on the challenge to consider the ethical implications of technology, publishing their own peer reviewed journal, the Journal of Ethics in Scientific and Technological Innovations (JESTI).

Sincerely, Miriam Rafailovich and Jonathan Sokolov

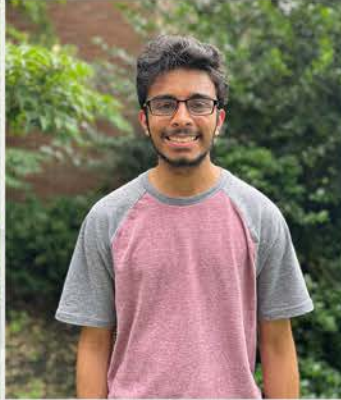
Miriam H. Rafailovich Jonathan Sokolov

The Garcia Center for Polymers at Engineered Interfaces was founded in 1996 and is named after the late Queens College professor, Narciso Garcia, who was a pioneer in the integration of education and research. The Center focuses on the broad application of materials research to engineering, medicine, and energy, and recently, AI, machine learning, and computational modeling. The Center also supports innovation through entrepreneurship and has multiple collaborations with industry and national laboratories. In the research program, high school students work together with undergraduates, PhD, post PhD and faculty who collaborate in addressing challenges at the cutting edge of modern science. The students are encouraged to publish in refereed scientific journals, present their results at national conferences, and develop patents to protect their intellectual property. Our goal is to convey to the students the excitement we enjoy daily in research and provide for them a supportive network within the scientific community. Research is a lifelong experience and we hope to remain a resource to our students long after "graduation".

High School Students



Haaris Alam



Ayush Arora



Tavan Bhatia



Michelle Bok



Caroline Brown



Maytal Chelst



Eric Chen



Sophia Chen



Derek Days



Sahana Dhama



Sicheng Dong



Konnie Duan



Sean Fang



Noah Fensterheim



Emma Gao



Navya Gautam

High School Students



Quinton Geller



Oran Goodman



Eric Guan



Michael He



Elaina Heghes



Eden Hen



Annie Hu



Shaheer Khan



Dohyun Kim



Juni Kim



Justin Kim



Muyao Li



Zixuan Lin



Matthew Lu



Thomas Luong



Rachel Na

High School Students



Deryn O'Leary



Gavin Onghai



Yuhao (Ben) Pan



Ohm Patel



Pratham Patel



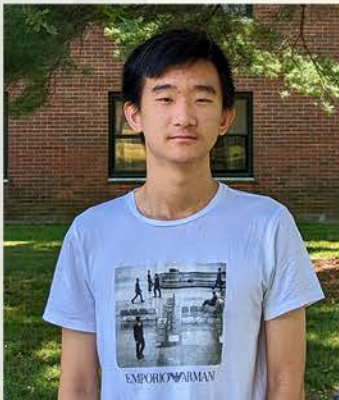
Sohan Paul



Darshini Podder



Briana Poon



Ming Qi



Ziyi (Rick) Qian



Harsha Rajkumar



Siri Reddy



Judah Rosenthal



Gabriel Rothman



Amit Saha



Hannah Saks

High School Students



Alex Samadi



Eliana Samuels



Rommy Sasson



Hillel Schein



Chengwei Shang



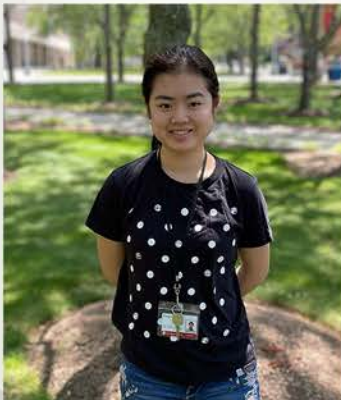
Matthew Sharin



Aleena Sheikh



Minsik (Andrew) Shin



Evelyn Shue



Helee Shukla



Tanya Shukla



Ekam Singh



Eshan Singhal



Arkajyoti (Arka) Sinha



Sahil Sood



Nikhita Srinivas

High School Students



Rebecca Sullivan



Angeline Sun



Edward Sun



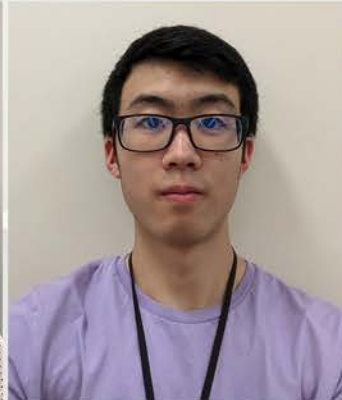
LeAnn Tai



Hannah Tao



David Tarrab



Dongli (Tony) Tian



Shreya Tiwari



Anya Vaish



Lorenzo Verona



Alex Wang



Laura (Zihan) Wang



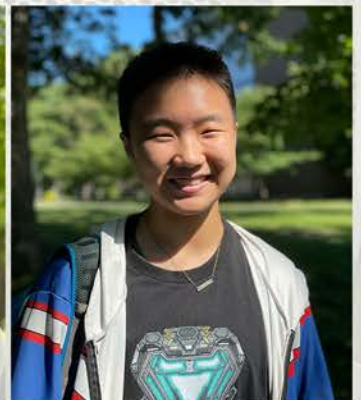
Vincent Wang



Yuhe (Luciana) Wei



Benjamin Wen



Sherlyn Wu

High School Students



Yubo Wu



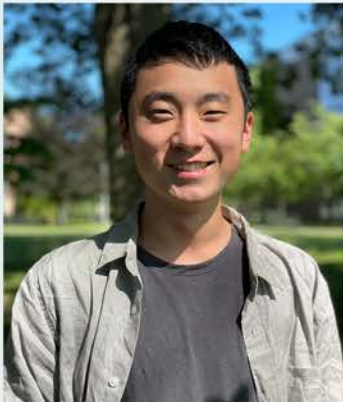
Yuhang Wu



Evan Xie



Rongrong Yan



Yi (Steven) Yang



Andy Yao



Sarah Yim



Shirley Xuan Ying Yu



Ivan Yuan Junior



Andrew Yuen



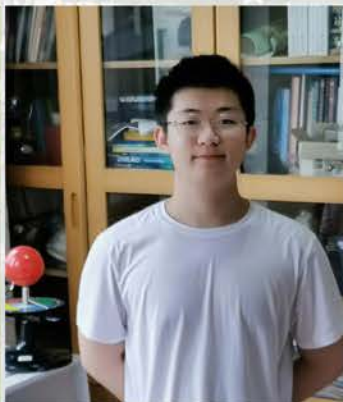
Andrew Zhang



Jerry Zhang



Ruijia (Gabo) Zhang



Shaoxi Zhang



Youyou (Yoyo) Zheng



Anthony Zhu

Research Experience for Undergraduates (REU)



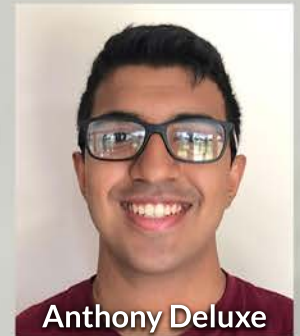
Christian Apostol



Allen Bethancourt



Anna Cho



Anthony Deluxe



Christopher Gazis



Megha Gopal



Joelle Gregoire Lincoln



Noah Kim



Ian Lau



Huiting Luo



Rena Max



Emir Mulic



Nicole Niculescu



Diya Rai-Gersappe



Melany Ramos Fernandez



Hugh Rosshirt



Sooraj Shah



Elizabeth Zhang

Graduate Students



Yiwei Fang



Haoyan Feng



Shi Fu



Adam Hansen



Jessica Hofflich



Yu-Chung Lin



Ziyuan Niu



Md Farabi Rahman



Aniket Raut



Robert Wong



Yifan Yin



Ziji (Jason) Zhang

Faculty & Staff



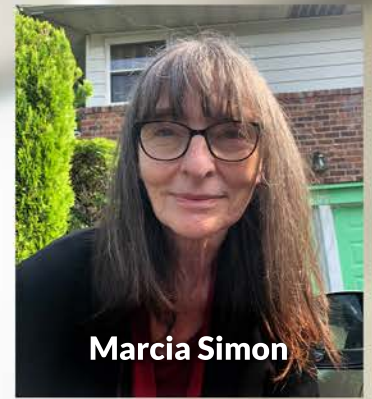
Jonathan Sokolov



Miriam Rafailovich



Michael Cuiffo



Marcia Simon



Dennis Gallanakis



Dilip Gersappe



Rebecca Isseroff



Brooke Ellison



Pawel Polak



Chander Sadasivan



Steven Walker



Yuefan Deng



Nilanjan Chakraborty



Herb Weiss



John Jerome



Kuan-Che Feng

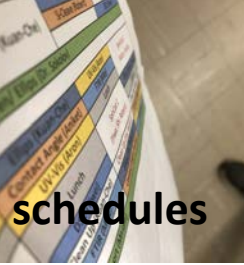


Peng Zhang

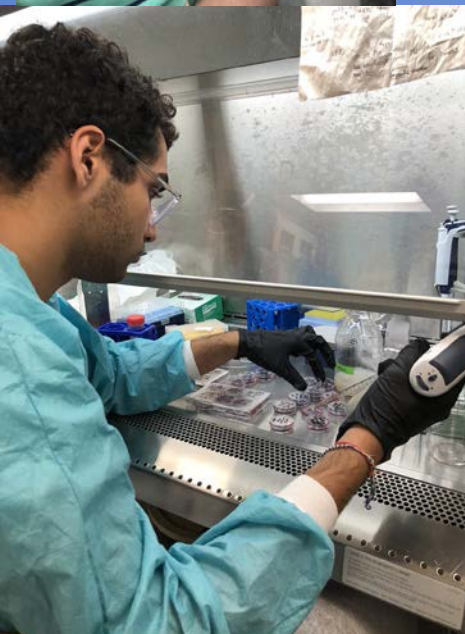
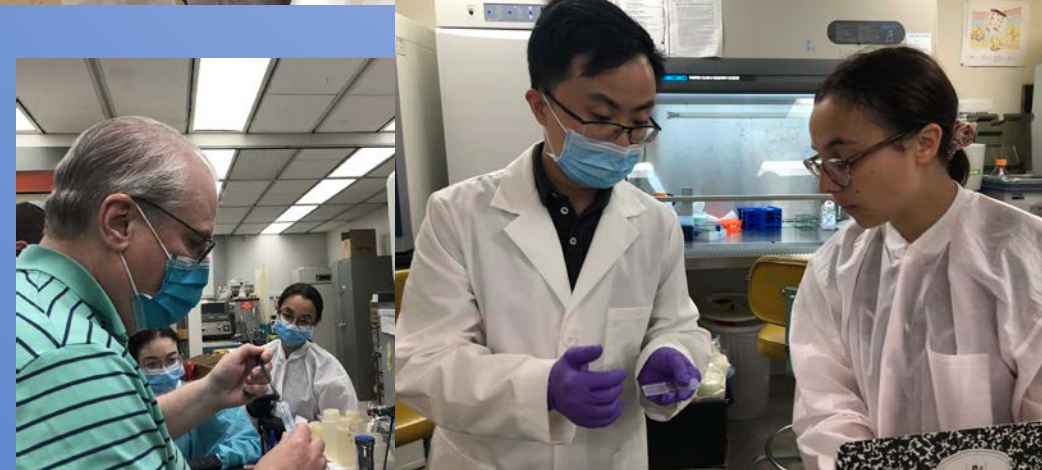


Aaron Sloutski

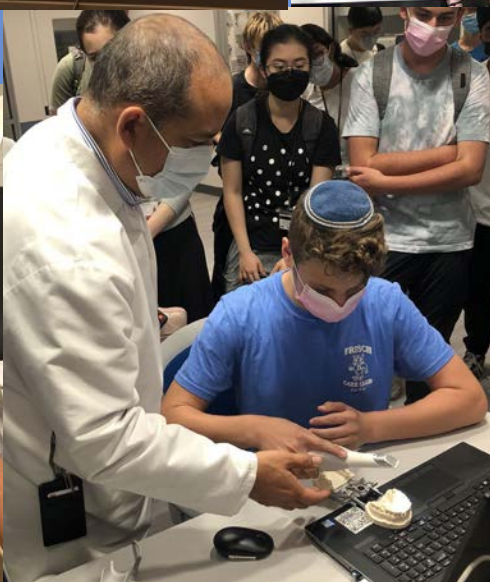
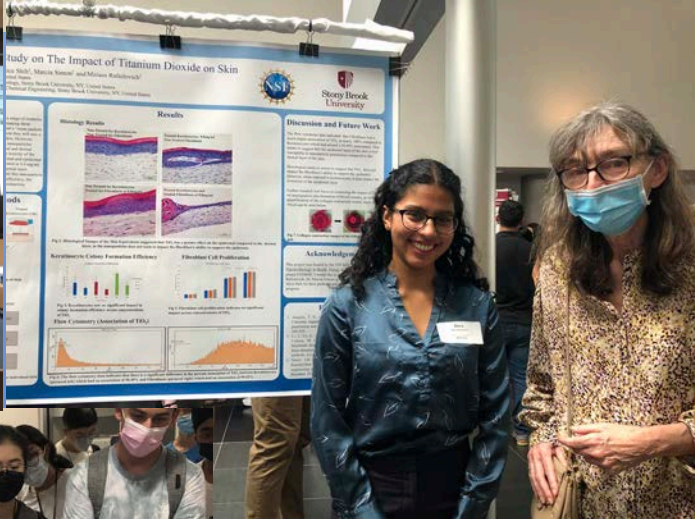
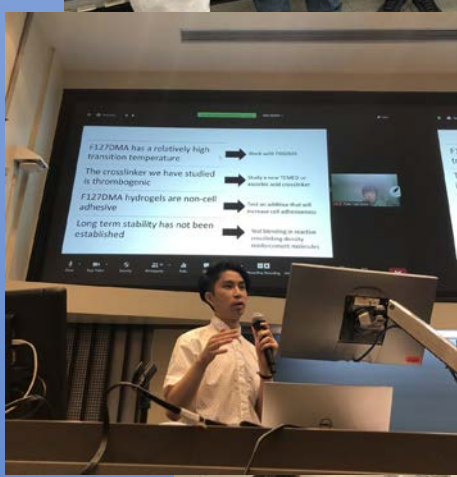
The first week –research bootcamp



In the lab and working on projects



In the lab and working on projects



Canoeing!

On The



Water

Fishing!



Fun Times!





Learning and Touring



Outdoor Adventures



Symposium





Summer Scholar Schedule of Weekly Activities

Each day starts with a mandatory group meeting at 10 AM!

Daily Schedule: Week of 6/27

| Monday – 6/27 | Tuesday – 6/28 | Wednesday – 6/29 | Thursday – 6/30 | Friday – 7/1 |
|---|---|--|---|--|
| <p>10:00 – 10:40: Introduction & Welcome</p> <p>10:40 – 11:30: Prof. Dilip Gersappe: Modeling Materials</p> <p>11:30 – 12:15: Prof. Peng Zhang: In silico biology</p> <p>12:15 – 12:45: Prof. Alfredo Fontanini: Research Overview at Stony Brook</p> <p>12:45 – 1:15: Lunch: Bagels on the Lawn</p> <p>1:15 – 2:15: Library Lecture: Clara Tran</p> <p>2:15 – 3:05: Prof. Kwan Woo Shin-- Research in Korea</p> <p>3:10 – 4:00: Prof. Stephen Walker: The Microbiome</p> | <p>10:00 – 10:15: Organizational Meeting</p> <p>10:15 – 12:15: Mandatory EH&S Chemical Training</p> <p>12:15 – 1:00: Lunch: with your REUs and Group</p> <p>1:00 – 1:30: Excel with Error Bars: Adam Hansen</p> <p>1:30 – 2:20: Dr. Ping Liu: Modeling Matter</p> <p>2:20 – 3:10: Dr. Gurtej Singh: Bioprinted Human Skin Models with Embedded Vascular Networks</p> <p>3:10 – 4:00: Prof. Pawel Polak: Image analysis</p> | <p>10:00 – 10:15: Organizational Meeting</p> <p>10:15 – 11:30: Mandatory EH&S Biosafety Training</p> <p>11:30 – 12:30: Lunch: With your REU and group</p> <p>12:30 – 4:00: Facilities Tour</p> | <p>10:00 – 10:15: Organizational Meeting</p> <p>10:15 – 11:15: Rebecca Isseroff: The Lab Notebook; Graphene</p> <p>12:30 – 1:00: Lunch with your group</p> <p>1:45 – 2:15: Safety Exam</p> <p>2:15 – 3:10: Dr. Nilanjan Chakraborty: Robotics</p> <p>3:10 – 4:00: Dr. Steve Larson: Biopolymers and the Army Corps of Engineers</p> <p>4:30 – 5:30: Baseball Challenge: NY vs Out of Town Feat. Dunkin Donuts + Baskin Robbins</p> | <p>10:00 – 10:30: Fire Safety Training</p> <p>10:30 – 11:15: Dr. Chander Sadasivan: Polymer Embolic Agents</p> <p>11:15 – 11:30: Organizational Meeting</p> <p>11:30 – 12:40: Pizza Working Lunch</p> <p>12:40 – 2:15: Journal Club Presentations</p> |

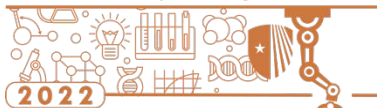


Summer Scholar Schedule of Weekly Activities

Each day starts with a mandatory group meeting at 10 AM!

Daily Schedule: Week of 7/4

| Monday – 7/4 | Tuesday – 7/5 | Wednesday – 7/6 | Thursday – 7/7 | Friday – 7/8 |
|---|---|---|---|--|
|  <p>Happy Fourth of July!</p> | <p>10:00 – 10:10: Organizational Meeting</p> <p>10:10 – 10:30: Prof. Steve Schwarz: Spin-Casting</p> <p>10:30 – 11:20: Prof. Chang Yon Nam: ALD Metal Deposition</p> <p>11:20 – 12:00: Lunch</p> <p>12:00 – 4:00: Spin-Casting Experiment Part 1</p> | <p>10:00 – 10:30: Organizational Meeting: Review of statistics and a puzzle</p> <p>10:30 – 4:00: Spin-Casting Experiment Part 2</p> | <p>10:00 – 10:30: Organizational Meeting</p> <p>10:30 – 11:20: Dr. Samantha Lucker: Soil Research</p> <p>11:20 – 12:00: Prof. Brooke Ellison: Holistic Ethics</p> <p>12:00 – 12:45: Working Lunch with Your Group:</p> <p>12:45 – 1:30: Review of Statistics I</p> <p>1:30 – 2:20: Research Talk 1: Prof. Jonathan Sokolov DNA</p> <p>2:20 – 3:30: Research Talk 2: Fuel Cells, Stem Cells and Embolisms</p> <p>3:30 – 4:00: Statistics II: Laboratory write up</p> | <p>10:00 – 10:15: Organizational Meeting</p> <p>10:15 – 12:00: Group presentations</p> <p>12:00 – 12:20: Pizza Lunch</p> <p>12:20 – 1:00: Skin: Prof. Marcia Simon</p> <p>1:00 – 2:30: Research Project Talks</p> |



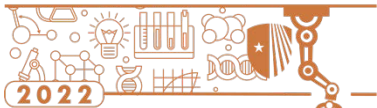
GARCIA

Summer Scholar Schedule of Weekly Activities

Each day starts with a mandatory group meeting at 10 AM!

Daily Schedule: Week of 7/11

| | Monday – 7/11 | Tuesday – 7/12 | Wednesday – 7/13 | Thursday – 7/14 | Friday – 7/15 |
|--|--|--|--|---|--|
| <p>Sunday – 7/10: <i>Nassau Pops Symphony Orchestra in Concert at Heckscher State Park and Trip to Mall (Sunday 7/10 from 5:30-9:30)</i></p> | <p>10:00 – 10:30: Organizational Meeting & Group Picture</p> <p>10:30 – 11:00: Rui Liu: The Human/Computer Interface</p> <p>11:00 – 1:45: Research Talks and Lunch (see schedule)</p> <p>1:45 – 4:00: Selection of Projects</p> <p>6:00 – 9:30: Celtic Quest Fishing and Bagels</p> | <p>10:00 – 11:00: Organizational Meeting & Rebecca Isseroff: Information session on the ISEF competition</p> <p>11:00 – 12:00: Dr. Kuan-Che Feng: Writing SOPs for Cell Lab Work I</p> <p>2:00 – 3:00: Dr. Ying Liu: SOP Lecture and Quiz</p> <p>3:00 – 4:00: Writing SOP for your project</p> | <p>10:00 – 10:30: Organizational meeting Final Project Assignment</p> <p>10:30 – 4:00: Work! (According to your group's schedule)</p> <p>4:30 – 5:30: Table Tennis Challenge - Yu-Chung Lin</p> | <p>10:00 – 10:30: Organizational Meeting: Donna Tuminello Filing for IP Protection</p> <p>10:30 – 4:00: Work! (According to your group's schedule)</p> | <p>10:00 – 10:15: Organizational Meeting: Green Energy Alternative for the Shinnecock Nation</p> <p>10:15 – 11:15: Student research update talks</p> <p>11:15 – 2:30: Work! (According to your group's schedule)</p> <p>12:00 – 1:00: Friday Pizza Social</p> <p>1:30 – 2:30: ERDC meet up</p> |



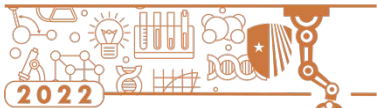
GARCIA

Summer Scholar Schedule of Weekly Activities

Each day starts with a mandatory group meeting at 10 AM!

Daily Schedule: Week of 7/18

| | Monday – 7/18 | Tuesday – 7/19 | Wednesday – 7/20 | Thursday – 7/21 | Friday – 7/22 |
|---|--|---|--|---|---|
| Sunday – 7/17: <i>Trip to BNL's Summer Sunday at the Vanderbilt Museum (10am-2pm)</i> | 10:00 – 10:15: Organizational Meeting & Research Updates: Fuel Cells and FACS 10:15 – 11:00: Dalia Leibowitz: Careers in Medical Device Applications at Medtronic 11:00 – 4:00: Work! (According to your group's schedule) | 10:00 – 10:15: Organizational Meeting 10:15 – 4:00: Work! (According to your group's schedule) 3:30 – 4:00: Research Update: DISC 7:00 – 7:30: Ice Cream Gathering | 10:00 – 10:30: Organizational meeting & Science Demonstration 10:30 – 11:00: Ikshu Pandey: Words From A Garcia Graduate 11:00 – 4:00: Work! (According to your group's schedule) 12:00 – 12:30: Yuefan Deng Lab Group Research Update 3:30 – 4:00: Research Updates & Ice Cream Social: Spin-Casting | 10:00 – 10:30: Organizational Meeting 10:30 – 10:45: Student research update talks – Neurogenic Differentiation 10:45 – 4:00: Work! (According to your group's schedule) 3:30 – 4:00: Research Updates & Ice Cream Social: Yuefan Deng Research Groups | 10:00 – 10:15: Organizational Meeting 10:15 – 11:15: Research Updates 11:15 – 2:30: Work! (According to your group's schedule) 12:00 – 1:00: Annual Garcia BBQ |
| | | | | |  |



GARCIA

Summer Scholar Schedule of Weekly Activities

Each day starts with a mandatory group meeting at 10 AM!

Daily Schedule: Week of 7/25

| | Monday – 7/25 | Tuesday – 7/26 | Wednesday – 7/27 | Thursday – 7/28 | Friday – 7/29 |
|--|---|---|--|---|---|
| Sunday – 7/24: <i>Trip to BNL's Summer Sunday on Atoms Feat. Ice Cream @ Dunkin' Donuts (10am-2pm)</i> | 10:00 – 10:15: Organizational Meeting 10:15 – 11:00: Dr. Richard Clark: Tunability of Multi-Functional Fibronectin Peptide for Defined Wound Therapy 11:00 – 4:00: Work! (According to your group's schedule) 3:30 – 4:00: Research Updates & Ice Cream Social | 10:00 – 3:00: Annual Garcia Canoe Trip on the Nissequogue River  3:00 – 4:00: Work! (According to your group's schedule) | 10:00 – 10:15: Organizational meeting 10:15 – 11:00: Dr. Julie Arslanoglu – Metropolitan Museum of Art: The Science of Art Restoration 11:00 – 4:00: Work! (According to your group's schedule) 12:00 – 12:30: REU Organizational Meeting 3:30 – 4:00: Research Updates & Ice Cream Social | 10:00 – 10:15: Organizational Meeting 10:45 – 10:45: Professor Robert Crease – The Death of BNL's High Flux Beam Reactor 10:45 – 11:30: Research Updates I 10:45 – 4:00: Work! (According to your group's schedule) 3:30 – 4:30: Research Updates II & Mr. Softee Ice Cream Social  | 10:00 – 1:00: Garcia 2022 Mid-Summer Research Symposium  |



Summer Scholar Schedule of Weekly Activities

Each day starts with a mandatory group meeting at 10 AM!

Daily Schedule: Week of 8/1

| Monday – 8/1 | Tuesday – 8/2 | Wednesday – 8/3 | Thursday – 8/4 | Friday – 8/5 |
|---|--|---|---|---|
| <p>10:00 – 10:15: Organizational Meeting</p> <p>10:15 – 10:45: Professor Jon Longtin, Dean of Stony Brook University College of Engineering and Applied Sciences: Engineering at Stony Brook</p> <p>10:15 – 10:45: Research Update: DISC</p> <p>11:00 – 4:00: Work! (According to your group's schedule)</p> | <p>10:00 – 3:00: Visit to the MET Research Labs</p> <p>THE MET</p> <p>10:00 – 4:00: Work! (According to your group's schedule)</p> | <p>10:00 – 10:15: Organizational meeting</p> <p>10:15 – 4:00: Work! (According to your group's schedule)</p> | <p>10:00 – 10:15: Organizational Meeting</p> <p>10:15 – 10:45: Vagelos Integrated Program at UPenn</p> <p>10:45 – 11:45: Professor Eyal Zussman: Fire Research at the Technion</p> <p>11:45 – 4:00: Work! (According to your group's schedule)</p> | <p>10:00 – 10:15: Organizational meeting</p> <p>10:15 – 4:00: Work! (According to your group's schedule)</p> |

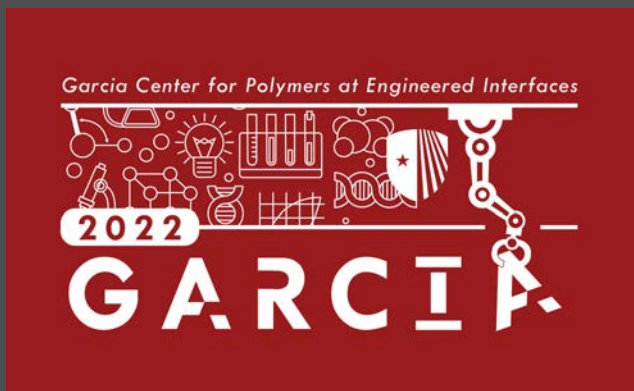


Summer Scholar Schedule of Weekly Activities

Each day starts with a mandatory group meeting at 10 AM!

Daily Schedule: Week of 8/8

| Monday – 8/8 | Tuesday – 8/9 | Wednesday – 8/10 | Thursday – 8/11 | Friday – 8/12 |
|---|---|--|---|--|
| <p>10:00 – 10:15: Organizational Meeting</p> <p>10:15 – 11:00: Marla Boots: Submission of Abstracts to the MRS Conference</p> <p>11:00 – 4:00: Work! (According to your group's schedule)</p> | <p>10:00 – 10:15: Organizational meeting</p> <p>10:15 – 4:00: Work! (According to your group's schedule)</p> <p>1:00 – 3:00: Sloths and Ice Cream Sloth Encounter LI & Carvel</p> | <p>10:00 – 10:15: Organizational meeting</p> <p>10:15 – 4:00: Work! (According to your group's schedule)</p> <p>3:00 – 4:00: Ethics Journal Organizational Meeting</p> | <p>10:00 – 10:15: Organizational Meeting</p> <p>10:15 – 11:15: Dr. Jonathan Garlick, Tufts University</p> <p>11:15 – 4:00: Work! (According to your group's schedule)</p> | <p>10:00 – 1:00: Garcia 2022 End-of-Summer Research Symposium</p>  |



Please join us:

Garcia 2022 Summer Research Symposium

Friday, July 29th, 10am – 1pm

SAC Ballroom A, Stony Brook University & Via Zoom

Greeting by

Steve Vaccarelli, Trust Officer,
Brown Brothers Harriman Trust Company, N.A.

Representing the
Louis Morin Charitable Trust

Guest Speaker:

Professor Alfredo Fontanini, MD, PhD
Professor & Chair, Department of
Neurobiology and Behavior

**Science Presentations by
Garcia 2022 Summer Research Scholars**

**Musical Arrangement by
Garcia Students and Prof.
John Jerome**

Please RSVP, Attend via Zoom, or Contact Us at: bit.ly/garcia2022symposium

Garcia Center for Polymers
at Engineered Interfaces

AT STONY BROOK UNIVERSITY

Garcia Center for Polymers at Engineered Interfaces

2022

GARCIA



Please join us:

Garcia 2022 End-of-Summer Virtual Research Symposium

Date:
Friday, August 12th
10am – 12pm

Zoom Link at: bit.ly/garcia2022symposium

Greeting by
Steve Vaccarelli, Trust Officer,
Brown Brothers Harriman Trust Company, N.A.
Representing the
Louis Morin Charitable Trust

Guest Speaker:
Dr. Isaac Cohen
VP, Corporate R&D Innovation
Estee Lauder Companies

Science Presentations by Garcia 2022 Summer Research Scholars

Attend via Zoom, Contact Us, or View Program at: bit.ly/garcia2022symposium

2022 Garcia Program End-of-Summer Virtual Research Symposium

Garcia Center for Polymers at Engineered Interfaces



" The highlight of Garcia is undoubtedly the interdisciplinary experience. Though our projects varied from machine learning to DNA research to materials engineering, we are united by the goal to learn and the goal to discover. This unified diversity that pulls 'GARCIA' together is expressed in the design. The hands-on skills we gained from participating in exciting, cutting-edge research was truly irreplaceable. Thank you to Garcia 2022 for the forever-cherished memories and opening our eyes to life as a scientist."

Leann Tai '22

| | |
|---------|---|
| 10:00AM | <p>Welcome Mr. Steve Vacarelli, Brown Bros Harriman and the Morin Charitable Trust</p> |
| | <p>Keynote Address Dr. Isaac Cohen, Estee Lauder Companies</p> |
| 10:15AM | <p>Session 0: Ethical Considerations in Science and Engineering Chair: Maytal Chelst</p> |
| | <p>A Salty Situation: Is Desalination an Ethical Solution to Water Scarcity? Konnie Duan, Harvard-Westlake High School, Studio City, CA Tony Tian, Mulgrave School, West Vancouver, BC, Canada Thomas Luong, Plano West Senior High School, Plano, TX Ben Pan, Stuyvesant High School, New York, NY Sarah Yim, Seoul International School, Seongnam, South Korea</p> |
| | <p>Gene Therapy: Making a Person Better or Making a Better Person? Ayush Arora, Munster High School, Munster, IN Maytal Chelst, Samuel H. Wang Yeshiva University for Girls, Hollis, NY Eliana Samuels, Yeshiva University High School for Girls, Hollis, NY Shreya Tiwari, Westwood High School, Austin, TX Evelyn Shue, Richard Montgomery High School, Rockville, MD Angeline Sun, Taipei American School, Taipei, Taiwan Anyva Vaish, Tesla STEM High School, Redmond, WA</p> |
| | <p>Ethical Challenges in Designing Research of Stratospheric Aerosol Injection: An Overview of the Risk-Knowledge Tradeoff Quinton Geller, Los Alamos High School, Los Alamos, NM Ivan Yuan, Shanghai High School International Division, Shanghai, Shanghai, China Vincent Wang, Irvington, Fremont, CA Anthony Zhu, Barrington High School, Barrington, IL</p> |

| | |
|---------|--|
| | <p>The Influence of Government Funding in the Scientific Research Process and Results</p> <p>Maytal Chelst, Samuel H. Wang Yeshiva University for Girls, Hollis, NY Emma Gao, The Harker School, San Jose, CA Eric Guan, North Carolina School of Science and Math, Chapel Hill, NC Eden Hen, SAR High School, Bronx, NY Evelyn Shue, Richard Montgomery High School, Rockville, MD Andy Yao, Herbert Henry Dow High, Midland, MI</p> |
| 10:25AM | <p>Session I: Biopolymers Chair: Huiting Luo</p> |
| | <p>The Influence of Rhizobium Tropici Produced EPM Biopolymer on Green Bush Bean Root and Plant Growth</p> <p>Yoyo Zheng, Asheville School, Asheville, NC Laura Wang, Mulgrave School, West Vancouver, BC, Canada Shirley Yu, Collingwood School, West Vancouver, BC, Canada</p> |
| | <p>An Evaluation of the Physical, Antimicrobial, Antiviral, and Toxic Properties of Rhizobium tropici ATCC 49672 Extracellular Polymeric Materials (EPM)</p> <p>Maytal Chelst, Samuel H. Wang Yeshiva University for Girls, Hollis, NY Eliana Samuels, Yeshiva University High School for Girls, Hollis, NY Gabriel Rothman, The Frisch School, Paramus, NJ</p> |
| | <p>Properties and applications of Biopolymer (EPS) and Nanocellulose Fibrils with Clay in Solution</p> <p>Rick Qian, Wayzata High School, Plymouth, MN Steven Yang, Amador Valley High School, Pleasanton, CA</p> |
| | <p>Molecular Dynamics Simulations of Soil-Strengthening Nanocomposite Hydrogels</p> <p>Arkajyoti Sinha, Lexington High School, Lexington, MA Jerry Zhang, Minnetonka Senior High School, Minnetonka, MN Vincent Wang, Irvington, Fremont, CA Anthony Zhu, Barrington High School, Barrington, IL</p> |
| 10:35AM | <p>Session II: In Silico and In Vitro Biology</p> |
| | <p>A Machine Learning Approach to Molecular Dynamics Predictions of SARS-CoV-2 Spike Protein Denaturation at Varying Temperatures and pH Levels</p> <p>Ayush Arora, Munster High School, Munster, IN Anyva Vaish, Tesla STEM High School, Redmond, WA Evan Xie, The Pingry School, Basking Ridge, NJ</p> |

| | |
|---------|--|
| | <p>Creating Coarse-Grained Models of Solvated Fibrinogen to Expedite Molecular Dynamics Simulations</p> <p>Eric Chen, Wayzata High School, Plymouth, MN</p> |
| | <p>Accelerating Multiscale Blood Flow Modeling with Computational Fluid Dynamics</p> <p>Amit Saha, Great Neck South High School, Great Neck, NY</p> |
| | <p>Generalized Lennard-Jones Equation for Ellipsoids using Physics-Informed Neural Network</p> <p>Yuhe (Luciana) Wei, Rutgers Preparatory School, Somerset, NJ</p> |
| | <p>Investigating Virus-Induced Thrombogenicity at the Molecular Level</p> <p>Justin Kim, Jefferson Forest High School, Forest, VA Matthew Lu, Chapel Hill High School, Chapel Hill, NC Ekam Singh, Washington High School, Fremont, CA LeAnn Tai, Arnold O. Beckman High School, Irvine, CA</p> |
| | <p>In Silico Modeling of the Ideal Binding Sites for Polylactic Acid Chains and Fibrinogen</p> <p>Rommy Sasson, Brooklyn Technical High School, Brooklyn, NY Michael He, Scripps Ranch High School, San Diego, CA</p> |
| | <p>Optimization of Learned-Jefferys Orbits Equation for Platelet Rotation in Online Machine Learning through Learned Parametrization of Fluid-Structure Interaction, Obsolete Deviation, and Deforming Capability</p> <p>Pratham Patel, North Carolina School of Science and Mathematics, Cary, NC</p> |
| | <p>CG-RNN - A Recurrent Neural Network for Coarse-Grained Force Field Prediction</p> <p>Eshan Singhal, The Oakridge School, Arlington, TX</p> |
| | <p>The Effect of P12 on Fibrinogen Fiber Formation in an <i>in vitro</i> Bovine Model</p> <p>Rommy Sasson, Brooklyn Technical High School, Brooklyn, NY</p> |
| | |
| 10:50AM | <p>Session III: Renewable Energy Generation Chairs: Yifan Yin and Haoyan Fang</p> |
| | <p>Using Acid-Treated Cellulose Fiber Membranes to Enhance the Performance of Proton Exchange Membrane Fuel Cells</p> <p>Thomas Luong, Plano West Senior High School, Plano, TX Ben Pan, Stuyvesant High School, New York, NY Sean Fang, Maggie Walker Governors School, Richmond, VA Konnie Duan, Harvard-Westlake High School, Studio City, CA Helee Shukla, New Hyde Park Memorial High School, New Hyde Park, NY Quinton Geller, Los Alamos High School, Los Alamos, NM</p> |

| | |
|---------|---|
| | <p>Investigating the Silver Nanoparticle Catalysis Mechanism in Alkaline Anion Exchange Membrane Fuel Cells</p> <p>Konnie Duan, Harvard-Westlake High School, Studio City, CA Quinton Geller, Los Alamos High School, Los Alamos, NM Helee Shukla, New Hyde Park Memorial High School, New Hyde Park, NY Thomas Luong, Plano West Senior High School, Plano, TX Ben Pan, Stuyvesant High School, New York, NY Sean Fang, Maggie Walker Governors School, Richmond, VA</p> |
| | <p>Surface Passivation Using 2D Perovskites Toward Efficient and Stable Perovskite Solar Cells</p> <p>Zixuan Lin, Shenzhen Middle School, Shenzhen, Guangdong, China Muyao Li, Shenzhen Middle School, Shenzhen, Guangdong, China Chengwei Shang, The Experimental High School Attached to Beijing Normal University, Beijing, China</p> |
| | <p>Investigating the effect of charging methods on dendrite formation in LiPF₆- and NaPF₆-electrolyte alkali-metal batteries through Lattice-Boltzman methods</p> <p>Tony Tian, Mulgrave School, West Vancouver, BC, Canada Ming Qi, University High School, Irvine, CA</p> |
| | |
| | <p>Science At-Home Video - The Leidenfrost Effect</p> |
| | |
| 11:00AM | <p>Session IV: Neurologic and Osteologic Differentiation of Dental Pulp Stem Cells Chair: Anna Cho</p> |
| | <p>Evaluating the Effect of Increased Resorcinol Diphenyl Phosphate (RDP) Concentrations in Clay on the Neurogenic Differentiation of Human Dental Pulp Stem Cells (hDPSCs)</p> <p>Hillel Schein, Davis Renov Stahler Yeshiva High School for Boys, Woodmere, NY Rebecca Sullivan, Yeshiva University High School for Girls, Hollis, NY Oran Goodman, The Frisch School, Paramus, NJ Nikhita Srinivas, Lausanne Collegiate School, Memphis, TN Sahil Sood, Lambert High School, Suwanee, GA Alexander Wang, Sewickley Academy, Sewickley, PA</p> |
| | <p>Investigating the Effect of Static Magnetic Fields on the Differentiation of DPSCs into Neurons</p> <p>Oran Goodman, The Frisch School, Paramus, NJ Nikhita Srinivas, Lausanne Collegiate School, Memphis, TN Rebecca Sullivan, Yeshiva University High School for Girls, Hollis, NY Hillel Schein, Davis Renov Stahler Yeshiva High School for Boys, Woodmere, NY Alexander Wang, Sewickley Academy, Sewickley, PA Sahil Sood, Lambert High School, Suwanee, GA</p> |

| | |
|---------|---|
| | <p>Investigating The Effect of a Dynamic Magnetic Field on The Rate of DPSC Neurogenic Differentiation</p> <p>Alex Wang, Sewickley Academy, Sewickley, PA Sahil Sood, Lambert High School, Suwanee, GA Rebecca Sullivan, Yeshiva University High School for Girls, Hollis, NY Hillel Schein, Davis Renov Stahler Yeshiva High School for Boys, Woodmere, NY Nikhita Srinivas, Lausanne Collegiate School, Memphis, TN Oran Goodman, The Frisch School, Paramus, NJ</p> |
| | <p>The Effect of Microsphere Growth and Static Magnetic Field on Osteogenic Differentiation of Dental Pulp Stem Cells</p> <p>Angeline Sun, Taipei American School, Taipei, Taiwan</p> |
| | |
| 11:15AM | <p>Session V: Robotics-Digital Analysis and Control</p> <p>Chairs: Hugh Rosshirt and Rena Max</p> |
| | <p>VR-Based Approach for Guiding a Robot in Manipulation Tasks</p> <p>Andy Yao, Herbert Henry Dow High, Midland, MI Eden Hen, SAR High School, Bronx, NY Siri Reddy, Horace Greeley High School, Chappaqua, NY</p> |
| | <p>Convolutional Neural Network Guided Point Cloud Segmentation</p> <p>Edward Sun, Torrey Pines High School, San Diego, CA Benjamin Wen, Aragon High School, San Mateo, CA</p> |
| | <p>A Cross-Platform Transfer</p> <p>Alex Samadi, Jericho Senior High School, Jericho, NY Sergio Rosa, South Side High School, Rockville Centre, NY</p> |
| | <p>Emotion Detection Using Deep Learning in Conjunction with Digital Image Speckle Correlation</p> <p>Eric Guan, North Carolina School of Science and Math, Chapel Hill, NC Juni Kim, Stanford Online High School, Redwood City, CA Judah Rosenthal, Davis Renov Stahler Yeshiva High School for Boys, Woodmere, NY David Tarrab, Ramaz Upper School, New York, NY Yubo Wu, Canyon Crest Academy, San Diego, CA</p> |
| | |
| 11:20AM | <p>Session VI: TiO₂ Nanotoxicology & DNA Sequencing Chips</p> |
| | <p>Impact of TiO₂ Nanoparticles on Skin Dynamics in Conjunction with Analysis of Treated Skin Organotypics Impact of Titanium Dioxide (TiO₂) Nanoparticles on Bacterial Infection Resistance of Fibroblasts and HUVEC Cells/Gene Expression</p> <p>Navya Gautam, Hauppauge High School, Hauppauge, NY Annie Hu, Great Oak High School, Temecula, CA Darshini Podder, Jericho High School, Jericho, NY Harsha Rajkumar, Fremont Christian High School, Fremont, CA</p> |

| | |
|---------|--|
| | <p>Matthew Sharin, Lawrence High School, Cedarhurst, NY Sherlyn Wu, Lawrence High School, Cedarhurst, NY Sarah Yim, Seoul International School, Seongnam, South Korea Jeffery Zhang, Shenzhen Middle School, Shenzhen, Guangdong Province, China</p> |
| | <p>Determining the Efficacy of Using Transposase (Tn5) to Cut DNA on PMMA Surfaces</p> <p>Tanya Shukla, Ardsley High School, Ardsley, NY Yuhang Wu, Worcester Academy, Worcester, MA</p> |
| | <p>Deposition of DNA onto Polymethacrylate (PMMA) Thin Film Gratings in Preparation for the Tagmentation of DNA with Tn5 Transposase</p> <p>Rachel Na, Friends Academy, Locust Valley, NY Deryn O'Leary, Our Lady of Mercy Academy, Syosset, NY Hannah Saks, Walt Whitman High School, Huntington Station, NY</p> |
| | <p>Determining the Extent to Which Sodium Dodecyl Sulfate Could Desorb DNA from Flat Surfaces</p> <p>Derek Days, Noble and Greenough, Newton, MA Ohm Patel, Patchogue-Medford High School, Medford, NY</p> |
| | |
| | <p>Video: Life in Garcia 2022</p> |
| | |
| 11:35AM | <p>Session VII: Repurposing Cellulose & Longest Living Oral Bacteria Chairs: Tony Deluxe and Elizabeth Zhang</p> |
| | <p>Long Term Survival of E. Faecalis</p> <p>Michelle Bok, Seoul International School, Seoul, Gyeonggi-do, South Korea Andrew Zhang, Del Norte High School, San Diego, CA Shreya Tiwari, Westwood High School, Austin, TX</p> |
| | <p>Deweaving Cotton Cloth using Non-Toxic and Environmentally Friendly Methods Repurposing Waste Fabric by Synthesizing Silver Nanoparticles on Deweaved Cotton Fibers</p> <p>Ivan Yuan Junior, Shanghai High School International Division, Shanghai, Shanghai, China Hannah Tao, Academy for Information Technology, Scotch Plains, NJ Andrew Yuen, Jericho High School, Jericho, NY Aleena Sheikh, MDQ Academy, Brentwood, NY</p> |

| | |
|---------|--|
| 11:40AM | <p>Session VIII: Liquid Embolic Agents Chair: Megha Gopal</p> |
| | <p>Optimizing a Minimally Invasive Reverse Thermo-Responsive Liquid Embolic Agent Polymer Treatment for Brain Aneurysms</p> <p>Noah Fensterheim, Ida Crown Jewish Academy, Skokie, IL Elaina Heghes, South Side High School, Rockville Centre, NY Shaheer Khan, Half Hollow Hills High School East, Dix Hills, NY Dohyun Kim, Seoul Foreign School, Seoul, Seoul, South Korea Briana Poon, Arlington High School, Lagrangeville, NY Evelyn Shue, Richard Montgomery High School, Rockville, MD Lorenzo Verona, American School of Milan, Milan, Lombardy, Italy</p> |
| | <p>Cell-Adhesiveness of Poly(vinyl Alcohol) and Additives as Potential Vascular Graft Material</p> <p>Caroline Brown, Williamsville North High School, Williamsville, NY Sophia Chen, Sage Hill School, Newport Coast, CA Sahana Dhama, The Wheatley School, Old Westbury, NY Emma Gao, The Harker School, San Jose, CA</p> |
| | |
| 11:45AM | <p>Session IX: Polymer Blends</p> |
| | <p>Optimizing Conductivity and Strength of Biodegradable Polymer Graphene Nanoplatelet Nanocomposites via 3D-Printing</p> <p>Tavan Bhatia, Staples High School, Westport, CT Haaris Alam, Portola High School, Irvine, CA Ruijia (Gabo) Zhang, Ed W Clark High School, Las Vegas, NV Gavin Onghai, Earl L Vandermulen, Port Jefferson, NY</p> |
| | <p>Flame-Retardant Polymer Blends Using Biopolymers</p> <p>Minsik Shin, Seoul International School, South Korea</p> |
| | |
| 11:50AM | <p>Session X: Spin-Casting Polymer Thin Films</p> |
| | <p>Spincasting to Determine Molecular Weights of Polystyrene Samples</p> <p>Sean Fang, Maggie Walker Governors School, Richmond, VA Alex Wang, Sewickley Academy, Sewickley, PA Justin Kim, Jefferson Forest High School, Forest, VA Arkajyoti Sinha, Lexington High School, Lexington, MA Sahil Sood, Lambert High School, Suwanee, GA Thomas Luong, Plano West Senior High School, Plano, TX</p> |
| | <p>An Inexpensive Method for Determining Molecular Weight</p> <p>Arkajyoti Sinha, Lexington High School, Lexington, MA Sean Fang, Maggie Walker Governors School, Richmond, VA Justin Kim, Jefferson Forest High School, Forest, VA</p> |

| | |
|---------|---|
| | Alex Wang , Sewickley Academy, Sewickley, PA Sahil Sood , Lambert High School, Suwanee, GA Thomas Luong , Plano West Senior High School, Plano, TX |
| | |
| | ReGroup Magazine – A Student-Led Magazine to Communicate Science |
| | |
| 12:00PM | Concluding Remarks |



Garcia 2022 Logo designed by LeAnn Tai

*We gratefully acknowledge support from
the Louis Morin Charitable Trust*

Session 0: Ethical Considerations in Science and Engineering

Chair: Maytal Chelst

Journal of Ethics in Scientific and Technological Innovation (JESTI)

Maytal Chelst¹, Konnie Duan², Navya Gautam³, and Anya Vaish⁴

¹Samuel H. Wang Yeshiva University High School for Girls, ²Harvard-Westlake High School, ³Hauppauge High School, and ⁴Tesla STEM High School



Ethical Topics:

- Privacy
- Genetics
- Aging
- Sustainability
- Government
- Geoengineering
- Vaccines
- Stem Cells
- Drugs

Mentors:

- Dr. Brooke Ellison
- Dr. Miriam Rafailovich
- Jessica Hofflich

Highlighted Today:

A Salty Situation: is Desalination an Ethical Solution to Water Scarcity?

Konnie Duan, Thomas Luong, Ben Pan, Tony Tian, and Sarah Yim

Gene Therapy: Making a Person Better or Making a Better Person?

Ayush Arora, Maytal Chelst, Eliana Samuels, Shreya Tiwari, Evelyn Shue, and Angeline Sun

Ethical Challenges in Designing Research of Stratospheric Aerosol Injection: An

Overview of the Risk-Knowledge Tradeoff
Quinton Geller, Ivan Yuan, Vincent Yang, and Anthony Zhu

The Influence of Government Funding in the Scientific Research Process and Results

Maytal Chelst, Emma Gao, Eric Guan, Eden Hen, Evelyn Sue, and Andy Yao

A Salty Situation: Is Desalination an Ethical Solution to Water Scarcity?

Konnie Duan¹, Thomas Luong², Ben Pan³, Hannah Tao⁴, Tony Tian⁵, Sarah Yim⁶

¹Harvard-Westlake High School, Studio City, CA, ²Plano West Senior High School, Plano, TX, ³Stuyvesant High School, New York, NY, ⁴Academy for Information Technology, Scotch Plains, NJ, ⁵Mulgrave School, West Vancouver, BC, Canada, ⁶Seoul International School, Seongnam, South Korea

As water scarcity becomes more severe, many populations have been building and relying on desalination plants. However, controversy has arisen because of the wide range of environmental problems desalination can cause. The increasing popularity and disputes regarding desalination beg the following question: When, if ever, is it ethical to adopt desalination programs, despite potential long-term damage to the environment? This question calls upon the consideration of various factors, like access to clean water, sustainability, and economic affordability, and ethical frameworks, such as environmental justice and utilitarianism. The aim of this paper is to establish conditions when desalination programs are ethical and discuss methods to maximize benefits and minimize harms.

Access to clean drinking water was explicitly recognized as a fundamental human right by the 2010 United Nations General Assembly. From a humanitarian perspective, desalination is a step towards guaranteed universal access to this human right and thus can be a necessary practice, especially for water-scarce regions where desalination is the only viable source of clean drinking water.

However, the various forms of environmental damage caused by desalination tells a different story. Most desalination plants are powered by fossil fuels, which contributes to greenhouse gas emissions, and a smaller number are powered by electricity, which releases cooling waters and air toxins.¹ Furthermore, the process of water intake by desalination plants can suck in small marine organisms along with the source water or impinge them on intake screens, causing loss of abundance and biodiversity in the ecosystem.² Finally, the byproduct brine, with dangerously high concentrations of salt, heavy metals, radioactive material, and pollutants, is typically dumped into the marine environment following reverse osmosis. There, it inevitably wreaks havoc on the ecological community and soil composition, increases sea temperature near the discharge site, and can even alter the quantity of dissolved oxygen in the water.³

Currently, research is being done to investigate potential modifications that can mitigate these detrimental effects, but most of these innovations are not yet ready to be used on a large scale.² We concluded that desalination programs are only ethical if the benefit of clean and safe water for a population outweighs the massive environmental harm. Using Bentham's utility calculus, it can be determined if, where, and when desalination projects are justified. This paper suggests how future research, foresight, and management can maximize benefits and minimize harms as we improve desalination to ensure safe, clean, and accessible water for everyone.

¹ Logan, Bruce E. "The Global Challenge of Sustainable Seawater Desalination." *Environmental Science & Technology Letters*, vol. 4, no. 6, June 2017, pp. 197–197. DOI.org (Crossref), <https://doi.org/10.1021/acs.estlett.7b00167>.

² Ihsanullah, Ihsanullah, et al. "Desalination and Environment: A Critical Analysis of Impacts, Mitigation Strategies, and Greener Desalination Technologies." *Science of The Total Environment*, vol. 780, Aug. 2021, p. 146585. ScienceDirect, <https://doi.org/10.1016/j.scitotenv.2021.146585>.

³ Saadaoui I., et al. "Characteristics of Desalination Brine and Its Impacts on Marine Chemistry and Health, With Emphasis on the Persian/Arabian Gulf: A Review." *Frontiers in Marine Science*, vol. 9, April 2022, <https://doi.org/10.3389/fmars.2022.845113>.

Gene Therapy: Making a Person Better or Making a Better Person?

Ayush Arora¹, Maytal Chelst², Gabriel Rothman³, Eliana Samuels², Angeline Sun⁴, Shreya Tiwari⁵, and Anya Vaish⁶

¹Munster High School, ²Samuel H. Wang Yeshiva University High School for Girls, ³The Frisch School, ⁴Taipei American School, ⁵Westwood High School, and ⁶Tesla STEM High School

In 1990, Ashanti de Silva, a four-year-old child with severe combined immunodeficiency, was the first human to have a successful usage of gene therapy. Nearly thirty years later, in 2018, He Jiankui, a Chinese scientist, used CRISPR-Cas9, a gene editing tool, to create a gene-edited baby for the first time. As a result of this success, there has been a drastic uptick in the number of people looking into potential gene-editing treatments (Figure 1). (Editors, 2021) However, at the same time, a worldwide debate was sparked over the efficacy and morality of this innovative technology.

While idealistically gene therapy seems to solve many issues associated with harmful genetic mutations, in actuality editing a human’s genome has a whole host of ethical issues that need to be addressed before research is continued. The primary question that would need to be addressed is the institution of a bright line - the line between making someone better (replacing/removing malignant genes/genetic mutations) and creating a better person. Once parameters are set, the issue of accessibility must be taken into account. Gene therapy is costly and therefore only a small percentage of people would

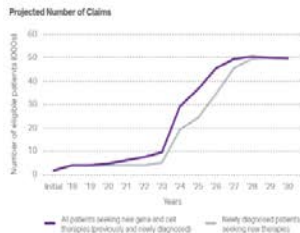


Figure 1. This figure shows the projected number of patients seeking gene therapy in previous years and in the years to come. Due to the advancements in the technology of the field, it is likely that the numbers will go up tremendously over the next few years and beyond because of the unparalleled potential gene therapy provides as a treatment for a number of otherwise incurable diseases. (Editors, 2021)

have it as a treatment option or have it generally available. (Sahli, 2021) Ethically, a treatment as innovative and potentially helpful as gene therapy should be available to all, regardless of monetary means. If the parameters are set in a way that editing can occur for purposes beyond that of addressing malignant genes, it is possible for those with the monetary means to use them in various ways that are not accessible to others, ultimately further widening the current worldwide socioeconomic gap.

There are many ethical concepts prevalent with regard to this moral dilemma, including those of autonomy and consequentialism. With the implementation of this technology, there is the potential for non-consensual genes to be harmfully edited, as well as the inevitable reinforcement of inequalities and damaging beauty standards. By looking through various ethical lenses, it can be concluded that gene therapy, despite its potential benefits in improving human health and wellbeing, requires strict restrictions on the status quo in order to provide the most collectively beneficial impact for the individuals utilizing this unique scientific advancement.

| DRUG NAME | MANUFACTURER | INDICATION | COST |
|---------------------------------------|----------------------|---|-------------------------|
| Luxturna (voretigene alipogene eye) | Spark | Inherited retinal disease | \$900,000 for both eyes |
| Kymriah (tisagenlecleumab) | Novartis | Acute lymphocytic leukemia Diffuse large B-cell lymphoma | \$475,000 \$372,000 |
| Yescarta (axicabtagene ciloleucel) | AbbVie | Large B-cell lymphoma and follicular lymphoma | \$373,000 |
| Zincapuma (betamagatadine ophthalmic) | Aveksis | Spinal muscular atrophy | \$3.125 million |
| Tecartus (ditigaligene desferrioxal) | AbbVie | Mantle cell lymphoma | \$373,000 |
| Breyanzi (lisocabtagene maraleucel) | BMS | Large B-cell lymphoma | \$400,300 |
| Alneca (delatigenericecel) | BMS and bluebird bio | Multiple myeloma | \$418,500 |

Figure 2. This table shows a number of new gene therapy drug treatments along with the disease that is being treated and the patient cost for each drug. This table portrays the high costs of different gene therapy treatments. (Sahli, 2021)

have it as a treatment option or have it generally available. (Sahli, 2021) Ethically, a treatment as innovative and potentially helpful as gene therapy should be available to all, regardless of monetary means. If the parameters are set in a way that editing can occur for purposes beyond that of addressing malignant genes, it is

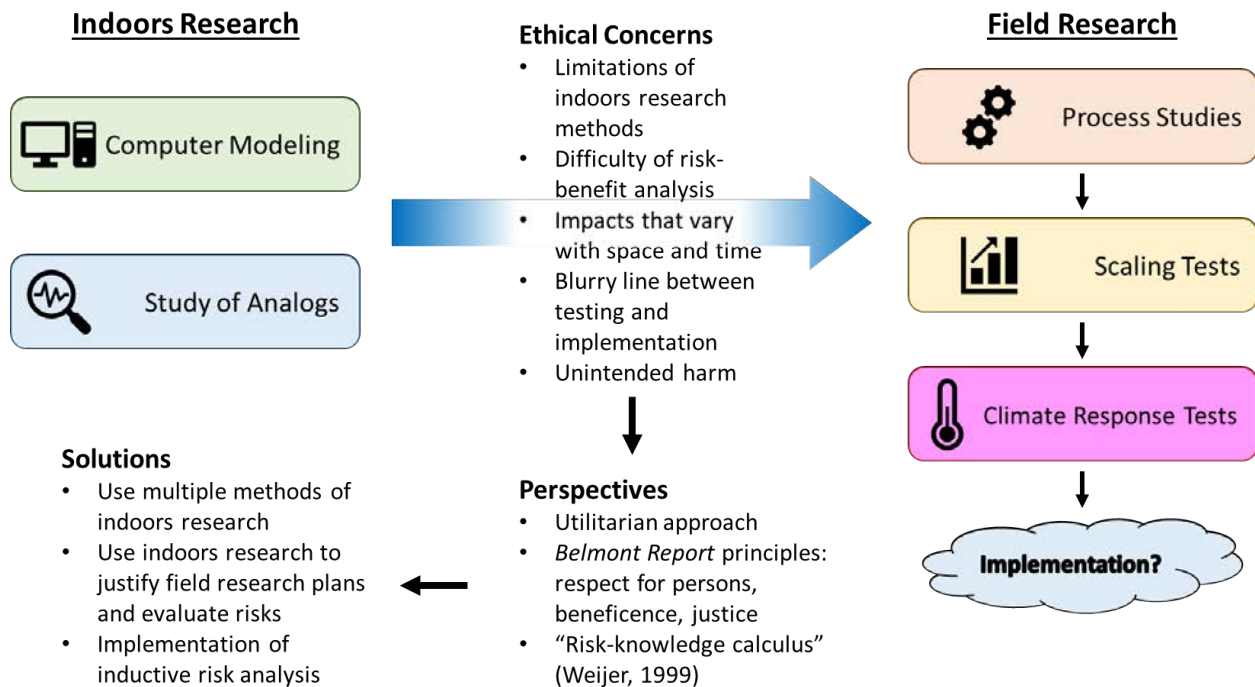
Editors. “The Surprising Impact of Gene Therapies.” *MedImpact*, Apr. 2021, www.medimpact.com/resources/client-news/surprising-impact-gene-therapies.
Sahli, Brett. *Cost Management for Sky-High, High-Cost Gene Therapy*, Aug. 2021, www.primetherapeutics.com/news/cost-management-for-sky-high-high-cost-gene-therapy/.

Ethical Challenges in Designing Research of Stratospheric Aerosol Injection: An Overview of the Risk-Knowledge Tradeoff

Ivan Yuan¹, Anthony Zhu², Vincent Wang³, Quinton Geller⁴

¹Shanghai High School International Division, Shanghai, China 200231, ²Barrington High School, Barrington, IL 60010, ³Irvington High School, Fremont, CA 94539, ⁴Los Alamos High School, Los Alamos, NM 87544

Stratospheric aerosol injection (SAI) has received much attention for its supposed effects of increasing albedo to delay the effects of climate change. Previous research has been conducted on models, but presently require small-scale field experiments to reduce uncertainties in parameters and risks (MacMartin and Kravitz, 2019). There are many ethical considerations when transitioning from indoors to field research of SAI. One consideration is the scale of impact. The impact of SAI can vary by both the time and geographic scales (Morrow et al., 2009). SAI research tends to have little to no benefits for the people who currently bear the risk from the experiment and mostly benefits people in the future. Furthermore, regional differences must be accounted for when conducting field tests. Another pertinent ethical consideration is the error and risk involved in computer models of SAI. Although models and simulations are less potentially damaging than field research, reliance on them is itself ethically dubious due to the very real possibility that they can be misleading or completely incorrect as a result of inductive error. Even still, we conclude that field research should only be conducted either to 1) reduce uncertainties of models by providing parameters or 2) confirm indoor research supported by multiple methods of research.



MacMartin, Douglas G., and Ben Kravitz. "The engineering of climate engineering." *Annual Review of Control, Robotics, and Autonomous Systems* 2.1 (2019).

Morrow, David R., Robert E. Kopp, and Michael Oppenheimer. "Toward ethical norms and institutions for climate engineering research." *Environmental Research Letters* 4.4 (2009): 045106.

The Influence of Government Funding on the Scientific Research Process and Results

Maytal Chelst¹, Emma Gao², Eric Guan³, Eden Hen⁴, Evelyn Shue⁵, Andy Yao⁶

¹Samuel H. Wang Yeshiva University High School for Girls, Hollis, NY, 11598, ²The Harker School, San Jose, CA 95129, ³North Carolina School of Science and Math, Durham, NC, 27705 ⁴SAR High School, Bronx, NY, 10471

⁵Richard Montgomery High School, Rockville, MD, 20852 ⁶Herbert Henry Dow High School, Midland, MI, 48640

Funding, be it from non-profit organizations, corporations, or even the government itself, is key to proper research. The United States government has consistently increased annual funding for research and development, with the amount of federal research funding growing from \$3.5 billion in 1955 to a whopping \$138.9 billion in 2019 (Figure 1).¹

However, although the total amount of federal funding has continued to climb, the percentage of total basic research funding in the US provided by the federal government has shrunk in recent years.² And as the federal share of research funding diminishes, the select projects that the government does choose to fund become subject to more scrutiny, raising questions regarding what

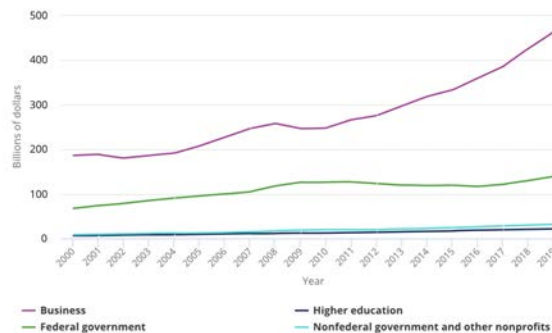


Figure 1. U.S. R&D expenditures, by source of funds: 2000–19¹

research the government decides to fund and how federal funding affects the procedure and results of research.

For one, researchers receiving funds from the government can feel pressured to produce certain desired results, which may impact the credibility of their studies or influence the direction of their work. Additionally, research projects funded by the government may lack transparency for reasons of national security, stifling adequate regulation and public backlash. This paper analyzes the ramifications of government funding on research through three case studies involving the application of facial recognition to the public, the engineering of biological weapons, and fraudulent reports from university research departments.

Facial recognition technology’s potential to be widely used in society has catalyzed a political and ethical debate fueled by fear of authoritarianism. Governmental interest in this crucial but still-developing field poses a moral question for researchers regarding the acceptance of federal funding when such funding might enable their research to be used in ways that violate ethics and human rights.

Federal funding of biological weapons, meanwhile, has sparked concerns about transparency and the public’s right to knowledge. During the development of these weapons, the US government withholds significant information despite the potential for this technology to kill millions.

Finally, conditions that come attached with federal funds provide a unique incentive for researchers to manipulate data or other aspects of their projects to achieve desirable outcomes. With critical funding on the line, some universities have resorted to reporting false data and results for their research projects.

From examining these three cases, this paper aims to tackle crucial and relevant questions regarding the ethics of federal funding and the effect that government involvement can have on research.

¹ National Science Board, National Science Foundation. 18 Jan. 2022. *Science and Engineering Indicators 2022: The State of U.S. Science and Engineering*. NSB-2022-1. Alexandria, VA. Available at <https://nces.nsf.gov/pubs/nsb20221>.

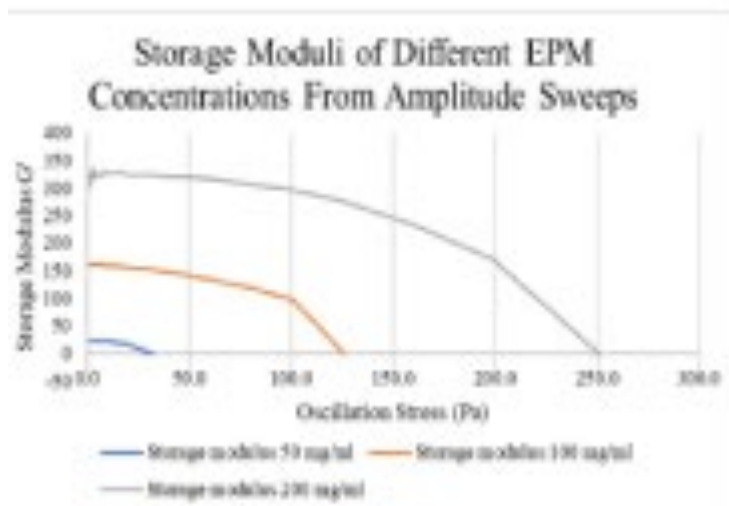
² Mervis, Jeffrey. “Data Check: U.S. Government Share of Basic Research Funding Falls below 50%.” *Science.org*, 9 Mar. 2017, <https://www.science.org/content/article/data-check-us-government-share-basic-research-funding-falls-below-50>.

Session 1: Biopolymers

Chairs: Huiting Luo, Yiwei Fang,
Dr. Kuan-Che Feng



Figure 1. Clay-biopolymer network formation simulation visualized in VMD [3]



The Influence of *Rhizobium Tropici* Produced EPM Biopolymer on Green Bush Bean Root and Plant Growth

Huiting Luo¹, Shirley Xuan Ying Yu², Youyou Zheng³, Zihan Wang⁴, Melany Ramos Fernandez⁵, Marcia Simon⁶, Miriam Rafailovich¹

¹Department of Materials Science and Chemical Engineering, Stony Brook University, Stony Brook, NY 11794, ²Collingwood School, West Vancouver, BC, Canada, ³Asheville School, Asheville, NC 28806, ⁴Mulgrave School, West Vancouver, BC, Canada, ⁵Physical Sciences, Suffolk County Community College, Selden, NY 11784, Department of Oral Biology and Pathology, ⁶Stony Brook University School of Dental Medicine, Stony Brook, NY 11794

Soil erosion is a global environmental concern caused by natural forces such as precipitation and flood as well as agricultural activities¹. Vegetation with a rich biomass system can be used for erosion control by altering soil properties, such as aggregate stability, hydraulic function, and shear strength. Modern agriculture often relies on chemical fertilizers to enhance root growth, resulting in toxic runoff, environmental contamination, and significant CO₂ emissions during production of chemical fertilizers. Our research investigated the use of EPM (ethanol precipitable material), biodegradable and environmentally friendly biopolymer-based substrates, to enhance root and plant growth.

Two EPM biopolymers are produced from bacteria *Rhizobium tropici* at Stony Brook School of Dental Medicine following the procedure of Staudt et al². One control group (tap water) and four EPM groups (EPM 1 and EPM 2 in concentrations 50 mg/L and 100 mg/L) were prepared. To test the effectiveness of biopolymers EPM 1 and EPM 2, green bush beans were germinated, watered, and analyzed to investigate both root and stem growth. Three petri dishes were used for each treatment, with five green bush bean seeds on each petri dish, watered with 50 mL of tap water or EPM solution daily. After three weeks, the plants and roots mass were analyzed to investigate whether the EPM biopolymer influenced the roots versus the stems differently.

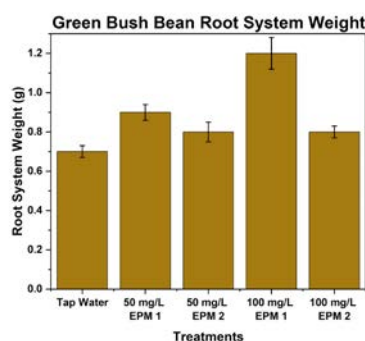


Figure 1. Root system weight of green bush bean plants

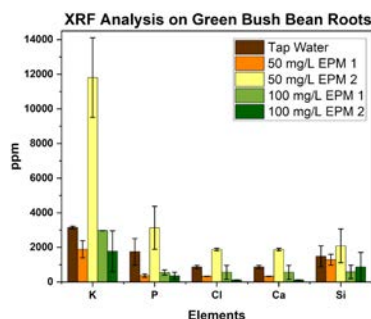


Figure 2. XRF analysis on green bush bean roots

As shown in Figure 1, green bush beans treated with EPM solutions have larger root mass than the control. Especially, plants watered with 100 mg/L EPM 1 had a 71% increase compared to the control group. According to Figure 2, biopolymers generally enhance root absorption. Roots treated with 50 mg/L EPM 2 contained the highest amount of K—which is a key nutrient to root growth. However, 50 mg/L EPM 2 was not the most enhancing treatment in root growth by mass from Figure 1. One possible reason would be that the K uptake exceeded the optimal K for root development. A previous study³ has shown that the root mass of melons decreased when the K concentration was over 118 mg/L. Data were collected for the plant's stem and leaf as well, along with its height.

Through the analysis, EPM treated green bush bean plants were found to have higher root mass, biomass, and higher plant height than plants watered with tap water, showing their potential in enhancing soil erosion resistance. From the results, it can be concluded that EPM 1 tends to better develop the root system, while EPM 2 tends to better develop the stem and leaf growth of green bush bean plants.

¹Nasir Ahmad, Nur Syabeera, et al. "A Systematic Review of Soil Erosion Control Practices on the Agricultural Land in Asia." *International Soil and Water Conservation Research*, vol. 8, no. 2, 2020, pp. 103–115., <https://doi.org/10.1016/j.iswcr.2020.04.001>.

²Staudt, Ann K., et al. "Variations in Exopolysaccharide Production by *Rhizobium Tropici*." *Archives of Microbiology*, vol. 194, no. 3, 2011, pp. 197–206. *Crossref*, <https://doi.org/10.1007/s00203-011-0742-5>.

³Saghaiesh, Sakineh Pourranjbari, and Mohammad Kazem Souri. "ROOT GROWTH CHARACTERISTICS OF KHATOUNI MELON SEEDLINGS AS AFFECTED BY POTASSIUM NUTRITION." *Acta Scientiarum Polonorum Hortorum Cultus*, vol. 17, no. 5, 2018, pp. 191–98. *Crossref*, <https://doi.org/10.24326/asphe.2018.5.17>.

An Evaluation of the Physical, Antimicrobial, Antiviral, and Toxic Properties of *Rhizobium tropici* ATCC 49672 Extracellular Polymeric Substances (EPS)

Maytal Chelst¹, Eliana Samuels¹, Gabriel Rothman², Dr. Kuan-Che Feng³, Yiwei Fang³, Adam Hansen³,
Dr. Stephen Walker⁴, Dr. Marcia Simon⁴, Dr. Miriam Rafailovich³

¹Samuel H. Wang Yeshiva University High School for Girls, 86-86 Palo Alto St, Hollis, NY 11423; ²The Frisch School, 120 W Century Rd, Paramus, NJ 07652; ³Department of Material Science and Engineering, Stony Brook University, Stony Brook, NY 11794; ⁴Department of Oral Biology and Pathology, Stony Brook University, Stony Brook, NY 11794

Rhizobia bacteria create a symbiotic relationship with legume plants by forming root nodules as a site for nitrogen fixation providing plants with ammonia from atmospheric nitrogen. During the process of this symbiosis, natural gel-like biopolymers are secreted by the rhizobia known as extracellular polymeric substances (EPS). (Maróti & Kondorosi, 2014; Wang et al., 2018) These biopolymers have many functions in the rhizosphere including soil particle adhesion as well as water and nutrient retention. Because of these desirable features and functions, the biopolymers are currently being tested by the United States Engineer Research and Development Center (ERDC) to strengthen soil to limit soil erosion and ensure slope stability of berms as an environmentally beneficial alternative to potentially toxic and/or non-biodegradable standard petrochemical treatments. (Larson, 2016) In order for these biopolymers to be put to widespread use, it is essential to further characterize the EPM (ethanol precipitable material; non-dialyzed EPS) and determine any potential effects on the environment including those on bacteria, viruses, and mammalian cells.

The biopolymers' rheological properties were tested by conducting an amplitude sweep, an angular frequency test, and a shear rate test. These tests were conducted in order to learn the EPM's rheological properties to optimally utilize its strength, reaction to stress, and resistance to frequency in soil treatments. Most significantly, using amplitude sweeps it was determined that as the concentration increases, the amount of pressure needed both to distort the EPM (i.e. the storage modulus) and the amount of pressure needed to break the EPM also substantially increases (Figure 1). A Langmuir-Blodgett (LB) film was then prepared in order to view the polymer under an Atomic Force Microscope (AFM) to provide insight into the topography and internal structure of the polymers. The results from the LB/AFM analysis are still pending.

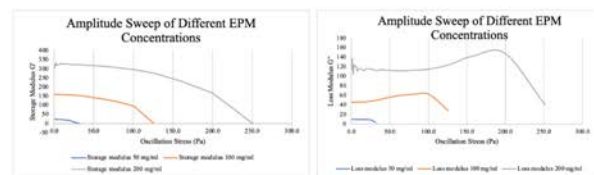


Figure 1. Rheology Amplitude Sweep Results. After doing an amplitude sweep with the rheometer for different concentrations of the EPM, the breaking point of the polymer for each concentration was determined and graphed above. The trend showed that as the concentration got higher, the breaking point got higher in terms of the amount of stress required to break the EPM. In addition, the storage and loss moduli went up with the concentration. This shows that the polymer becomes stronger and harder to break and/or distort as the concentration is elevated.

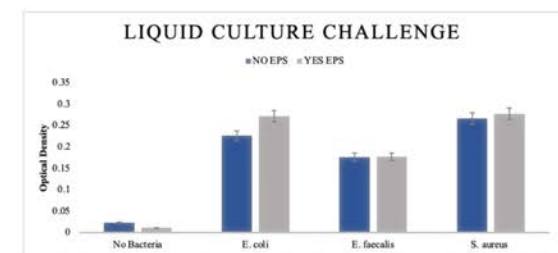


Figure 2. Liquid Culture Challenge Results. The liquid culture challenge (with BHI media) was tested with three different species of bacteria (*E. coli*, *E. faecalis*, and *S. aureus*). The difference between the presence and absence of the polymer is not statistically significant (P(T<=t) two-tail: 42%) indicating the biopolymer most likely has no antibacterial properties.

are still pending. The ultimate goal of the study is to determine why the biopolymers have the effect they do on the surrounding environment and to get a deeper understanding of the chemical properties involved in the mechanisms of the biopolymers.

The EPM's antimicrobial properties were tested using *E. coli*, *S. aureus*, and *E. faecalis* with agar diffusion assay and liquid culture challenge (with BHI media) and found to not inhibit bacterial growth (Figure 2). Toxicity was tested as a function of exposure time with three different cell types (HUVEC, MDCK2, and gingival keratinocytes) incubation with EPM (10mg/ml and 1mg/ml) for 1 hour were found to be non-toxic. Using human dermal fibroblasts, EPM (0mg/ml, 0.5mg/ml, 0.05mg/ml) with an incubation period of three days were found to be non-toxic. The results of the antiviral testing

Larson, S., Lord, E., Corcoran, M., Nijak Jr., G., & Nestler, C. (n.d.). *ERDC knowledge core: Home - HPC*. ERDC Library. Retrieved August 10, 2022, from <https://erdc-library.erdcdren.mil/jspui/>

Maróti, G., & Kondorosi, É. (1AD, January 1). *Nitrogen-fixing rhizobium-legume symbiosis: Are polyploidy and host peptide-governed symbiont differentiation general principles of endosymbiosis?* *Frontiers*. Retrieved August 10, 2022, from <https://www.frontiersin.org/articles/10.3389/fmicb.2014.00326/full>

Wang, Q., Liu, J., & Zhu, H. (1AD, January 1). *Genetic and molecular mechanisms underlying symbiotic specificity in legume-rhizobium interactions*. *Frontiers*. Retrieved August 9, 2022, from <https://www.frontiersin.org/articles/10.3389/fpls.2018.00313/full>

Deposition of DNA onto Polymethacrylate (PMMA) Thin Film Gratings in Preparation for the Tagmentation of DNA with Tn5 Transposase

Rachel Na¹, Deryn O'Leary², Hannah Saks³, Jonathan Sokolov⁴

¹*Friends Academy, Locust Valley, NY 11560*, ²*Our Lady of Mercy Academy, Syosset, NY 11791*, ³*Walt Whitman High School, Huntington, NY 11743*, ⁴*Stony Brook University, Stony Brook, NY 11794*

In recent years, next-generation sequencing (NGS) has had significant applications in high-throughput sequencing. However, all current technologies, such as Illumina and even Pacific Bioscience's RS, are only able to generate less than a few tens of kilobases and have difficulty labeling and reassembling repeatomes [1]. Considering that the human genome has 3.2 billion base pairs with intricate and repetitive structural variations, much of the genome that has a role in gene expression and diseases is at risk of being lost using current sequencing methods [2,3]. The NGS library preparation process can result in the loss of information regarding spatial organization, making reassembly difficult [1]. Previous studies have explored ways to simplify long-range sequencing (LGS) and preserve spatial orientation by combing DNA on polymethacrylate (PMMA) coated silicon wafers as preparation for sequencing [1].

This study examines the application of depositing DNA onto flat polydimethylsiloxane (PDMS) samples which can then be stamped onto a PMMA-coated and grated silicon wafer to suspend the DNA (bridging) and provide steric clearance for the transposase to simultaneously cut and label the DNA strands. This method allows NGS to be analyzed with minimal risk of losing important genome information.

Two methods of depositing DNA were tested. The first method that was explored was stamping DNA onto Si wafers. Samples of PDMS were dipped into solutions with different concentrations of λ DNA (NEB) in either DNase or TE buffer with varying concentrations of NaCl to promote DNA adhesion to PDMS. Glycerol was added to some solutions at a 1% (v/v) concentration to encourage the DNA to transfer from the PDMS to the Si grating. The samples were then imaged with a LEICA fluorescence microscope at 10x and 63x magnification. If the DNA appeared to be stretched out and favorable for stamping, the sample was stamped onto a PMMA-coated Si wafer for various lengths of time using various weights. The width and type of grating (linear or offset) were also experimented with. The second method tested was spin casting DNA onto the Si grating. Static spinning and dynamic spinning were both analyzed. Some solutions were made with 10 mM of MgCl₂ to increase adsorption of DNA onto the PMMA. For static spinning, a droplet of DNA solution was placed at the center of the Si wafer and was incubated for various lengths of time. The wafer was then spun at either 2500 rpm or 5000 rpm. For dynamic spinning, a pipette was used to deposit the DNA solution at the edge of the wafer while it was spinning.

Results indicated that PDMS that was cured in a 60°C oven for 2 days increased the adhesion of DNA on the PDMS. However, this made it difficult for the DNA to be stamped and transferred onto the Si wafer. PDMS that was heated for less time (4 hours versus 48 hours) resulted in less crosslinking of polymers on the surface, causing coiling of the DNA. The NaCl also made it difficult to transfer the DNA, causing the DNA to rip and not bridge. To solve this problem, glycerol was added instead of salt to aid transfer. Additionally, it was found that finer gratings were preferable because the DNA did not have to stretch as far to bridge. A solution with a concentration of 2.5 ng λ DNA per μ L of DNase buffer with 1% (v/v) added glycerol deposited on PDMS and stamped across an 8.6 μ m linear grating for 15 seconds and no weight yielded the best results.

For static spin casting, different solution incubation times and spin speeds did not significantly change results. For dynamic drops, a rotation rate of 5000 rpm showed some bridging but also caused breakage of the DNA strands as the speed was too fast. Overall, spin casting yielded some adequate results, but they were difficult to replicate. More research is required to find the preferable conditions for spin casting.

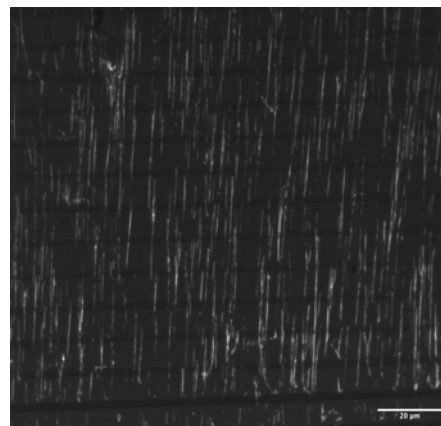


Figure 1. Fluorescence microscope image of 2.5 ng λ DNA per μ L of DNase buffer with 1% (v/v) added glycerol stamped onto PMMA-coated Si (8.6 μ m grating)

[1] Cho, NaHyun & Goodwin, Sara & Budassi, Julia & Zhu, Ke & McCombie, W. & Sokolov, Jonathan. (2017). Fragmentation of Surface Adsorbed and Aligned DNA Molecules using Soft Lithography for Next-Generation Sequencing. *Journal of Biosensors & Bioelectronics*. 08. 10.4172/2155-6210.1000247.

[2] Budassi, Julia & Cho, NaHyun & Del Valle, Anthony & Sokolov, Jonathan. (2021). Microfluidic delivery of cutting enzymes for fragmentation of surface-adsorbed DNA molecules. *10.1101/2021.03.31.437857*.

[3] Amarasinghe, S.L., Su, S., Dong, X. et al. Opportunities and challenges in long-read sequencing data analysis. *Genome Biol* 21, 30 (2020). <https://doi.org/10.1186/s13059-020-1935-5>

Properties and applications of Biopolymer (EPS) and Nanocellulose Fibrils with Clay in solution

¹Rick Qian, ²Yi Yang, ³Yiwei Fang, ³Miriam Rafailovich

¹Wayzata High School, ²Amador Valley High School, ³Stony Brook University

Water is characterized by high boiling, melting, and critical temperatures, large specific heat, and high surface tension, and it is of great interest to study these properties in solutions of biological compounds. EPS Biopolymer and nanocellulose fibrils have been considered as a material to be added in soil to aid in water retention and soil compaction [1] [2]. With the onset of climate change, water retention and soil compaction have become more important due to the growing problem of soil erosion to protect the environment; biopolymers and nanocellulose may be the answer.

In this study, we began by preparing solutions of biopolymer, nanocellulose, and water with clay. We created EPS biopolymer solutions at four different concentrations, 200 mg/mL, 100 mg/mL, 50 mg/mL, and 10 mg/mL, and Nanocellulose concentrations at 10 mg/mL. For each concentration of biopolymer and nanocellulose, and pure water, four samples were made, containing no clay, 5% clay by mass, 10% clay by mass, and 20% clay by mass. We ran Differential Scanning Calorimetry (DSC) on these solutions to test the freezing point depression and enthalpy of freezing. Next, we created a 100 mg/L nanocellulose solution to compare with a pre-prepared solution of 100 mg/L biopolymer on the goniometer, both

without clay. We dropped the two solutions and pure water (shown in figure 1) on uncleaned silicon wafers and ran the goniometer to measure how the contact angle changed over time through photos taken at 60 second intervals. Finally, we measured the water retention ability of biopolymer, nanocellulose, and water on the triple-cleaned silicon wafers using a microscale and timer, finding how long it took for each solution to evaporate.

Significant differences have been found between different concentrations of biopolymer, nanocellulose, and the control for water retention, melting point depression, evaporation rates, and the way with which evaporation occurs on a drop. Figure 2 shows the percentages of non-freezable water in different solutions, indicating that the higher the concentration of biopolymer, the more non-freezable water is present in the solution, while nanocellulose does have a higher non-freezable water percentage than water at the same concentration. Figure 3 indicates the results of the microscale evaporation rate test, showing

that biopolymer has a much lower evaporation rate compared to the water control and the nanocellulose, while nanocellulose performed around as well as the water control. This result highlights how adding biopolymer to water results in better water retention. Figure 4 shows relative amounts of evaporation height-wise and width-wise to determine how biopolymer, nanocellulose, and the water control evaporates. The graph indicates that the biopolymer evaporates height-wise, creating a coffee-ring type shape as it evaporates.

The water control and the nanocellulose evaporate the same way -- through shrinking that keeps the water droplet intact. Figure 5 demonstrates that the amount of freezing point depression from biopolymer also increases with increasing concentration, and nanocellulose has a lower freezing point compared to biopolymer at equal concentrations.

Overall, EPS biopolymer acts as a better source for water retention compared to nanocellulose. Furthermore, the higher the concentration of EPS biopolymer, the larger the percent of non-freezable water. The next steps for further study include using different pH to determine water retention and percent freezable water to better model soil.

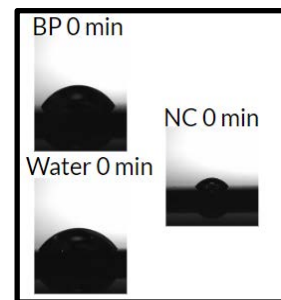


Figure 1. Droplet shape of solutions at initial contact angle measurement

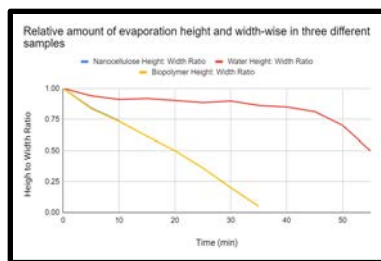


Figure 3

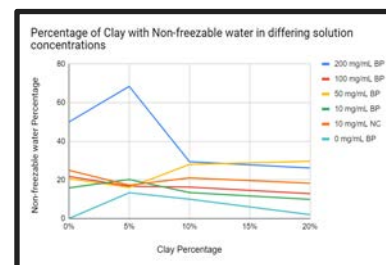


Figure 2

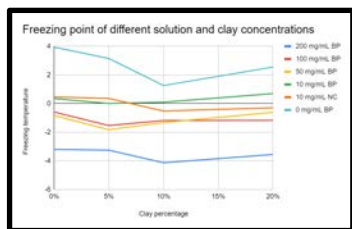


Figure 5

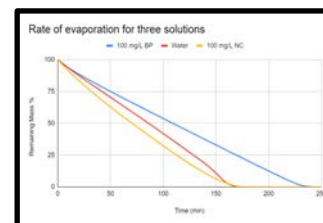


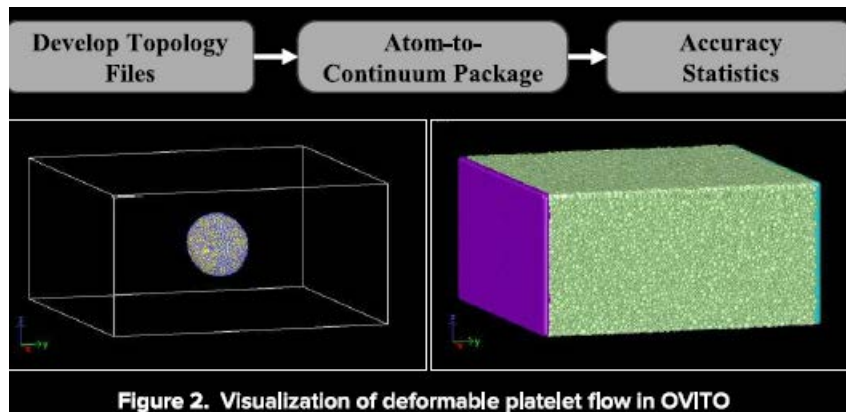
Figure 4

[1] Ruth M. Barajas, Vanessa Wong, Karen Little, Antonio Patti, Gil Garnier. Carboxylated Nanocellulose Superabsorbent: Biodegradation and Soil Water Retention Properties. 2021. <https://doi.org/10.21203/rs.3.rs-474606/v1>

[2] Tereza Cristina Luque Castellane, Manoel Victor Franco Lemos, Eliana Gertrudes de Macedo Lemos. Evaluation of the biotechnological potential of Rhizobium tropici strains for exopolysaccharide production. *Carbohydrate Polymers*, Vol. 111, 191-197, 2014. <https://doi.org/10.1016/j.carbpol.2014.04.066>

Session 2: In Silico and In Vitro Biology

Chairs: Ziyuan Niu, Ziji Zhang, Yicong Zhu, Bernard Essuman



| ML Model | RMSE | Simulation RMSE |
|-------------|----------------------|----------------------|
| kNN - RMSD | 0.050nm | 0.049nm |
| RF - RMSD | 0.069nm | 0.049nm |
| NN - RMSD | 0.045nm | 0.049nm |
| NN - Hbonds | 7.09 | 7.86 |
| NN - SASA | 12.69nm ² | 13.79nm ² |

Molecular Dynamics (MD) Simulations of Soil-Strengthening Nanocomposite Hydrogels

Jerry Zhang¹, Vincent Wang², Anthony Zhu³, Arkajyoti Sinha⁴, Shoumik Saha⁵, Dilip Gersappe⁵, Miriam Rafailovich⁵
¹Minnetonka High School, Minnetonka, MN 55345, ²Irvington High School, Fremont, CA 94539, ³Barrington High School, Barrington, IL 60010, ⁴Lexington High School, Lexington, MA 02421, ⁵Department of Materials Science and Chemical Engineering, Stony Brook University, Stony Brook, NY 11794

Recent experiments suggest that adding clay-based nanofiller to biopolymer solutions form soil-strengthening hydrogels that can potentially replace the energy-intensive and unsustainable concrete.¹ Past molecular dynamics (MD) simulations also demonstrate that polyelectrolytes undergo adsorption to oppositely-charged fillers.² Thus, we seek to investigate the effect of charge on molecular features such as network formation, cluster geometry, and polymer adsorption onto filler particles as well as its effect on mechanical system properties including viscosity and elastic moduli, ultimately allowing us to determine whether or not gelation occurs.

We use the LAMMPS³ software to model the gelation of polymer-filler solutions. We initialize systems with solvent particles, 30-bead polymer chains with counterions, and 19-bead filler particles with counterions. Polymers were connected using bonds defined by the finitely extensible nonlinear elastic (FENE) potential. We simulate soft-sphere potential in an nVT ensemble. Then, we simulate simple 12-6 Leonard-Jones potential in an nPT ensemble to reach equilibrium. The system is given charges and equilibrated a second time under an nPT ensemble using electrostatic potentials. For our tests, we vary the charge magnitude of each biopolymer bead uniformly. After each system has been equilibrated with electrostatic interactions, we perform a number of tests under nVT conditions. First, we use the Green-Kubo relation to calculate viscosity by integrating the stress autocorrelation function (SAF) with respect to time. Next, we use the step-strain test (SST) to determine the mechanical stability of each system. We elongate the system by a strain of 20% and observe the stress during a relaxation period of 500τ . Then, we compute the radial distribution function (RDF) of the polymers with respect to the fillers in order to measure adsorption. Finally, we test cluster formation by applying a network clustering algorithm (NCA). If clustering occurs, we quantify cluster geometry and network formation by calculating the gyration tensor, allowing us to determine asphericity, acylindricity, and relative shape anisotropy.

For charge magnitudes of $q=1$ and $q=2$, the SAF decayed to a value of zero as shown in Figure 1, suggesting that gelation did not occur. Similarly, as seen in Figure 2, the SST decayed to a value of zero for both $q=1$ and $q=2$, confirming that gelation did not occur. Compared to the RDF of the properly-gelated reference system, the charge systems showed weak peaks of the polymer-filler RDF around the cluster cut-off length of 1.2σ as shown in Figure 3. Therefore, our data supports the conclusion that polymer-filler adsorption does not occur at those particular charge magnitudes.

Though these results seem to signify that charged systems do not induce gelation, we do observe increasing viscosity with charge magnitude, suggesting that larger charge magnitudes could induce gelation. For our future work, we plan to study these larger charge systems as well as different charge distributions and polymer architectures. If these other charge systems do in fact induce gelation, experimental teams can then manufacture or culture biopolymers with the specific charge properties, relative to the fillers. In summary, we will continue to explore charged biopolymer-filler solutions from an MD approach to hopefully gain valuable insight that could enable exciting applications such as eco-friendly concrete alternatives or agricultural soil additives to combat soil erosion and increase water retention.

We thank Shoumik Saha and Dr. Dilip Gersappe for their mentorship in this project. We also thank Dr. Miriam Rafailovich and the Garcia Program for providing us the opportunity to conduct this research.

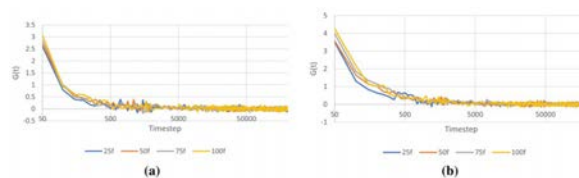


Figure 1: Stress autocorrelation function for (a) $q=1$ and (b) $q=2$.

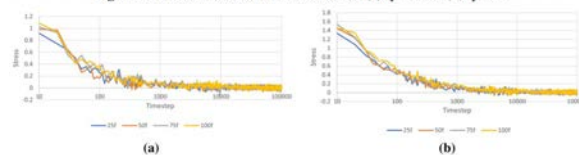


Figure 2: Step-strain test for (a) $q=1$ and (b) $q=2$.

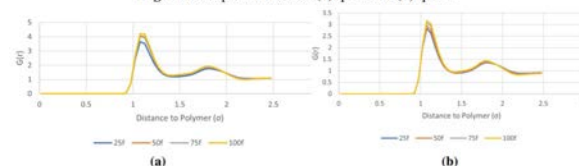


Figure 3: Radial distribution function of polymers with respect to filler for (a) $q=1$ and (b) $q=2$.

¹ Chang, I., et al. "Soil strengthening using thermo-gelation biopolymers." *Construction and Building Materials*, vol. 77, 2015, pp. 430-438, doi.org/10.1016/j.conbuildmat.2014.12.116

² Panchagnula, V. "Molecular Dynamics Simulations of Polyelectrolyte Multilayering on a Charged Particle." *Langmuir*, vol. 21, no. 3, pp. 1118-1125, doi.org/10.1021/la047741o

³ Plimpton, S. "Fast Parallel Algorithms for Short-Range Molecular Dynamics." *Journal of Computational Physics*, vol. 118, no. 1, 1995, pp. 1-19, doi.org/10.1006/jcph.1995.1039

A Machine Learning Approach to Molecular Dynamics Predictions of SARS-CoV-2 Spike Protein Denaturation at Varying Temperatures and pH Levels

Ayush Arora¹, Anya Vaish², Evan Xie³, Ziyuan Niu⁴, Yuefan Deng⁴, Peng Zhang⁴

¹Munster High School, Munster, IN 46321, ²Tesla STEM High School, Redmond, WA 98053, ³The Pingry School, Basking Ridge, NJ 07920, ⁴Department of Applied Mathematics & Statistics, Stony Brook University, Stony Brook, NY 11794

As of August 2022, COVID-19, caused by the SARS-CoV-2 virus, has resulted in approximately 587 million cases and 6.4 million deaths.¹ Understanding the infectivity of the virus under various environmental conditions is essential to developing more effective methods of combatting it. The viral infection is initiated when the SARS-CoV-2 spike protein (S-protein) binds to the human angiotensin-converting enzyme 2 (ACE-2) receptor.² This project examines the temperature and pH conditions under which the S-protein denatures, rendering the virus particle incapable of attacking human cells.

Traditionally, atom-to-atom molecular dynamics simulations, which individually model the millions of atoms within a protein and the interactions between them, have been used to accurately study proteins.³ However, the computational cost of running these simulations makes them impractical for studying the denaturing of the S-protein under a comprehensive range of temperature and pH values. Therefore, this project uses machine learning to create a series of predictive models that can learn denaturing points from limited simulation data of specific temperature (3°C, 20°C, and 37°C) and pH (1, 2, 3, 4, 5) values. This is achieved by predicting the root-mean-square deviation (RMSD), number of P-W (protein to water) H-bonds, number of MC-MC (main chain to main chain) H-bonds, and solvent accessible surface area (SASA) for a given temperature and pH. These metrics measure different structural changes in the S-protein, so they correlate with the denaturing of the S-protein.

Due to the sparsity of the training data, models were evaluated using k-fold cross validation to ensure accurate predictions on new input values. The equilibrium RMSD was identified by the horizontal asymptote of the exponential curve fitted to the RMSD graph. Numerous different models were developed and optimized with different machine learning algorithms and forms of input data. In the end, the full-curve feed-forward neural network was the best performing model because it achieved the lowest root mean square error (RMSE) of 0.0449nm and was able to model a continuous function. This was lower than the simulation's RMSE of 0.0487nm (a result of random factors influencing the output of each run), demonstrating the efficacy of this model.

The full-curve feed-forward neural network was applied to the MC-MC H-Bonds and SASA, with slight adjustments to the data preprocessing: output values were scaled between zero and one for training and the line of best fit with smallest slope was used to identify equilibrium values. After optimization on the learning rate, network structure, and number of epochs, the MC-MC H-Bonds model achieved an RMSE of 7.09, which was lower than the simulation's RMSE of 7.86, and the SASA model achieved an RMSE of 12.69nm², which was lower than the simulation's RMSE of 13.79nm².

The trends discovered by the models for these three metrics were visualized using heatmaps (Figure 1).

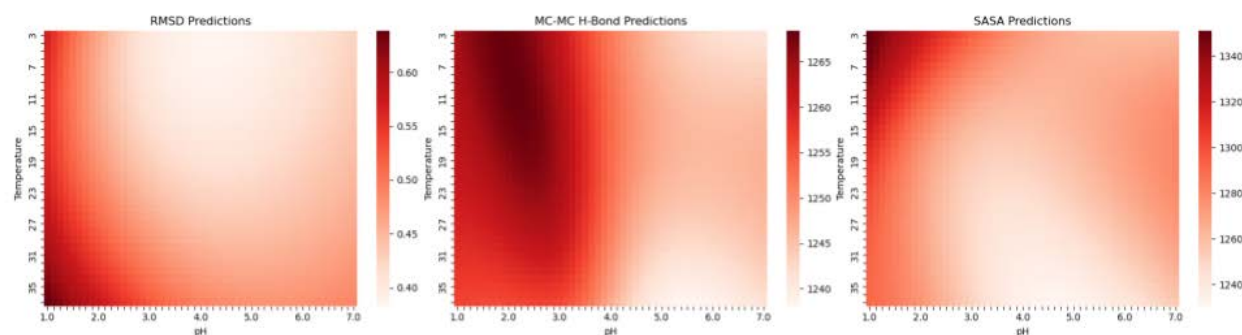


Fig. 1 Heatmap visualization of each model's predictions on temperatures ranging from 3°C to 37°C and from pH1 to pH7.

Moving forward, we will develop a model for the last metric, P-W H-Bonds, and a model that uses the predictions of the four metric models to classify whether or not the S-protein denatures.

¹ John Hopkins University. (2022, August 10). *Covid-19 Dashboard*. Johns Hopkins Coronavirus Resource Center. Retrieved August 10, 2022, from <https://coronavirus.jhu.edu/map.html>

² He Y, Zhou Y, Liu S, Kou Z, Li W, Farzan M, Jiang S. Receptor-binding domain of SARS-CoV spike protein induces highly potent neutralizing antibodies: implication for developing subunit vaccine. *Biochem Biophys Res Commun*. 2004 Nov 12;324(2):773-81. doi: 10.1016/j.bbrc.2004.09.106. PMID: 15474494; PMCID: PMC7092904.

³ Khan, F. I., Lobb, K. A., & Lai, D. (2022). The molecular basis of the effect of temperature on the structure and function of SARS-COV-2 spike protein. *Frontiers in Molecular Biosciences*, 9. <https://doi.org/10.3389/fmolb.2022.794960>

Creating Coarse-Grained Models of Solvated Fibrinogen to Expedite Molecular Dynamics Simulations

Eric Chen¹ Ziji Zhang² Peng Zhang^{2,3} Yuefan Deng² Miriam Rafailovich⁴

¹Wayzata High School, Plymouth, Minnesota 55446, ²Department of Applied Mathematics and Statistics, Stony Brook University, Stony Brook, NY 11794, ³Department of Biomedical Engineering, Stony Brook University, Stony Brook, NY 11794, ⁴Department of Materials Science and Chemical Engineering, Stony Brook University, Stony Brook, NY 11794.

Accurate molecular dynamics (MD) simulations often require computers to simulate thousands or millions of individual atoms. These *all-atomic* simulations are computationally intensive, inefficient, and often fail to reach simulation times exceeding milliseconds [2]. Coarse graining alleviates these limitations by reducing an all-atomic model to a skeleton with fewer particles while preserving accuracy by ensuring that the interparticle forces closely resemble those of the all-atomic model [2]. As such, coarse graining is valuable in modern biology as a way of efficiently and accurately simulating proteins at long timescales.

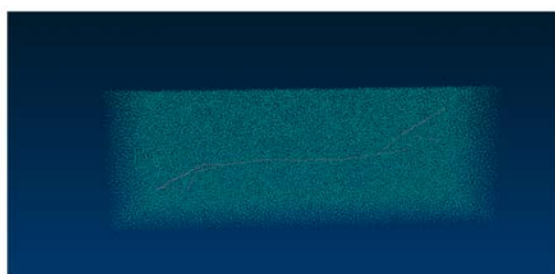


Figure 1: A coarse-grained model of fibrinogen solvated in MARTINI coarse-grained model of water. 91,203 particles total.

Fibrinogen has special significance in modern biology due to its role in creating fibrin, a protein central to thrombosis and vascular injury recovery [1]. Therefore, expediting MD simulations of fibrinogen with coarse graining is vital. A coarse-grained model of fibrinogen in a vacuum was created by [3] in 2021. However, because fibrinogen is naturally solvated, a solvated coarse-grained model of fibrinogen is desired. In this paper, we create such a model by combining the existing coarse-grained model of fibrinogen in a vacuum with the MARTINI coarse-grained model for water. We then compare our new coarse-grained model of solvated

fibrinogen with the baseline all-atomic model of solvated fibrinogen to examine accuracy. If successful, our new coarse-grained model will boost pharmaceutical research in important areas including thrombosis prevention.

To this end, we created the coarse-grained model for fibrinogen in a water box (**Figure 1**) and rendered an all-atomic model of fibrinogen in a water box (**Figure 2**) using Visual Molecular Dynamics (VMD). We intend to conduct energy-minimization simulations on these two models using NAMD. As a preliminary test, we ran these simulations for 1000 time steps. The results of this preliminary test demonstrate the stability of our models, ensuring their feasibility over a larger time interval. Our next step is to run the simulations on a supercomputer for a significantly longer interval, which will conclude in approximately 7 days. At that time, we will take measurements like the root-mean-square-deviation (RMSD) and root-mean-square-fluctuation (RMSF) and create graphical representations like Ramachandran Plots from the simulation results. We can then determine the efficacy of our coarse-grained model by comparing the measurements and examining the similarity between our coarse-grained model and our all-atomic model.

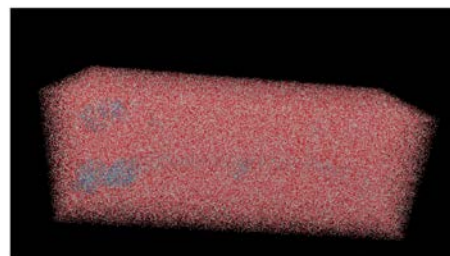


Figure 2: An all-atomic model of solvated fibrinogen. 1,532,046 particles total.

[1] Herrick, S., Blanc-Brude, O., Gray, A., and Laurent, G. (1999). Fibrinogen. *The international journal of biochemistry & cell biology*, 31(7):741–746

[2] Husic, B. E., Charron, N. E., Lemm, D., Wang, J., Pérez, A., Majewski, M., Krämer, A., Chen, Y., Olsson, S., de Fabritiis, G., et al. (2020). Coarse graining molecular dynamics with graph neural networks. *The Journal of chemical physics*, 153(19):194101

[3] Zhang, Z., Zhang, P., Rafailovich, M., Simon, M., and Deng, Y. (2021). Ai-guided multiscale biomechanical model of fibrinogen: correlating with in vitro results. *International Fibrinogen Research Society Workshop*

Accelerating Multiscale Blood Flow Modeling with Computational Fluid Dynamics

Amit Saha¹, Yicong Zhu², Peng Zhang², Yuefan Deng²

¹Great Neck South High School, Great Neck, NY 11020, ²Department of Applied Mathematics and Statistics, Stony Brook University, Stony Brook, NY 11794

Cardiovascular disease (CVD) is responsible for upwards of 17.9 million deaths per year. CVD-related death commonly occurs on account of platelet-mediated thrombosis, where platelets aggregate within blood vessels. Under this context, modeling blood flow is of principal importance to both elucidate the mechanisms behind thrombi formation and to design more effective therapeutics for treating CVD.

Blood flow modeling is a natural setting for multiscale modeling (MSM), which involves the use of conservation laws derived from physics at multiple different length and time scales. Previous literature indicates that the use of coupled coarse-grained molecular dynamics and dissipative particle dynamics is highly accurate for MSM simulations of blood flow and platelet-mediated thrombosis. However, evaluation of both molecular dynamics (MD) and dissipative particle dynamics (DPD) are computationally difficult, making blood flow modeling for therapeutic applications prohibitively difficult.

In order to make such simulations more feasible, this project examines the usability of neural network accelerated computational fluid dynamics (CFD), which uses the continuum approximation of fluids, as a *much* faster alternative to dissipative particle dynamics. Furthermore, we aim to implement CFD utilizing an AI-based algorithm to adaptively timestep the simulation in order to increase computational efficiency, as CFD resolves at much longer timescales than does DPD or MD.

We first generated a set of topology files representing deformable platelets undergoing pressure-driven flow. Then, we utilized LAMMPS to simulate the dynamics and flow of these deformable platelets with periodic boundary conditions. Preliminary results indicate **9x** speedup for coupled CFD-MD simulations relative to MD-DPD methods, even without neural network acceleration. This indicates a vast

decrease in computational cost, making blood flow simulation far more accessible for therapeutic design. Validation testing for neural network methods show a speedup of 2.3 orders of magnitude with comparable accuracy, indicating great potential for neural networks in accelerating MSM simulations.

The next steps for the project are to develop more neural network methods and implement them in LAMMPS, as well as developing the aforementioned AI algorithm to exploit the higher time scales upon which CFD develops.

[1] Bell, J. B., Garcia, A. L., & Williams, S. A. (2007). Numerical methods for the stochastic Landau-Lifshitz Navier-Stokes equations. *Physical Review E*, 76(1), 016708.

[2] Han, C., Zhang, P., Zhu, Y., Cong, G., Kozloski, J. R., Yang, C. C., ... & Deng, Y. (2022). Scalable multiscale modeling of platelets with 100 million particles. *The Journal of Supercomputing*, 1-18.

[3] Zhu, Y., Zhang, P., Han, C., Cong, G., & Deng, Y. (2021, June). Enabling ai-accelerated multiscale modeling of thrombogenesis at millisecond and molecular resolutions on supercomputers. In *International Conference on High Performance Computing* (pp. 237-254). Springer, Cham.

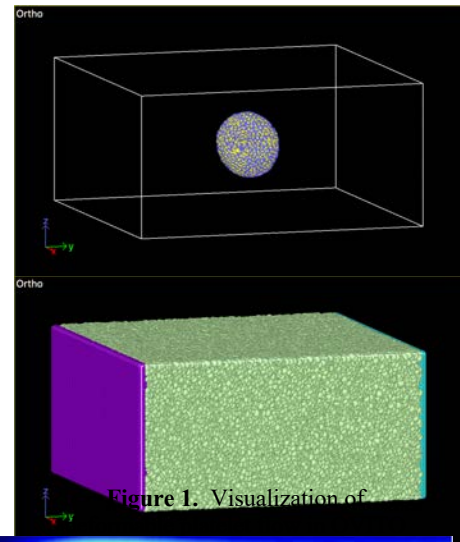
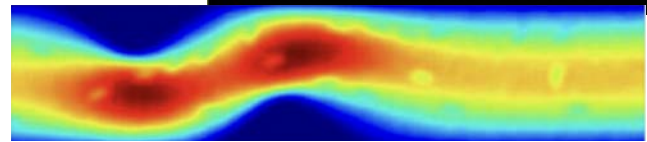


Figure 1. Visualization of



| Method | Velocity Error | Inference Time | Epoch Time |
|--------------|----------------|----------------|------------|
| PINO | 1.6% | 0.011s | 52.43s |
| Spectral CFD | n/a | 2.2s | n/a |

Figure 2. Neural network accuracy statistics and DPD flow data

Generalized Lennard-Jones Equation for Ellipsoids using Physics-Informed Neural Network

Yuhe Wei¹, Ziji Zhang², Yicong Zhu², Peng Zhang², Yuefan Deng²

¹Rutgers Preparatory School, NJ 08873

²Department of Applied Mathematics and Statistics, Stony Brook University, Stony Brook, NY 11794

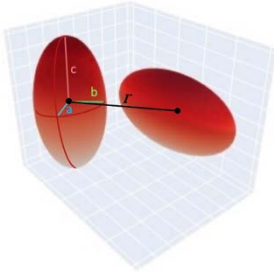


Fig. 1 Experiment Setup Illustration

Platelet dynamics plays an essential role in understanding the mechanisms of blood clotting that can be simulated *in silico* with molecular dynamics (MD). However, the extreme computational workload demand of MD simulations often hinders the study of long-time bioprocess. Our work aims to simplify the computation of Lennard-Jones (LJ)¹ potentials, which is the intermolecular force fields between interacting platelets, by proposing a generalized equation for theoretically similar ellipsoid models. This work introduces an analytic approach of data analysis with the multivariate adaptive regression spline (MARS)² model and physics-informed neural network (PINN) to discover the governing prediction model derived from a nonlinear system of input parameters. By using a massive training set with more than 200K samples and 10 independent variables, our

models describe the predicted equation that governs the integrated potentials between interacting ellipsoids while significantly reducing the computation time.

In our dataset generated from numerical experiments, we collected 10 input independent variables mapped with 1 output target variable of LJ potential. We let B_1 and B_2 be the two interacting platelets, a, b, c be the length of semi-axis, r be the distance between B_1 and B_2 , θ and ϕ be the relative rotation angle of B_1 and B_2 , respectively (Fig. 1). With the large set of input variables, we performed a quantile transformation³ to convert the LJ potential dependent variable to a Gaussian distribution (Fig. 2), thereby improving the precision of the predictive model. The transformed histogram and qq-plot visualization is shown in Fig. 3. Based on the transformed dataset, we used the Earth-function based MARS model to find the prediction curve of max degree of 3 (Fig. 4), with a RMSE of 0.5187.

We are implementing a PINN of the governing equation to learn about the target parameters ($\lambda_1, \lambda_2, \lambda_3$) that are described below:

$$LJP = \lambda_1 \lambda_2 [\lambda_3 \left(\frac{\sigma}{h_{12}}\right)^7 - \left(\frac{\sigma}{h_{12}}\right)],$$

where λ_1, λ_3 denote the force-field parameters and λ_2 represents the function for relative orientation and position of the ellipsoids. We will assess the PINN training with a customized loss function to penalize the difference between predicted LJ potential and the true LJ potential value for further analysis and find the generalized equation by investigating the physics-guided equation⁴ in the neural network framework.

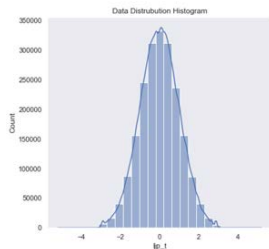


Fig.2 Data Distribution Histogram After Quantile Transformation

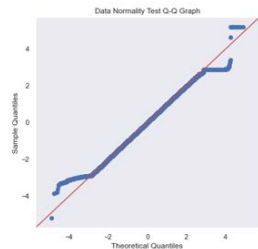


Fig3. Data Normality Test Q-Q Plot

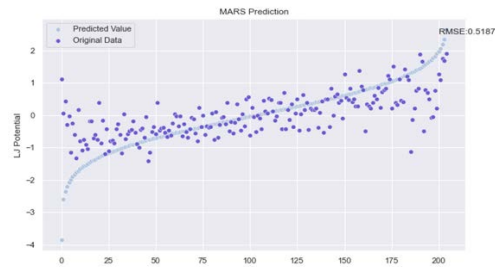


Fig4. MARS Prediction Graph

¹“Lennard-Jones Potential.” https://en.wikipedia.org/wiki/Lennard-Jones_potential

²Friedman, Jerome H. 1991. “Multivariate Adaptive Regression Splines.” *The Annals of Statistics*. JSTOR, 1–67.

³Gilchrist, W. (2000). *Statistical Modelling with Quantile Functions (1st ed.)*. Chapman and Hall/CRC. <https://doi.org/10.1201/9781420035919>

⁴Everaers, R., and M. R. Ejtehadi. “Interaction potentials for soft and hard ellipsoids.” *Physical Review E* 67, no. 4 (2003): 041710.

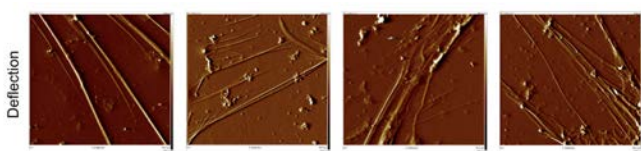
Investigating Virus-Induced Thrombogenicity at the Molecular Level

Justin Kim¹, Matthew Lu², Ekam Singh³, LeAnn Tai⁴, Joelle Gregoire Lincoln⁵, Kuan-Che Feng⁶, Adam Hansen⁷, Miriam Rafailovich⁶

¹Jefferson Forest High School, Forest, VA, 24551, ²Chapel Hill High School, NC, 27516, ³Washington High School, CA, 94536, ⁴Arnold O. Beckman High School, Irvine, CA, 92602, ⁵Brown University, Providence, RI, 02912, ⁶Department of Materials Science and Chemical Engineering, Stony Brook University, Stony Brook, NY 11794, ⁷Department of Biomedical Engineering, Stony Brook University, Stony Brook, NY 11794

Fibrinogen is a plasma-soluble glycoprotein that is responsible for thrombogenesis, the formation of blood clots. While thrombogenesis is an important process, excessive blood coagulation can cause serious health conditions such as strokes, heart attacks, and embolisms. The purpose of this project was to investigate the correlation between virus-induced lipid secretion and fibrinogen fiber formation. This project can provide insights into the mechanisms of thrombosis associated with the SARS-CoV-2 virus, as well as how to treat those afflicted.

To study the formation of fibrinogen fibers on surfaces, solutions of 20 mg/ml, 3 mg/ml polybutadiene solutions, 30 mg/ml polylactic acid, 15 mg/ml polystyrene were spun onto silicon wafers for their



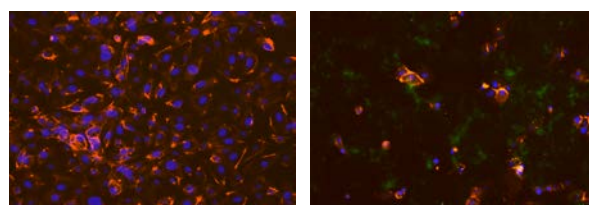
| PS | PB | PLA | PB |
|-----------|-----------|-----------|-----------|
| 15 | 20 | 30 | 3 |
| mg/ ml | mg/ ml | mg/ ml | mg/ ml |

thrombogenic and biocompatible nature. Fibrinogen was added to the films, imaged through AFM, and analyzed for morphological properties. Madin-Darby canine kidney (MDCK-2) cells and H1N1-infected human umbilical vein endothelial cells (HUVEC) were plated and infected with the H1N1 virus into each well.

Human gingival keratinocytes as models of epithelial cells were also infected with H1N1 through direct infection and conditional media taken from previous MDCK-2 cultures. After fixing and drying, cultures were stained for actin, lipids, and DNA, followed with EVOS microscopy analysis.

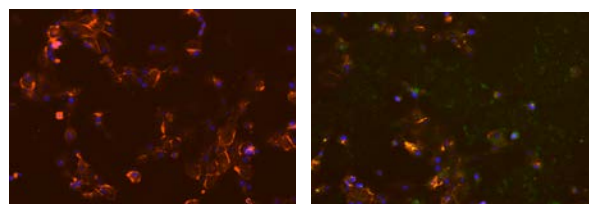
The deflection images of fibrinogen reveal that fibrinogen is able to form fibers on flat, hydrophobic surfaces. MDCK-2 cells infected with H1N1 secreted lipid droplets while neither HUVEC cultures (control, direct H1N1 infection) displayed lipid droplet formation. However, HUVEC treated with the conditional media obtained from H1N1 infected MDCK-2 cultures developed lipid showers, demonstrating that the hydrophobic secretions of an infected culture spreads to nearby tissue at the systemic scale. The same results were observed with human gingival models.

Knowing that viral infection causes canine epithelial-like tissue to become hydrophobic, the next steps are to test the formation of fibrinogen fibers on infected human cells. P12, a fibronectin-derived peptide, due to its abilities to prevent fibrinogen polymerization and thrombogenesis in virus-infected cell cultures. This project will reveal fibrinogen fibers that form after viral infection is due to the lipid showers in epithelial tissue that make the environment suitable for blood coagulation.



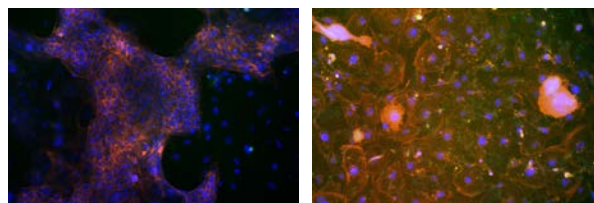
HUVEC
Control

MDCK-2 Direct
Infection



HUVEC Direct H1N1
Infection

HUVEC +
Conditional Media



KC Direct
Infection

KC + Conditional
Media

[1] Jin, Ng Zhang, and Subash C. B. Gopinath. "Potential Blood Clotting Factors and Anticoagulants." *Biomedicine & Pharmacotherapy*, vol. 84, 2016, pp. 356–65. *Crossref*, doi:10.1016/j.biopha.2016.09.057.[2] Ebony A Monson, Alice M Trenerry, Jay L Laws, Jason M Mackenzie, Karla J Helbig, Lipid droplets and lipid mediators in viral infection and immunity, *FEMS Microbiology Reviews*, Volume 45, Issue 4, July 2021, fuua066, <https://doi.org/10.1093/femsre/fuua066>

In Silico Modeling of the Ideal Binding Sites for Polylactic Acid Chains and Fibrinogen

Rommy Sasson¹, Michael He², Bernard Essuman³, Yuefan Deng⁴, Peng Zhang⁴

¹Brooklyn Technical High School, 29 Fort Greene Pl, Brooklyn, NY 11217, ²Scripps Ranch High School, 10410 Falcon Way, San Diego, CA 92131, ³Departments of Biochemistry and Applied Mathematics, Stony Brook University, Stony Brook, NY 11794, ⁴Department of Applied Mathematics, Stony Brook University, Stony Brook, NY 11794

The implantation of medical devices that interact with the circulatory system has been linked to the development of thrombosis, which can result in strokes or heart attacks. In order to develop non-thrombogenic materials, we must create models to simulate how fibrinogen binds to different materials. Simulating the P-12 peptide inhibited fibrinogen binding to different surfaces will provide insight on the risk factors posed by different implants [1]. This knowledge can be implemented in the recommended treatment options for patients as well as in the design of safer biomedical devices in the future.

Fibrinogen is a glycoprotein complex composed of 3 domains, of which the D domains have more hydrophobic regions than the E domain, meaning that the D domains are highly hydrophobic while the E Domain is more neutral. Polylactic acid is a hydrophobic surface, which means that the above regions adsorb onto it [2].

In order to develop such a model, this investigation identifies the most favorable binding locations for Polylactic Acid (PLA) polymers on the human fibrinogen molecule, specifically ID 3GHG. Taking the 3 separated domains of fibrinogen in Chimera (Left D Domain, E Domain, and Right D



Figure 1: Image of Fibrinogen with optimally bound polymer chains (red) superimposed on top

Domain), PLA chains of length 3 and 5 are docked using Autodock Vina in order to determine the respective binding sites with the lowest Root Means Square Deviation (RMSD). The resulting structures are then superimposed onto a model of the complete fibrinogen protein, as can be seen in Figure 1. This gave us a model of fibrinogen where PLA was bound to the most likely spots. Then, the RMSD of the binding sites is compared across the three domains.

In our comparison of the docking scores, we compared PLA chains of length 3 and 5 bound to the Right D Domain, the Left E Domain, and the E Domain. The results showed that the highest binding efficiency, with the most negative score (the more energy released during bonding, the higher the binding affinity and the more negative the score), was between the Right D Domain and the 5 length PLA chain at -6.1, followed by the Left D Domain and the 5 length PLA chain at -6. The E Domain and the 5 length PLA chain had a score of -5.7, and the 3 length PLA chain binding scores were a lower. These results demonstrate that the D domains have higher binding affinities with PLA, most likely as a result of higher hydrophobicity. They also show how increasing the length of the PLA chains directly correlate to higher binding affinities.

¹ Doilidov, A., El-Saieha, S., Fariaa, S., & Lo, P. (n.d.). (rep.). The Effect of P12 Peptide on Fibrinogen Fiber Formation and Endothelial Cell Attachment on Polystyrene (pp. 19–23). JUCER.

² J.Koo, D. Galanakis, Y. Liu, A. Ramek, A. Fields, X. Ba, M. Simon, and M. H. Rafailovich, *Biomacromolecules* 2012 13 (5), 1259-1268

Optimization of Learned-Jeffery Orbits Equation for Platelet Rotation in Online Machine Learning through Learned Parametrization of Fluid-Structure Interaction, Oblate Deviation, and Deforming Capability

Pratham Patel¹, Yicong Zhu², Peng Zhang², Yuefan Deng²

¹North Carolina School of Science and Mathematics, Durham, NC, 27705, ²Stony Brook University, Stony Brook, NY 1179

Molecular dynamics (MD) essentially describes how atoms and molecules interact together and is conducted through computation simulation. However, such modeling requires an immense amount of computing power in order to process all aspects of a biological model. Though many biological models have been simulated with the assistance of HPC, high performance computing, many models still require massive amounts of time to simulate. In fact, a full rotation of a platelet requires 54 hours of simulation [1]. Though there exist physics equations which govern over platelet motion, MD is required to discern their parameters.

To best optimize MD simulations, machine learning is utilized to learn the parameters of the century old Jeffery Orbits Equation (JOE). The equation is a model of the infinite platelet orbits and as they relate to the flow changes in biofluids. However, this century old equation does not account for shape varying objects, as well their changes within with flow [2]. To account for the idealistic nature of the Jeffery Orbits Equation, a new equation with added parameters was developed. The Learned Jeffery-Orbits Equation (L-JOE) (Figure 1) adds parameters including κ_0 , the fluid-object coupling constant, λ_0 for the coarse grained, and λ_1 for the fine-grained deviations from a perfect oblate. When such parameters are zero, however, the equation is the century old Jeffery Orbits equation.

The added parameters not only added an increased accuracy to the L-JOE, but are also dynamic in nature. Their reliance on the other various constants changed their own values and added to accuracy of the model as a whole. Previous to the creation of the L-JOE within a biomechanics-informed online learning (BIOL), large amounts of multiscale modeling (MSM) data was collected for ground truth data. Such MSM data is an optimal the training set for the BIOL.

The MSM data, however, still requires this data to be integrated within the Recurrent Neural Network. In future studies, the BIOL would still need to be continually optimized with dynamic parameters. The integration of such large ground truth data from the MSM simulation will certainly be monumental in increasing the accuracy within the model.

$$\dot{\phi}(\dot{\gamma}t) = \frac{1}{2}(\Lambda \cos 2\phi + 1 + \kappa_0)(1 + \lambda_0 + \lambda_1 \sin 2\phi)$$

Fig. 1 Learned Jeffery-Orbits Equation with added dynamic parameters [1]

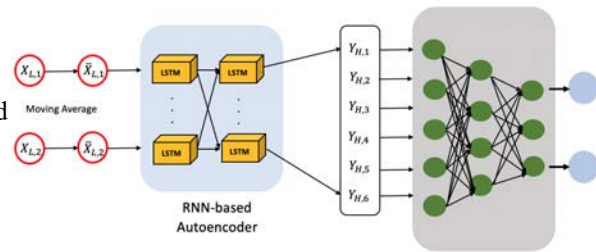


Fig. 2 Architecture of the BIOL model for platelet dynamic prediction [1]

[1] Zhang Z, Zhang P, Han C, Cong G, Yang C-C and Deng Y (2022) Online Machine Learning for Accelerating Molecular Dynamics Modeling of Cells. *Front. Mol. Biosci.* 8:812248. doi: 10.3389/fmolb.2021.812248

[2] Einarsson, J. & Candelier, Fabien & Lundell, Fredrik & Angilella, Jean-Régis & Mehlig, B.. (2015). Effect of weak fluid inertia upon Jeffery orbits. *Physical Review E.* 91. 10.1103/PhysRevE.91.041002.

CG-RNN: A Recurrent Neural Network for Coarse-Grained Force Field Prediction

¹Eshan Singhal, ²Ziji Zhang, ³Peng Zhang, ³Yuefan Deng

¹The Oakridge School, ²Stony Brook University, ³Stony Brook University, ⁴Stony Brook University

Simulating proteins in silico using Molecular Dynamics (MD) provides highly precise physics insights allowing experimentation without the need for laboratory procedure [1]. These simulations, however, require heavy computational workload with atomic level computations which is the major challenge for large proteins at long time scales. Thus, coarse graining (CG) algorithms have been studied which attempt to reduce the problem dimensions of the target allowing for longer simulations and more protein observations with a limited cost of accuracy [2]. Previous methods employ neural networks and graph neural networks with features calculated from the atomic simulation data to predict the energies and forces on each CG atom[3].

Thus, we propose a novel architecture by using Recurrent Neural Network (RNN) layers to improve accuracy of the algorithm. The intuition of using RNN is natural as this specializes in time step input data which applies directly to the coordinate-frame data whereas the current approach simply utilizes a dense network of linear layers [4]. Different variations of the typical RNN cell, GRU cell, and LSTM cell as well as combinations of the RNN component with a Dense layer component will be trained in an unsupervised approach and the CG simulation protein will be compared to the MD simulation using Kullback-Leibler (KL) Divergence and Mean Squared Error (MSE), obtained from the Ramachandran plots (**Figure 1**), and RMSD of the trajectories [5, 6].

Preliminary testing with 1,000 frame Alanine Dipeptide data demonstrates higher model accuracy for the RNN compared to the baseline model with an initial 17.9% reduction in KL Divergence. Further, complete testing of the developed model and baseline model is being accomplished with 100,000 frame Chignolin data on the IBM supercomputer with TICA energy plots (**Figure 2**) to derive final result metrics however similar accuracy results are expected.

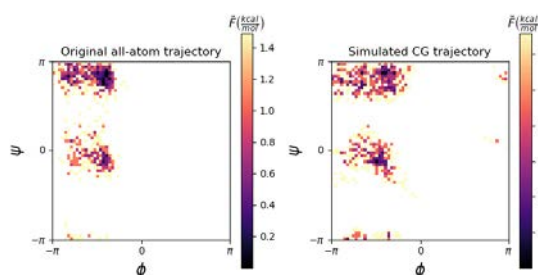


Figure 1 Alanine Dipeptide Ramachandran plot comparison for Baseline CG

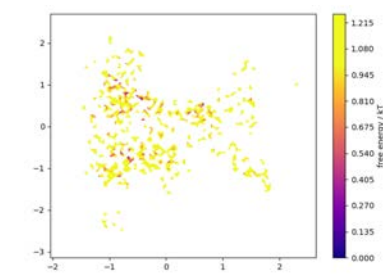


Figure 2 Chignolin sample TICA plot

[1] Computational Soft Matter: From Synthetic Polymers to Proteins, Lecture Notes, Norbert Attig, Kurt Binder, Helmut Grubmüller, Kurt Kremer (Eds.), John von Neumann Institute for Computing, Jülich, "NIC Series, Vol. 23, ISBN 3-00-012641-4, pp. 1-28, 2004.

[2] Kmiecik, S., Gront, D., Kolinski, M., Wieteska, L., Dawid, A. E., & Kolinski, A. (2016). Coarse-Grained Protein Models and Their Applications. *Chemical Reviews*, 116(14), 7898–7936. <https://doi.org/10.1021/acs.chemrev.6b00163>

[3] Husic, B. E., Charron, N. E., Lemm, D., Wang, J., Pérez, A., Majewski, M., Krämer, A., Chen, Y., Olsson, S., de Fabritiis, G., Noé, F., & Clementi, C. (2020). Coarse graining molecular dynamics with graph neural networks. *The Journal of Chemical Physics*, 153(19), 194101. <https://doi.org/10.1063/5.0026133>

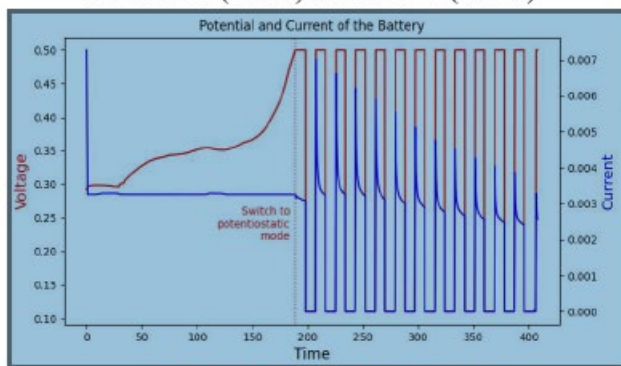
[4] Schuster, M., & Paliwal, K. (1997). Bidirectional recurrent neural networks. *IEEE Transactions on Signal Processing*, 45(11), 2673–2681. <https://doi.org/10.1109/78.650093>

[5] Levada, A. (2022). On the Kullback-Leibler Divergence between Pairwise Isotropic Gaussian-Markov Random Fields. *SSRN Electronic Journal*. <https://doi.org/10.2139/ssrn.4089590>

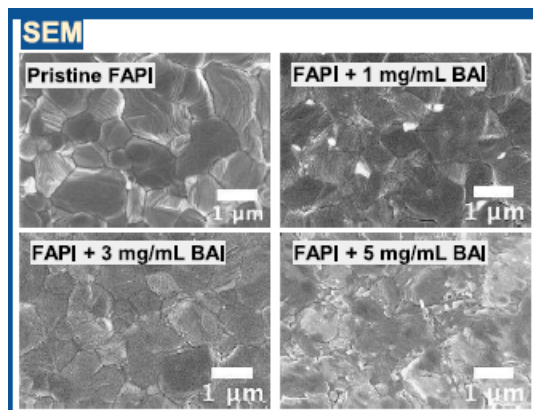
[6] Carugo, O., & Djinić-Carugo, K. (2012). A proteomic Ramachandran plot (PRplot). *Amino Acids*, 44(2), 781–790. <https://doi.org/10.1007/s00726-012-1402-z>

Session 3: Renewable Energy Generation

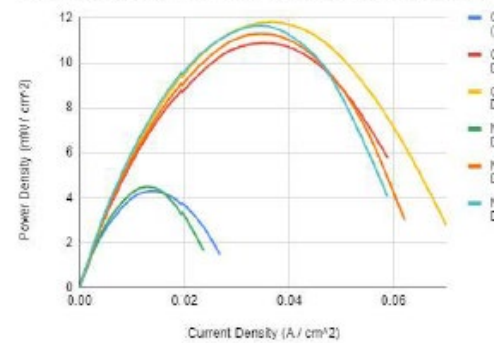
**Chairs: Aniket Raut, Haoyan Fang,
Yifan Yin, Zhuolin Xia,
Rebecca Isseroff**



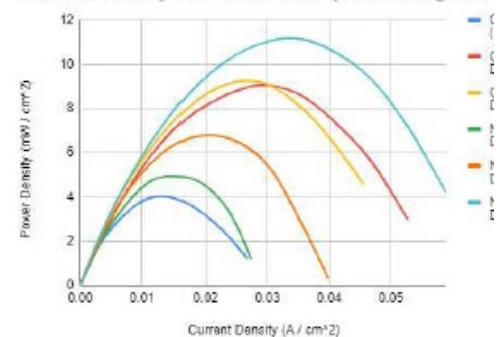
Charging the Li-Ion Battery



Current Density vs Power Density for 60 deg Cels



Current Density vs Power Density for 80 deg Cels



Using Acid-Treated Cellulose Fiber Membranes to Enhance the Performance of Proton Exchange Membrane Fuel Cells

Thomas Luong¹, Ben Pan², Sean Fang³, Konnie Duan⁴, Helee Shukla⁵, Quinton Geller⁶, Aniket Raut⁷, Haoyan Fang⁷, Farabi Rahman⁷, Rebecca Isseroff⁸, Miriam Rafailovich⁷

¹Plano West Senior High School, Plano, TX 75093, ²Stuyvesant High School, New York, NY 10282, ³Maggie L. Walker Governor's School, Richmond, VA 23220, ⁴Harvard-Westlake High School, Studio City, CA 91604, ⁵New Hyde Park Memorial High School, New Hyde Park, NY 11040, ⁶Los Alamos High School, Los Alamos, NM 87544, ⁷Department of Materials Science and Chemical Engineering, Stony Brook University, Stony Brook, NY 11794, ⁸Lawrence High School, Cedarhurst, NY 11516

Hydrogen fuel cells are an emerging form of green energy that can produce electricity with zero emissions from hydrogen and oxygen gas¹. Proton exchange membrane fuel cells (PEMFCs) are a popular type that uses a proton exchange membrane (PEM). However, one barrier to the widespread adoption of PEMFCs is the high cost of the Nafion membrane. Previous research has identified Resorcinol bis(diphenyl phosphate)(RDP) treated commercial cellulose filter paper as an alternative to Nafion membranes² due to the biodegradability, abundance, and low cost of the cellulose filter paper. This study aims to investigate the effectiveness of acid and RDP treatment on cellulose fiber membranes to increase the power output of PEMFCs.

Four samples of cellulose filter paper were tested: older Ahlstrom papers from 2019, similarly-dated Ahlstrom papers with a 24-centimeter diameter, Ahlstrom Munksjö papers from 2021, and Ahlstrom Munksjö papers from 2022. Early trials of the control groups with only RDP treatment show that the Ahlstrom papers from 2019 and Ahlstrom Munksjö papers from 2022 had the best power output, so the others were discarded from experimentation. The old Ahlstrom and new Ahlstrom Munksjö cellulose filter papers were treated with citric acid (C₆H₈O₇), phosphoric acid (H₃PO₄), or a combination of the two by submerging them in 200 mL of 1 M acid overnight. The cellulose filter papers were then washed using distilled water and coated with RDP with 6 drops onto one side and 3 drops on the other using a glass pipette. They were placed in an oven at 150°C for 20 minutes to allow the RDP to diffuse uniformly. Each sample was placed between two electrodes in the hydrogen fuel cell test station, and the PEMFC performance was recorded at various temperatures: 30°C, 60°C, 80°C, and 90°C.

Through scanning electron microscopy (SEM), the images produced demonstrated no significant morphological difference between the cellulose filter paper of the old Ahlstrom company and the new merger Ahlstrom Munksjö, suggesting similarity in chemical composition. Additionally, energy dispersive X-Ray spectroscopy (EDS) was utilized to produce an elemental composition spectrum for each sample; results indicated the presence of phosphorus from the RDP. As seen in Fig. 1, the control group of new cellulose paper treated with only RDP achieved a peak power density of 4.9 mW cm⁻² at 80°C. In comparison, the old cellulose paper treated with RDP and citric acid achieved a peak power density of 11.8 mW cm⁻², a 140% increase from the control group. For old cellulose paper treated with RDP and phosphoric acid, a peak power density of 10.9 mW cm⁻² was obtained at 60°C, a 120% increase from the control group. Additionally, new cellulose paper treated with a combination of 1M citric acid and phosphoric acid yielded a peak power density of 11.2 mW cm⁻² at 80°C, suggesting that combined acid treatment can increase stability of the membrane at higher temperatures.

Further research of RDP-treated cellulose filter paper as a viable alternative to Nafion for proton membrane exchange remains necessary. Continued investigation into different combinations of acid and molar concentration is underway to evaluate their potential effects on the PEMFC power output.

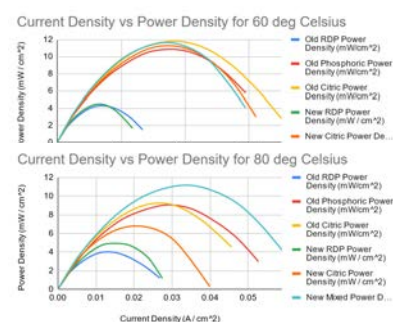


Fig. 1. Polarization curves for each membrane tested at 60°C and 80°C.

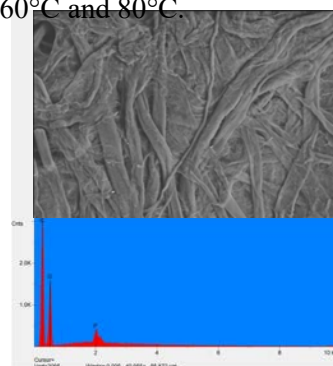


Fig. 2. EDS spectrum for 1 M phosphoric acid and RDP-treated new Ahlstrom Munksjö cellulose filter paper

¹ Tellez-Cruz, M.M.; Escorihuela, J.; Solorza-Feria, O.; Compañ, V. Proton Exchange Membrane Fuel Cells (PEMFCs): Advances and Challenges. *Polymers* 2021, 13, 3064. <https://doi.org/10.3390/polym13183064>

² Wang, Likun, et al. "Operation of Proton Exchange Membrane (PEM) Fuel Cells Using Natural Cellulose Fiber Membranes." *Sustainable Energy & Fuels*, The Royal Society of Chemistry, 30 July 2019, <https://doi.org/10.1039/C9SE00381A>

Investigating the Mechanism of Silver Nanoparticle Catalysts in Alkaline Anion Exchange Membrane Fuel Cells

Konnie Duan¹, Quinton Geller², Helee Shukla³, Thomas Luong⁴, Ben Pan⁵, Sean Fang⁶, Haoyan Fang⁷, Aniket Raut⁷, Farabi Rahman⁷, Miriam Rafailovich⁷
¹Harvard-Westlake High School, Studio City, CA 91604, ²Los Alamos High School, Los Alamos, NM 87544, ³New Hyde Park Memorial High School, New Hyde Park, NY 11040, ⁴Plano West Senior High School, Plano, TX 75093, ⁵Stuyvesant High School, New York, NY 10282, ⁶Maggie L. Walker Governor's School, Richmond, VA 23220, ⁷Department of Materials Science and Chemical Engineering, Stony Brook University, Stony Brook, NY 11794

To improve clean energy innovations, scientists have been researching alkaline anion exchange membrane fuel cells (AEMFCs), which can function in salt water and basic environments unlike other hydrogen fuel cells. However, AEMFCs, which require an expensive heavy-metal catalyst such as platinum (Pt) to achieve significant power output, have low durability. A previous study shows that the amount of Pt catalyst can be reduced if simultaneously used with a less costly catalyst, like silver (Ag) nanoparticles (NPs) capped with octanethiol or hexanethiol [1]. In our research, we treated AEMFCs with dodecanethiol (C₁₂)-protected AgNPs that were synthesized using the Brust-Schiffrin method. Several AEMFCs, one without AgC₁₂, one with a AgC₁₂ sprayed membrane, one with AgC₁₂ sprayed electrodes, and two each with a monolayer of AgC₁₂ NPs deposited on both sides of the membrane, were tested for maximum power density to better understand the mechanism. AgC₁₂ NP monolayers were also observed under a Transmission Electron Microscope (TEM) to better explain the results.

First, a Langmuir-Blodgett trough (LBT) produced an isothermal curve for the AgC₁₂ NPs and deposited a monolayer of AgNPs onto each of two membranes with an appropriate surface pressure (5 mN/m on one and 10 mN/m on the other). Then, a commercial airbrush was used to spray 1 μg/cm² of AgC₁₂ NPs on both sides of one membrane and 1 μg/cm² of AgC₁₂ NPs on two electrodes. About the same amount of AgNPs were applied via the LBT with the 10 mN/m surface pressure and each of the airbrush sprays. No matter if they were treated or untreated with AgNPs, all membranes tested were Sustainion® X37-50 Grade RT Membranes, and the all electrodes tested were Pt/C 20% Toray Paper electrodes with active areas of 5 cm² and electrode Pt loading of 0.76 mg/cm². As current was applied, the voltage increased and then decreased. The test was stopped when it declined to 0.1 V.

As seen in Figure 1, the control cell had a peak power density of 0.398 W/cm². The 5 mN/m and 10 mN/m surface pressure depositions had peak power densities of 0.380 W/cm² (4.52% decrease) and 0.451 W/cm² (13.3% increase) respectively. The AEMFC with AgC₁₂ NPs sprayed onto the membrane and the one sprayed onto the electrode reached maximums of 0.556 W/cm² (39.7% increase) and 0.469 W/cm² (17.8% increase) respectively. The membrane spray likely worked better than the electrode spray because of some synergy between the AgNPs and membrane. It remains unknown why there is less catalytic activity of deposited AgNPs, which are platelet-shaped after LBT application [2]. However, the AEMFC with the monolayer deposited at 10 mN/m had a slightly greater maximum power density than the one deposited at 5 mN/m, perhaps because it had more AgNPs to catalyze the reactions. As evidenced by the normal distribution curves in Figures 2 and 3, the compressed monolayer deposited at 10 mN/m was more uniform, which could also explain higher power output. In the future, durability tests will be conducted to investigate whether AgNPs enhance durability.

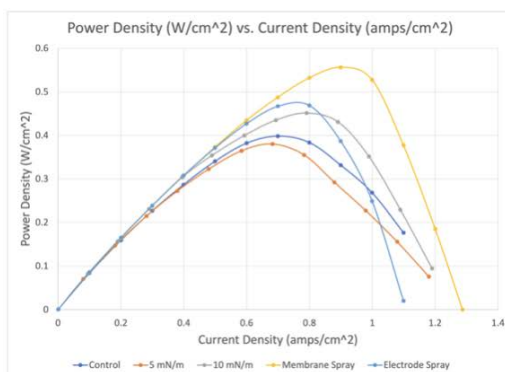


Figure 1: Power Density vs. Current Density for Different Application Methods of AgNPs

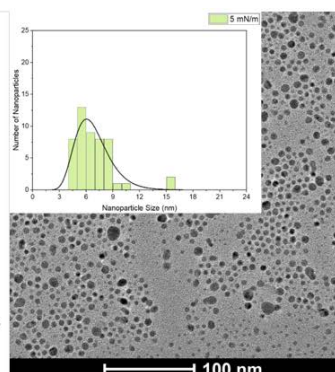


Figure 2: Number of NPs vs. NP Size (nm) for 5 mN/m S.P. Deposition

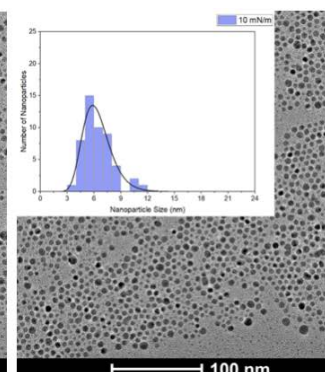


Figure 3: Number of NPs vs. NP Size (nm) for 10 mN/m S.P. Deposition

[1] Ahn, Andrew, et al. "Enhancing the performance of anion exchange membrane fuel cells (AEMFCs) using silver nanoparticles." *American Chemical Society*, 2021.

[2] Sun, Yuan, et al. "Characterization of palladium nanoparticles by using X-ray reflectivity, EXAFS, and electron microscopy." *Langmuir* 22.2 (2006): 807-816.

Surface Passivation Using 2D Perovskites toward Efficient and Stable Perovskite Solar Cells

Zixuan Lin¹, Muyao Li¹, Chengwei Shang², Yifan Yin³, Miriam Rafailovich³

¹Shenzhen Middle School, Shenzhen, China 518024, ²International Department, The Experimental High School Attached to Beijing Normal University, Beijing, China 100032, ³Department of Materials Science & Chemical Engineering, Stony Brook University, Stony Brook, NY 11794,

With our growing awareness of global warming, solar cells are being rapidly adopted into practical use as a renewable energy source. Perovskites is a class of organometallic materials known for their relatively low material cost and high power conversion efficiency (PCE) when serving as the active layer of solar cells. Perovskites have a hybrid organic-inorganic chemical formula of ABX_3 , in which A indicates a monovalent organic cation such as formamide (FA^+) and methylamine (MA^+) or cesium, B indicates a metal cation such as lead and tin, while X is a halide anion, and a cuboctahedral crystal structure with A occupying the center and octahedral $[BX_6]^{4+}$ clusters around it.² 3D perovskites such as formamidinium lead iodide (FAPbI₃) are most widely used due to their relatively high PCE, but they also exhibit low stability due to their inherent hydrophilicity; 2D perovskites such as n-Butylammonium lead iodide (BAPbI₃), on the other hand, exhibits superior moisture stability, but also has lower PCE owing to larger band gaps and poor charge transportation. Therefore, 2D/3D heterostructures fabricated by applying 2D perovskites as a passivation layer on top of a 3D active layer may possess the stability and efficiency of both materials.

The Perovskite Solar cells, as displayed in Figure 1-a, were prepared by first depositing c-TiO₂ and then m-TiO₂ on FTO glass through spin casting, with annealing applied after the deposition of each layer to form the electron transport layer (ETL). Then, 1.4M FAPbI₃ and 35 mol% MAcl in DMF/DMSO mixed solvent (v:v=4:1) was spun cast at 5000 rpm for 30s, and CB was dropped as anti-solvent at 15 s prior to the ending of the program, followed by annealing at 150 °C for 10 min. Next, different concentrations of BAI dissolved in IPA were coated at the top of 3D PVK by spinning at 3000 rpm for 30s, followed by annealing at 100 °C for 10 min. Then, Spiro-OMeTAD was spin coated onto the sample, forming the hole transport layer (HTL). Lastly, Au electrodes were deposited onto HTL by physical vapor deposition (PVD).

Scanning electron microscopy (SEM) was first conducted to investigate the surface morphology of perovskite films with or without 2D passivation. Compared to the pristine-FAPbI₃ film, FAPbI₃/BAI thin films showed less distinctive grain boundaries and more fully covered grains. While imperfections like not fully covered grains and rough surfaces arose in FAPbI₃ with 1 mg/mL and 5 mg/mL BAI, the FAPbI₃ with 3 mg/mL BAI yielded the optimal result with mostly fully covered grains. The X-ray diffraction (XRD) measurement shows the BAI coating didn't change the FAPbI₃ crystal structure. X-ray photoelectron spectroscopy (XPS) indicates that the structure of perovskite films near the surface is less stable. Finally, the device performance test was conducted as shown in Figure 1-b. FAPbI₃-3 mg/ml BAI yielded the optimal result with highest PCEs and lowest hysteresis compared with pristine-FAPbI₃, FAPbI₃-1 mg/ml BAI, and FAPbI₃-5 mg/ml BAI, indicating a significant improvement in both efficiency and stability of perovskite solar cells.

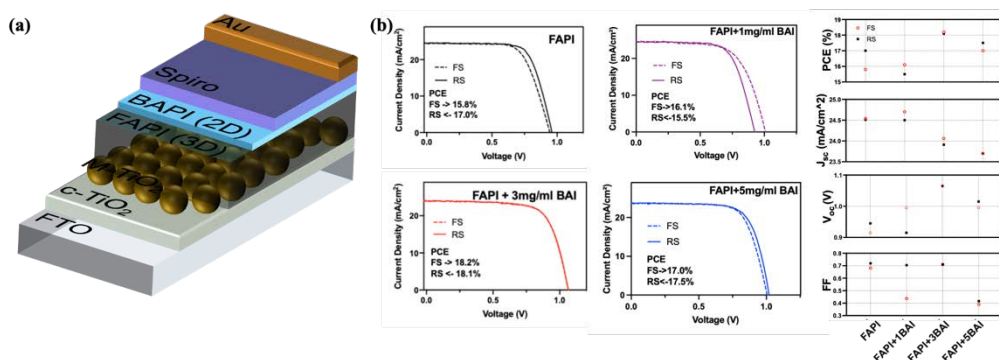


Figure 1: The structure of the perovskite solar cell (a) and the performance parameters of the four samples (b).

- (1) Chen, Y.; He, M.; Peng, J.; Sun, Y.; Liang, Z. Structure and Growth Control of Organic-Inorganic Halide Perovskites for Optoelectronics: From Polycrystalline Films to Single Crystals. *Adv. Sci.* **2016**, *3* (4), 1500392. <https://doi.org/10.1002/advs.201500392>.
- (2) Kim, E.-B.; Akhtar, M. S.; Shin, H.-S.; Ameen, S.; Nazeeruddin, M. K. A Review on Two-Dimensional (2D) and 2D-3D Multidimensional Perovskite Solar Cells: Perovskites Structures, Stability, and Photovoltaic Performances. *J. Photochem. Photobiol. C Photochem. Rev.* **2021**, *48*, 100405. <https://doi.org/10.1016/j.jphotochemrev.2021.100405>.

Investigating the effect of charging methods on dendrite formation in LiPF₆- and NaPF₆-electrolyte alkali-metal batteries through Lattice-Boltzmann methods

Ming Qi¹, Dongli Tian², Zhuolin Xia³, Dr. Dilip Gersappe³, Dr. Miriam Rafailovich³

¹University High School, Irvine, CA 92612, ²Mulgrave School, West Vancouver, BC V7S 3H9, ³Stony Brook University, Stony Brook, NY 11794

Lithium ion batteries have been recognized as having high energy densities and electrochemical potential, making them invaluable in consumer electronics (Goonan). However, lithium mining and processing has been shown to be very costly and harmful for the environment (Agusdinata). Consequently, more cost effective and sustainable alternative anode materials such as sodium are being investigated for their energy storage capacities and failure mechanisms. Yet, like lithium, the growth of dendrites on the anode surface is a prominent failure mechanism for sodium, constituting a major obstacle in the development of reliable, efficient, and safe sodium ion batteries as they cause reduced energy storage capacity and battery lifespan, as well posing serious safety concerns such as short circuits (Wang).

In this study, we aimed to further understand the mechanisms of dendrite formation and changes in the roughness of the solid electrolyte interphase in sodium ion batteries through computational modeling on the mesoscopic scale using Lattice-Boltzmann simulations. This analysis was first done on a system simulating sodium batteries undergoing the well-established switch charging method. Afterwards, we completed the same analysis with the pulse charging method, which has been shown to reduce dendrite growth in Li-ion batteries (Huang), and determined its viability in achieving similar results in charging Na-ion batteries. We finally then used our results to evaluate these charging methods and optimize their associated parameters.

Our simulations were written in C++ using the Lattice-Boltzmann simulation library Palabos, and were run on Stony Brook supercomputers. Our system consists of a half cell with a working electrode, virtual counter electrode, and electrolyte with a rough anode surface generated by algorithmic randomness. We found that for lithium pulse charging significantly reduced the size of the dendrite formations (Fig 1), ending with a final surface roughness of 2.39 compared with 3.12 for switch charging (Fig 2).

However, pulse charging took 31% longer to charge the battery to max capacity than switch.

As of the completion of this abstract we are running the pulse and switch charge simulations for the sodium ion batteries on the Seawolf supercomputer. We will compare these two charging methods for charging effectiveness and dendrite growth on sodium ion batteries, as well as contrast the reduction of dendrite formation in sodium and lithium for pulse charging against switch.

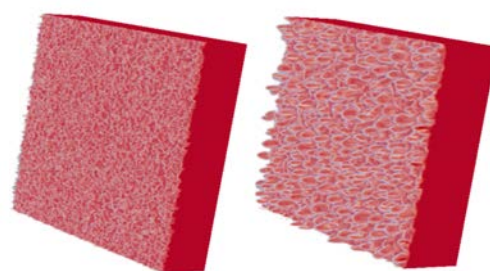


Figure 1: Visualization of Surface Morphology

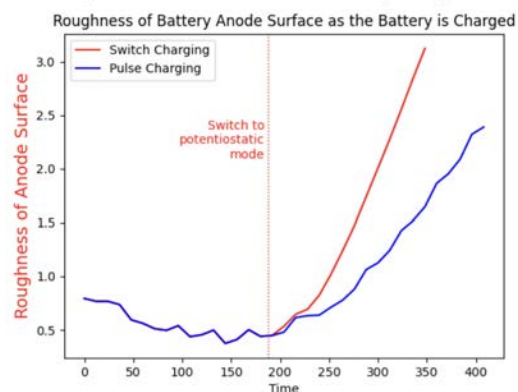


Figure 2: Results from Li-ion Battery Simulations

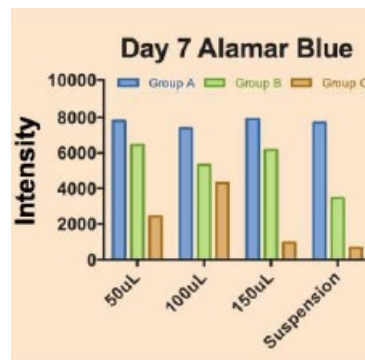
Agusdinata, Datu Buyung, et al. "Socio-Environmental Impacts of Lithium Mineral Extraction: Towards a Research Agenda." Environmental Research Letters, vol. 13, no. 12, Nov. 2018, p. 123001. DOI.org (Crossref), <https://doi.org/10.1088/1748-9326/aae9b1>.

Goonan, Thomas. Lithium Use in Batteries. USGS Numbered Series, 1371, U.S Geological Survey, 2012, https://pubs.usgs.gov/circ/1371/pdf/circ1371_508.pdf.

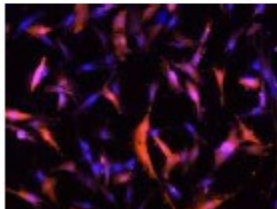
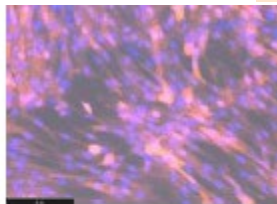
Wang, Yixian, et al. "A Sodium–Antimony–Telluride Intermetallic Allows Sodium-Metal Cycling at 100% Depth of Discharge and as an Anode-Free Metal Battery." Advanced Materials, vol. 34, no. 1, Jan. 2022, p. 2106005. DOI.org (Crossref), <https://doi.org/10.1002/adma.202106005>.

Session 4: Neurologic and Osteologic Differentiation of Dental Pulp Stem Cells

Chairs: Adam Hansen, Elias Georgas, Dr. Kuan-Che Fang



TCP
20X
DAPI and RFP



Pure PLA
20X
DAPI and RFP

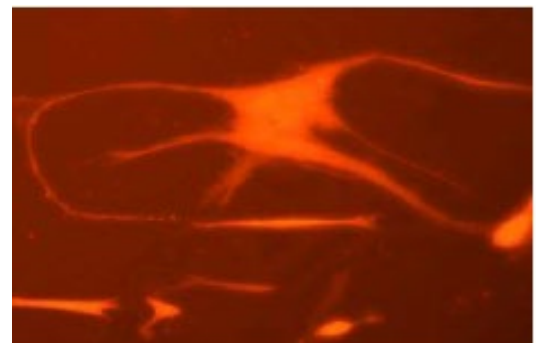


Fig 3: Day 9 EVOS 20x Mag PLA

Evaluating the Effect of Increased Resorcinol Diphenyl Phosphate Concentrations in Clay on the Neurogenic Differentiation of Human Dental Pulp Stem Cells

Hillel Schein¹, Rebecca Sullivan², Oran Goodman³, Nikhita Srivinas⁴, Sahil Sood⁵, Alex Wang⁶, Anna Cho⁷, Elias Georgas⁷, Adam Hansen⁸, Kuan-Che Feng⁸, Miriam Rafailovich⁸

¹Davis Renov Stahler Yeshiva High School for Boys, NY, 11598, ²Yeshiva University High School for Girls, NY, 11423, ³The Frisch School, NJ, 07652, ⁴Lausanne Collegiate School, TN 38120, ⁵Lambert High School, GA, 30024, ⁶Sewickley Academy Senior School, PA, 15143, ⁷Stony Brook University Biomedical Engineering Department, ⁸Stony Brook University Materials Science Department

Neurons are used to communicate information between the human body and the brain.¹ Currently, there is no cure for neurological diseases, however, clinical trials have shown stem cell differentiation to be a promising treatment for these conditions.² Human dental pulp stem cells (hDPSCs) are multipotent mesenchymal progenitor cells that have a high potential for self-renewal.³ In this experiment, hDPSCs were plated onto coated silicon wafers. This project examined the effect of surface chemistry on cell differentiation by adding varying concentrations of RDP-Clay to the silicon wafer coating and comparing the results. Resorcinol Diphenyl Phosphate (RDP) consists of one phosphate and two phenyl groups which alter the surface chemistry. The RDP was mixed with clay so that the phenyl groups would be adsorbed into the clay and freeing the phosphates to promote stem cell growth. Tissue Culture Plate (TCP) has been found to promote stem cell differentiation into neurons, however, it is not biocompatible. Therefore, PLA was tested as an alternative base for differentiation as it has already been proven to be safe for the human body. Poly(lactic acid) (PLA) is a biocompatible and biodegradable material which breaks down in the body within 2 years.⁴ PLA was chosen because of its biocompatibility and ability to promote stem cell growth.⁵

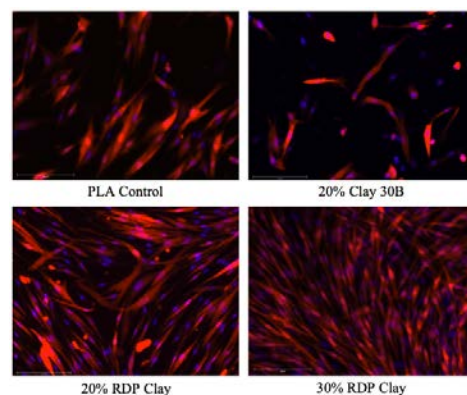


(Figure 1) - EVOS imaging day 9 under 20x magnification. The images show confluence cells and the beginnings of differentiation.

This project tested the hypothesis that an increased concentration of RDP-Clay mixed with PLA will result in a greater rate of differentiation of hDPSCs into neurons.

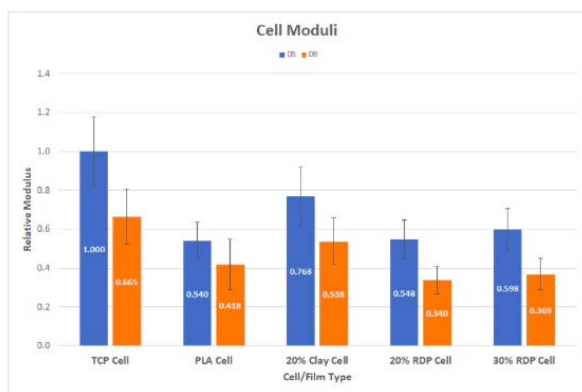


(Figure 2) - Cell modulus data from days 5 and 9 reflecting relative cell stiffness

Pure PLA, TCP, 20% RDP-Clay, 30% RDP-Clay, and 20% 30B clay were coated onto silicon wafers as surfaces for differentiating the dental pulp stem cells into neurons. Moduli and EVOS imaging were performed on day 5 before changing to neural media, and 9 days after changing to neural media to measure cell growth. Additionally on day 28, the cells will undergo RT-PCR as well as be observed under an EVOS microscope to determine if the cells differentiated into nerve cells. The days 5 and 9 moduli show that as time progressed, cell stiffness decreased which is common in cell differentiation (Figure 2).

¹ Woodruff, Alan. "What Is a Neuron?" *Queensland Brain Institute - University of Queensland*, 13 Aug. 2019, qbi.uq.edu.au/brain/brain-anatomy/what-neuron.

² Hernández, Rosa, et al. "Differentiation of Human Mesenchymal Stem Cells towards Neuronal Lineage: Clinical Trials in Nervous System Disorders." *Biomolecules & Therapeutics*, The Korean Society of Applied Pharmacology, 25 Oct. 2019, www.biomolther.org/journal/view.html?volume=28&number=1&spage=34&year=2020.

³ Sloan, Alistair J, and Rachel J Waddington. "Assessment of Pulp Vitality: A Review - Wiley Online Library." *International Journal of Paediatric Dentistry*, Wiley Online Library, 18 Dec. 2008, onlinelibrary.wiley.com/doi/full/10.1111/j.1365-263X.2008.00955.x.

⁴ Garlotta, Donald. "A Literature Review of Poly(Lactic Acid) - Journal of Polymers and the Environment." *SpringerLink*, Kluwer Academic Publishers-Plenum Publishers, Apr. 2001, link.springer.com/article/10.1023/A:1020200822435.

⁵ Hamad, K., et al. "Directory of Open Access Journals." *EXPRESS Polymer Letters*, Budapest University of Technology, 1 May 2015, doaj.org/article/9012242d000549918247c7fc699698b0.

Investigating The Effect of Static Magnetic Fields on the Differentiation of Dental Pulp Stem Cells into Neurons

Nikhita Srinivas^{1*}, Oran Goodman^{2*}, Rebecca Sullivan³, Hillel Schein⁴, Alexander Wang⁵, Sahil Sood⁶, Anna Cho⁷, Adam Hansen⁸, Kuan-che Feng⁸, Miriam Rafailovich⁸

¹Lausanne Collegiate School, TN 38120, ²The Frisch School, NJ 07652, ³Yeshiva University High School for Girls, NY 11423, ⁴Davis Renov Stahler Yeshiva High School for Boys, NY 11598, ⁵Sewickley Academy Senior School, PA 15143, ⁶Lambert High School, GA 30097, ⁷Department of Biomedical Engineering, Stony Brook University, NY 11790, ⁸Department of Materials Science and Engineering, Stony Brook University, NY 11790, *Equal Contribution

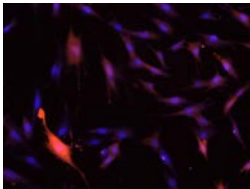


Fig 1: Day 5 EVOS Mag 20x PLA with mag field

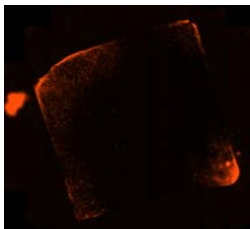


Fig 2: Day 9 Scan of Mag PLA with field

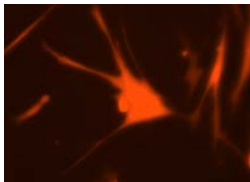


Fig 3: Day 9 EVOS 20x Mag PLA with field

Neurodegenerative disorders, the progressive loss of neurons leading to nervous system dysfunction, represent a growing health problem as neurons are not able to regenerate on their own if they sustain damage or injuries.¹ Finding a way to effectively generate neurons through the use of stem cells is increasingly important for neurodegenerative medicine. Dental Pulp Stem Cells (DPSCs) are a type of pluripotent stem cell that are able to proliferate efficiently which have been proven to be capable of neurogenic differentiability under certain circumstances.² Different environments, including static magnetic fields, have been shown in previous literature to have an effect on the differentiation of the DPSCs.³

The purpose of this study is to investigate the effect that a static magnetic field has on the generation of DPSCs into neurons. We spincoated silicon wafers with either pure Polylactic acid (PLA) or PLA with 20% Resorcinol Diphenyl Phosphate (RDP) clay at 2500 rpm for 30 seconds to create thin polymer films. DPSCs were then plated on the polymer films as well as on tissue culture plates (TCP) at an initial seeding density of 1.5×10^5 cells per sample and cultured with DPSC media (Alpha-MEM) for 3 days. After the third day of culturing, samples were switched to neural induction medium. Specific samples were further grown to day 5 and tested for modulus with no change of media. On day 5, before the cells were switched to neuronal media, modulus testing was performed on TCP and PLA cell controls to receive baseline rigidity data along with EVOS microscopy of the cells (Fig 1) to determine a baseline image of the cells before differentiation. The cells were then switched from the DPSC media to a neuronal media and placed in magnetic trays. Nine days after the media change, modulus testing was attempted on the cells undergoing magnetic treatment but was not completed due to a lack of cells. EVOS imaging of the cells showed a large decrease in plating efficiency and a scan of the whole silicon wafer showed cells on the outer edges of the wafer (Fig 2). Possible hypotheses for this change could be the interaction of the diamagnetic silicon wafer to the static magnetic field or the interaction of the RDP clay to the magnetic field as both have a magnetization. While there was a decrease in plating efficiency, the surviving cells on the plates exposed to the static magnetic field (Fig 3) showed cells that had a structure that looked closer to the structure of a neuron in comparison to

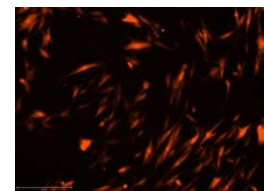


Fig 4: Day 9 EVOS 10x Mag PLA without field (control)

the controls (Fig 4), potentially because of the magnetic field.

Further investigations will use PLA molds instead of films on silicon wafers to determine the cause of the DPSC interaction with the static magnetic field. EVOS imaging and RT-PCR will be utilized to examine the differentiation of the DPSCs.

¹ Przedborski, Serge, et al. "Series Introduction: Neurodegeneration: What is it and where are we?", *The Journal of Clinical Investigation*, vol. 111, no. 1, 2003, <https://www.jci.org/articles/view/17522>. Accessed 9 August 2022.

² Ueda, Tomoyuki, et al. "Characteristics and Therapeutic Potential of Dental Pulp Stem Cells on Neurodegenerative Diseases", *Frontiers in Neuroscience*, vol. 14, 2020, <https://www.frontiersin.org/articles/10.3389/fnins.2020.00407/full>. Accessed 9 August 2022.

³ Sadri, Maryam, et al. "Static Magnetic Field Effect on Cell Alignment, Growth, and Differentiation in Human Cord-Derived Mesenchymal Stem Cells", *Cell Mol Bioeng*, vol. 10, no. 3, pg 249-262, 2017, <https://pubmed.ncbi.nlm.nih.gov/31719863/>. Accessed 9 August 2022.

Investigating The Effect of A Dynamic Magnetic Field on Rate of DPSC Neurogenic Differentiation

Alex Wang¹, Sahil Sood², Rebecca Sullivan³, Hillel Schein⁴, Nikhita Srivinas⁵, Oran Goodman⁶, Anna Cho⁷, Elias Georgas⁷, Adam Hansen⁸, Kuan-Che Feng⁸, Miriam Rafailovich⁸

¹Sewickley Academy Senior School, PA, 15143, ²Lambert High School, GA, 30024, ³Yeshiva University High School for Girls, NY, 11423, ⁴Davis Renov Stahler Yeshiva High School for Boys, NY, 11598, ⁵Lausanne Collegiate School, TN, 38120, ⁶The Frisch School, NJ, 07652, ⁷Stony Brook University Biomedical Engineering Department, NY, 11794, ⁸Stony Brook University Materials Science Department, NY, 11794

Neurodegenerative diseases pose a major health problem due to the intrinsic, non-dividing and non-regenerative nature of neurons. Damage to neuronal networks in the central nervous system (CNS) from traumatic injuries or neurodegenerative diseases are difficult to recover from, for CNS axon lesions reside in an environment that is inhibitory towards axon regeneration [1]. Therefore, it is imperative to develop a protocol to efficiently catalyze neurogenesis as a means to combat long-term neuronal damage. Dental pulp stem cells (DPSCs) are easily accessible multipotent stem cells with a high proclivity to differentiate into several cell lines [2]. Previous research has shown a significant increase in differentiation of DPSCs into neurons via plating on Poly-lactic Acid (PLA) and 20% resorcinol diphenyl phosphate (RDP) clay polymer blends [3]. Furthermore, separate literature indicated the usage of a spinning, dynamic magnetic field and superparamagnetic iron-oxide core and gold shell nanoparticles (NPs) induced axon growth in neurons [4]. In order to determine a method of increasing the likelihood of differentiation, we have researched the effects of a dynamic magnetic field (with iron-oxide core nanoparticle treatment and 20% RDP clay surface) on DPSC-based neurogenesis.

We spincoated 24 silicon wafers with either pure PLA or PLA with 20% RDP chloroform-based solutions at 2500 rpm for 30 seconds to create thin polymer films, with pure PLA acting as a control. Following, DPSCs were plated onto wafer surfaces at an initial seeding density of 1.5×10^5 and cultured with DPSC media (Alpha-MEM) for 3 days. On day 3, modulus testing was performed on tissue culture plate (TCP) and PLA cell controls to receive baseline rigidity data. On each plate, 3 cells were tested 3 different times, in total 9 tests per plate. Day 3 EVOS microscopy provided baseline images of undifferentiated DPSCs on PLA and TCP for morphological comparison during future EVOS tests (**FIG 1**). Following imaging and modulus testing, on day 3, DPSC media was exchanged for neuronal media. On day 1 following neuronal media change, cells were treated with NPs. On day 2, cells were treated with the dynamic for 30 minutes each, and would continue every other day for the next 6 days. On day 6, modulus testing was again performed. On day 9, EVOS microscopy was performed, showing increased neuronal-like morphology in the cells (**FIG 1**). Treated cells showed increased elongation and axonal development. On day 28, we will perform RT-PCR and expect Magnetic Field+NP plates to show the greatest amount of native neuron-like genetic markers.

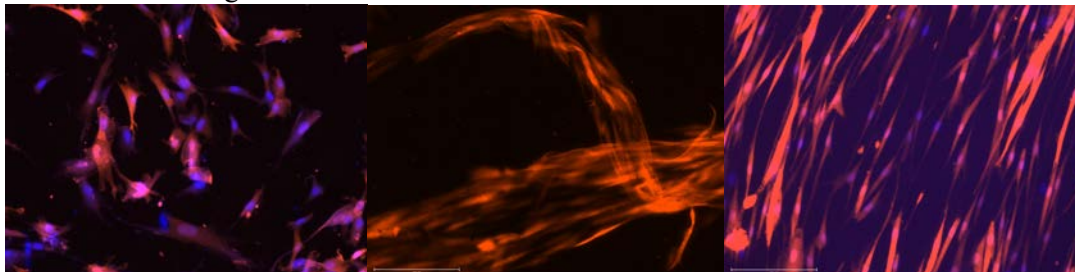


Figure 1. Day 3 PLA 20x EVOS; Day 9 PLA+Magnetic Field+NPs 20x EVOS; Day 9 PLA-Magnetic Field-NPs 20x EVOS

[1] Silver, Jerry, et al. "Central Nervous System Regenerative Failure: Role of Oligodendrocytes, Astrocytes, and Microglia." *Cold Spring Harbor Perspectives in Biology*, 7 Mar. 2015. National Library of Medicine, <https://doi.org/10.1101/cshperspect.a020602>. Accessed 3 Aug. 2022.

[2] Luo, Lihua et al. "Potential Roles of Dental Pulp Stem Cells in Neural Regeneration and Repair." *Stem cells international* vol. 2018 1731289. 7 May. 2018, doi:10.1155/2018/1731289

[3] Justin, Anya, et al. "Observing the Neurogenic Differentiation of Human Dental Pulp Stem Cells (hDPSCs) on Molded Poly-lactic Acid (PLA) Scaffolds with Varying Percentages of Resorcinol Diphenyl Phosphate (RDP) Clay." *Journal of Undergraduate Chemical Engineering Research*, pp. 61-65,

[4] Yuan, Muzhaozi, et al. "Promoting neuroregeneration by applying dynamic magnetic fields to a novel nanomedicine: Superparamagnetic iron oxide (SPIO)-gold nanoparticles bounded with nerve growth factor (NGF)." *Nanomedicine: Nanotechnology, Biology, and Medicine*, vol. 14, 25 Mar. 2018, pp. 1337-47.

The Effect of Microsphere Growth and Static Magnetic Field on Osteogenic Differentiation of Dental Pulp Stem Cells

Angeline Sun¹ Emir Mulic², Sooraj Shah², Kuan-Che Feng³

¹Taipei American School, Taipei, Taiwan, 11152; ²Stony Brook University, Stony Brook, NY 11794; ³Department of Materials Science and Chemical Engineering Stony Brook University, NY, 11794

This study aims to investigate the effect of microsphere formation and static magnetic fields on osteogenic differentiation. DPSCs were grown in the DPSC growth media (containing α -MEM, 10% FBS, and 1% penstrep). To make the cells aggregate into a microsphere, two types of wells were used to prevent adhesion to well surface: U-bottom non-adhesive 96-well plates and flat-bottom 96-well plates covered with 50, 75, 100, and 150 μ L 2% agarose in PBS in each well. Different volumes of agarose produce different degrees of curvature, thereby influencing the compactness of the microspheres. EVOS imaging in Figure 1 revealed that the agarose wells were better at forming dense aggregates compared to suspension wells. At 3, 5, and 7 days after microsphere formation, the cells were transferred and plated onto 6-well tissue culture plates. To determine the optimal type of well and incubation time, cell viability in wells under different conditions was determined using alamar blue assay. Measurements were taken every other day after plating to discern a pattern of cell growth. Ascorbic acid and β -glycerophosphate were added into the medium to induce osteogenic differentiation.

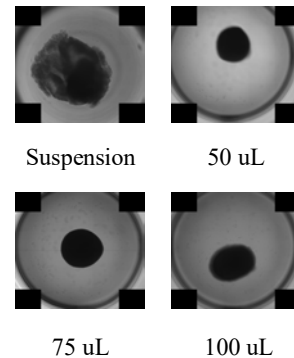


Figure 1. Microspheres under EVOS

The synergistic effect of magnetic fields and magnetic scaffolds has been demonstrated to enhance osteogenesis through activating signaling pathways [5]. For the magneto-mechanical stimuli, cells were plated onto different scaffolds and incubated under the presence or absence of magnetic fields. The three types of compression-molded scaffolds were pure polylactic acid (PLA), a biodegradable polyester frequently used in tissue engineering [6], 95% PLA and 5% RDP clay, and 90% PLA and 10% magnetic iron oxide microparticles. Using atomic force microscopy (AFM) to characterize surface topology, we found that all three scaffolds were of nanoscale roughness, with the scaffolds containing iron oxide being the roughest.

For both microsphere and magnetic field experiments, after 28 days of incubation, EVOS would be used to image cell morphology and the biomineralization. Raman spectroscopy and SEM would be used to learn about the crystallinity and element composition of biomineralization. RT-PCR would be performed to quantify mRNA of the following osteogenic-related genes: osteocalcin (OCN), dentin sialophosphoprotein (DSPP), and alkaline phosphatase (ALP). All results would be normalized with the housekeeping gene GAPDH related to Day 0.

- [1] Anitua, Eduardo, et al. "Progress in the Use of Dental Pulp Stem Cells in Regenerative Medicine." *Cytotherapy*, Elsevier, 12 Feb. 2018, <https://www.sciencedirect.com/science/article/pii/S1465324918300033>.
- [2] Mortada, Ibrahim, and Rola Mortada. "Dental Pulp Stem Cells and Osteogenesis: An Update." *Cytotechnology*, vol. 70, no. 5, 2018, pp. 1479–1486., <https://doi.org/10.1007/s10616-018-0225-5>.
- [3] Buduru, Smaranda Dana, et al. "The Potential of Different Origin Stem Cells in Modulating Oral Bone Regeneration Processes." *Cells*, vol. 8, no. 1, 2019, p. 29., <https://doi.org/10.3390/cells8010029>.
- [4] Bu, Nam-Ung, et al. "In Vitro Characterization of Dental Pulp Stem Cells Cultured in Two Microsphere-Forming Culture Plates." *Journal of Clinical Medicine*, vol. 9, no. 1, 2020, p. 242., <https://doi.org/10.3390/jcm9010242>.
- [5] Xia, Yang, et al. "Magnetic Field and Nano-Scaffolds with Stem Cells to Enhance Bone Regeneration." *Biomaterials*, vol. 183, 2018, pp. 151–170., <https://doi.org/10.1016/j.biomaterials.2018.08.040>.
- [6] Hamad, K., et al. "Properties and Medical Applications of Polylactic Acid: A Review." *Express Polymer Letters*, vol. 9, no. 5, 2015, pp. 435–455., <https://doi.org/10.3144/expresspolymlett.2015.42>.

Investigating Elasto-acoustic Gram as a Noninvasive Method for Early Detection of Arthritis and Subchondral Bone Alteration

Sahil Sood¹, Carmen Shum², Adnan Reyes³, Elias Georgas², Junhang Zhang³, Qifa Zhou³, Yi-Xian Qin²

¹Lambert High School, ²Department of Biomedical Engineering at Stony Brook University, ³Department of Biomedical Engineering at University of Southern California

Introduction: Osteoarthritis is a degenerative musculoskeletal disorder that progressively affects the joints of over 32 million adults, resulting in chronic pain and stiffness [1]. A hallmark of osteoarthritis is the degradation of articular cartilage and remodeling of subchondral bone, which causes aching, swelling in the knee, and a reduced range of mobility. In the status quo, diagnostics for osteoarthritis include joint aspiration, X-Ray, magnetic resonance imaging, and invasive scope. However, all of these options are suboptimal, as they are either highly invasive or subject the patient to high quantities of radiation. Conversely, the use of acousting techniques, such as elastography, can provide non-invasive, high quality images of cartilage degeneration in osteoarthritis. Shear wave elastography is a method of imaging that is able to detect tissue stiffness and damaged tissues. The objective of this study is to expand upon the previous use of this technology by our lab by increasing the sample size for noninvasive detection and correlation of cartilage surface to subchondral bone alteration.

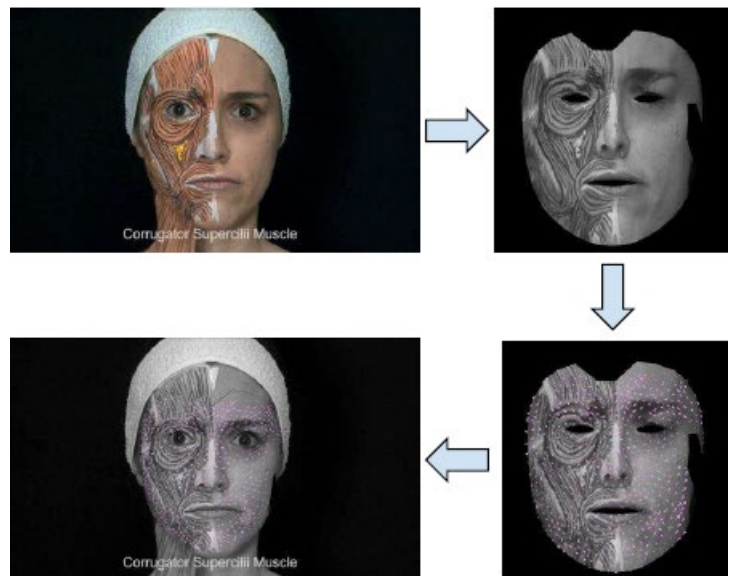
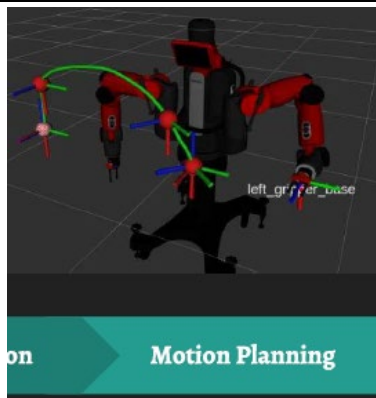
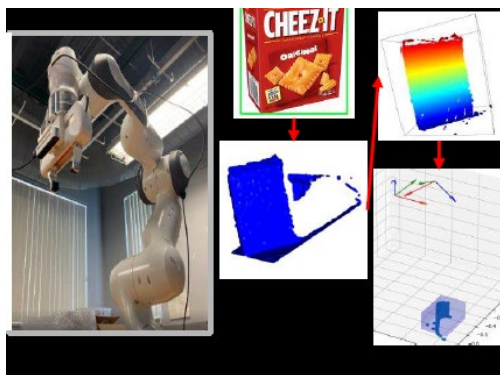
Materials and methods: Using both chemical and physical methods, samples were prepared to simulate the effects of cartilage surface defect and subchondral bone alteration. Using varying grades of sandpaper, cartilage surface roughness was modeled. There were 4 experimental groups: a control group, 150, 220, and 320 grit (Fig 1). This represents the loss of surface on articular cartilage in osteoarthritis patients. By running exposed cartilage over the varying grits of sandpaper in the x and y direction, cartilage degradation is obtained. In order to simulate subchondral bone defects, formic acid was utilized. There were 4 groups of subchondral bone defects: the control, 1%, 3%, and 7% formic acid, which was injected into the subchondral bone area of the sample to induce demineralization. The final group was a combination of the two methods, with sandpaper on the surface to cause surface degradation and formic acid in the subchondral bone area. Once osteoarthritis is "induced", the samples were tested to investigate the effect of cartilage degeneration on the bone mechanics. The use of shear wave elastography was employed to test the samples. In order to create a shear wave, vibrations from a mechanical shaker with a metal rod was placed on a sample along with the probe, and the shear wave speed was measured. The analysis with shear wave elastography was done in conjunction with a lab in California, and the results are still pending with regards to how the bone mechanics are affected and whether the elasto-acoustic gram is a successful non-invasive method for early detection of osteoarthritis.



1 - <https://www.mayoclinic.org/diseases-conditions/osteoarthritis/symptoms-causes/syc-20351925#:~:text=Osteoarthritis%20is%20a%20degenerative%20disease,pain%20and%20disability%20of%20osteoarthritis.>

Session 5: Robotics-Digital Analysis and Control

**Chairs: Dasharadhan Mahalingam,
Zhikang Dong, Jessica Hofflich,
Shi Fu**



VR-Based Approach for Guiding a Robot in Manipulation Tasks

Dr. Nilanjan Chakraborty¹, Dasharadhan Mahalingam², Andy Yao³, Eden Hen⁴, Siri Reddy⁵

¹Assistant Professor at Stony Brook University, Stony Brook, NY, 11794 ²Graduate Student at Stony Brook University, Stony Brook, NY, 11794 ³Herbert Henry Dow High School, Midland, MI, 48640 ⁴Salanter Akiba Riverdale High School, Bronx, NY, 10471 ⁵Horace Greeley High School, Chappaqua, NY, 10514

Learning from demonstration (LfD) is a technique that familiarizes a robot with a certain task through demonstrations, and has been gaining popularity due to the difficulty of manually programming robots to complete specific tasks. Of the three main categories of LfD demonstrations, teleoperation has emerged as more efficient and practical compared to more physical LfD procedures.¹ Specifically, virtual reality (VR) is a type of teleoperation technique that has proved to be a more effective and accurate method of simulating demonstrations compared to other systems such as using a PS3 controller.²

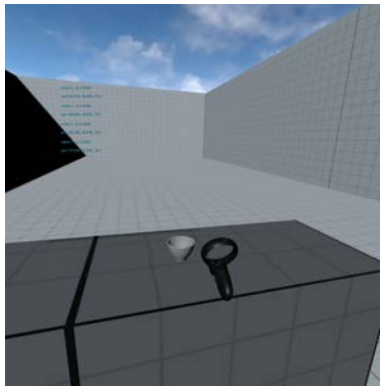


Figure 1. Virtual Environment (VE)

Using virtual reality (VR), this research aims to develop an LfD pipeline to allow for a faster and easier way of guiding a robot in performing manipulation tasks. A VR LfD pipeline would focus on the extraction of task constraints, task generalization, and motion planning in order to take the poses of a virtual object and translate that data into movements for the robot to execute. This pipeline was mainly developed using Python, C++, and ROS (Robot Operating System).

Within this paper, we show that recorded VR motion paths are capable of being interpreted into a set of screw-linear motions and associated inverse kinematic joint-space movements so that the Baxter Rethink Robotics machine executes a replication of the demonstrated task. Using both an Oculus Quest and Quest 2, a series of common movements involving household objects were recorded within Unreal Engine 4 in quaternion rotational and XYZ coordinate form, logged with the Android Debug Bridge, and processed through a WebSocket Python program that automatically sent the resulting pose and grip data to the ROS platform. Within ROS, using algorithms provided by the Interacting Robotic Systems Laboratory (IRSL) at the University, this data was translated into areas of interest, which allowed for the creation of end effector generalized screw-linear interpolation paths between areas of interest. Once the end effector had a set path, an inverse kinematic program (also from the IRSL) was used to calculate the angle and position of each of the related seven joints on the Baxter Robot, determining the pathing feasibility and allowing for execution.

While this research could have applications for almost any manipulation task, this study differs from others in that it is specifically intended to assist a robot in learning many routine tasks of daily life that would be of use to those with disabilities, such as pouring a liquid into a cup or stacking objects. To this end, one of the main benefits of a VR LfD pipeline would be giving a capable demonstrator the ability to guide a robot in performing an unexpected task remotely, rather than requiring the robot to be visited in person on every such occasion. This project opens the door for more research into applying and optimizing VR LfD pipelines now that such a pipeline has been created.

Using both an Oculus Quest and Quest 2, a series of common movements involving household objects were recorded within Unreal Engine 4 in quaternion rotational and XYZ coordinate form, logged with the Android Debug Bridge, and processed through a WebSocket Python program that



Figure 2. RVIZ Model of Baxter Rethink Robot

¹ Ravichandar, H., Polydoros, A. S., Chernova, S., & Billard, A. (2020). Recent Advances in Robot Learning from Demonstration. *Annual Review of Control, Robotics, and Autonomous Systems*, 3(1), 297–330. <https://doi.org/10.1146/annurev-control-100819-063206>

² Jackson, A., Northcutt, B. D., & Sukthankar, G. (2019). The Benefits of Immersive Demonstrations for Teaching Robots. *2019 14th ACM/IEEE International Conference on Human-Robot Interaction (HRI)*, 326–334. <https://doi.org/10.1109/HRI.2019.8673270>

Convolutional Neural Network Guided Point Cloud Segmentation

Edward Sun,¹ Ben Wen,² Aditya Patankar,³ Nilanjan Chakraborty³

¹Torrey Pines High School, 3710 Del Mar Heights Road, San Diego, CA 92130 ²Aragon High School, 900 Alameda de las Pulgas, San Mateo, CA 94402 ³Department of Mechanical Engineering, Stony Brook University, Stony Brook, NY 11790

Ailments like muscular dystrophy, cerebral palsy, arthritis, or severe spinal cord injuries can cause serious mobility impairments on one or many limbs, restricting an individual's ability to perform fundamental tasks. Living with such mobility impairments cause individuals to become highly dependent

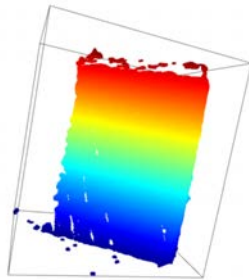


Fig. 1 segmented and bounded object

on the care from others. However, these limitations may be overcome with the usage of a robotic arm that assists with daily tasks. Previous studies have shown that caregiving time can be reduced by 41% with the aid of a Kinova Jaco robotic arm.¹ As these benefits in assistive robotics are realized, many private sector companies such as Jaco by Kinova and iARM by Exact Dynamics have commercialized such applications of robotics.² As dexterous manipulation is dependent upon proper point cloud segmentation objects, speed and accuracy must be considered in perception of objects to be grasped.³ Thus, in this study, we experimented with an end-to-end implementation of You Only Look Once (YOLOv5)⁴ guided point cloud segmentation to accurately localize grasping targets in a computationally efficient manner.

We utilized the Yale-CMU-Berkeley (YCB) objects dataset⁵ to customly train a YOLOv5 model. Assuming that the object is stationary and the base location of the robot arm is defined, we approached the localization problem by taking a single snapshot of the object with the Robot Operating System (ROS).

As one of the fastest object detection models, YOLOv5 was implemented in Python to label and localize the object with a bounding box. Then, with the given depth data and the location of the robot arm, the localized object would be transformed to 3D real world coordinates (Fig. 1) via a perspective projection from 2D to 3D and then a reference frame transformation from the local camera coordinate system to the global coordinate system (Fig. 2).

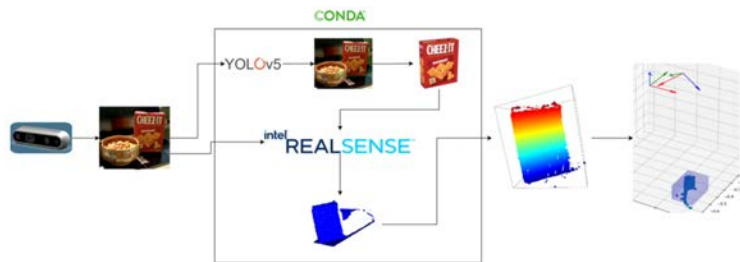


Fig. 2 Segmentation Pipeline

Post processing is performed to remove noisy points introduced on planes parallel to the surface backgrounds (e.g., table). DBSCAN is applied to the point cloud in order to cluster the point cloud. The cluster with the greatest number of points is assumed to be the object. A bounding volume is placed around the point cloud to better represent the true shape and orientation of the object. This procedure significantly improves the accuracy of the object's 3D point cloud segmentation. Further studies may seek to infer the full shape of the object and implement robotic grasping calculations based on the more accurate model.

¹Maheu, Veronique, et al. "Evaluation of the Jaco Robotic Arm: Clinico-Economic Study for Powered Wheelchair Users with Upper-Extremity Disabilities." 2011 IEEE International Conference on Rehabilitation Robotics, 2011, <https://doi.org/10.1109/icorr.2011.5975397>.

²Campeau-Lecours, Alexandre, et al. "Jaco assistive robotic device: Empowering people with disabilities through innovative algorithms." (2016). Available at https://www.resna.org/sites/default/files/conference/2016/other/campeau_lecours.html

³Duan, Haonan, et al. "Robotics Dexterous Grasping: The Methods Based on Point Cloud and Deep Learning." *Frontiers in Neurorobotics*, vol. 15, 2021, <https://doi.org/10.3389/fnbot.2021.658280>.

⁴Redmon, Joseph, et al. "You Only Look Once: Unified, Real-Time Object Detection." 2016 IEEE Conference on Computer Vision and Pattern Recognition (CVPR), 2016, <https://doi.org/10.1109/cvpr.2016.91>.

⁵Calli, Berk, et al. "The YCB Object and Model Set: Towards Common Benchmarks for Manipulation Research." 2015 International Conference on Advanced Robotics (ICAR), 2015, <https://doi.org/10.1109/icar.2015.7251504>.

A Cross-Platform Transfer

Hugh Rosshirt^{1*}, Alex Samadi², Sergio Rosa³, Mariam Rafailovich⁴

^{1*} Notre Dame University, Cleveland, Ohio; ² Jericho Senior High School, Jericho, New York; ³ South Side High School, Rockville Centre, New York, ⁴ Stony Brook University Department of Materials Science and Chemical Engineering}

Many people who are paralyzed rely on using an electric wheelchair to get from place to place. Quadriplegia occurs after a neck or spinal injury and is a form of paralysis where all four limbs are paralyzed. As people with quadriplegia are unable to move their limbs, they are dependent on their wheelchair but many improvements can be made. For the same reason that people who suffer from quadriplegia cannot move their limbs, their range of vision is limited. With this being a major issue for people with quadriplegia- we set out to create a solution for people with this issue. A tongue touch keypad (TTK) is a small keypad that is embedded into a retainer. With small sensor buttons, this keypad can act like a mouse for a computer. It was soon realized that to help people with quadriplegia, the use of a tongue touch keypad would be very practical. As rotating cameras have been available since the 1900s, we created a program that would be able to control these movements based on the location of the cursor and later based on buttons pressed on the user interface. As the mouse is moved to the left and right, the camera moves accordingly. Later with buttons, as the left or right button is clicked the camera follows. In most cases, this camera could be mounted on the top back part of an electric wheelchair allowing the driver to see behind and both sides of the wheelchair by moving a mouse. With a quadriplegic user, a tongue-touch keypad would be connected wirelessly to the controls of the camera to be used.

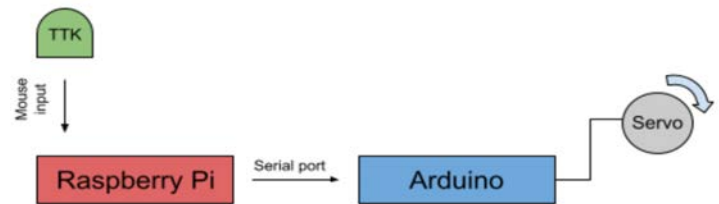


Figure 1: Transfer of TTK input to moving Servo

As shown in the figure, The tongue touch keypad would send mouse inputs to the Raspberry Pi. Once the Raspberry Pi detects these inputs, the Raspberry Pi would send these mouse inputs to the Arduino via serial port. While the camera would be mounted on the Servo, the Arduino would instruct the Servo which way to move. So in Sum, as buttons on the tongue touch keypad are pressed through a user interface, the tongue touch keypad would instruct the servo which way to move. Finally, as this system would be applied to an electric wheelchair, there would be a monitor mounted on one of the armrests that would display what the camera sees and two buttons. These buttons would be pressed to move the camera from side to side. And the camera would be clamped on the back of the wheelchair to make places visible that once were not. As this project can always be improved, we are working on making the receiver of the TTK Bluetooth so it will be compatible with more platforms. Additionally, we are working on adding another camera mounted on a second Servo strictly for the range of up and down. This would complete the range of vision for the user.

[1] Hangu Park and Maysam Ghovanloo. "An Arch-Shaped Intraoral Tongue Drive System with Built-in Tongue-Computer Interfacing SoC" 2014

[2] Hui Tang and D.J. Beebe. "An oral tactile interface for blind navigation" 2006

Emotion Detection Using Deep Learning in Conjunction with Digital Image Speckle Correlation

Eric Guan¹, Juni Kim², Judah Rosenthal³, David Tarrab⁴, Yubo Wu⁵, Rena Max⁶, Jessica Hofflich⁷, Zhikang Dong⁸, Shi Fu⁹, Pawel Polak¹⁰, Miriam Rafailovich¹¹

¹North Carolina School of Science and Math, Durham, NC 27705, ²Stanford Online High School, Redwood City, CA 94063, ³Davis Renov Stahler Yeshiva High School for Boys, Woodmere, NY 11598, ⁴Ramaz Upper School, New York, NY 10075, ⁵Canyon Crest Academy, San Diego, CA 92130, ⁶Department of Computer Science, University of Maryland, College Park, MD 20742, ¹⁰Department of Applied Mathematics and Statistics, Stony Brook University, Stony Brook, NY 11794, ¹¹Department of Materials Science and Chemical Engineering, Stony Brook University, Stony Brook, NY 11790

Detecting micro-motions of the face muscles has many practical applications. It can be used to identify muscle paralysis, distinguish people from each other, gauge reaction time, detect deep fake videos, and measure people's emotions. Digital Image Speckle Correlation (DISC), first developed for materials science to understand mechanical stress, is a promising tool for muscle movement detection because it can detect extremely small movements in the face. DISC compares pairs of frames and generates a vector map by tracking the movement of pixels between the frames.

We first detect the face in each frame of the videos using the open-source Mediapipe library developed by Google. In order to mitigate head movement in the video, we use the face tracking capabilities of Mediapipe library and the affine transformation to create a canonical face. Resulting canonical face images are the same size and position for each frame and can be compared using DISC.

The DISC computations are carried out using Optical Flow methods from the open-source library OpenCV. The resulting vector field is plotted on the canonical images and inverse mapped using the affine mapping, converting the face back to the original video frames. The whole process produces a video analogous to the original input but with the overlay of the vector map tracking the micromovements in the face (Fig. 1).

These new videos are fitted into a 3D Convolutional Neural Network (CNN) for emotions classification. The fitting is done using two publicly available datasets (CK+¹ and DAiSEE²). The project will be accompanied with a website where users can upload their own videos and get results with the characterization of the emotions from the image.

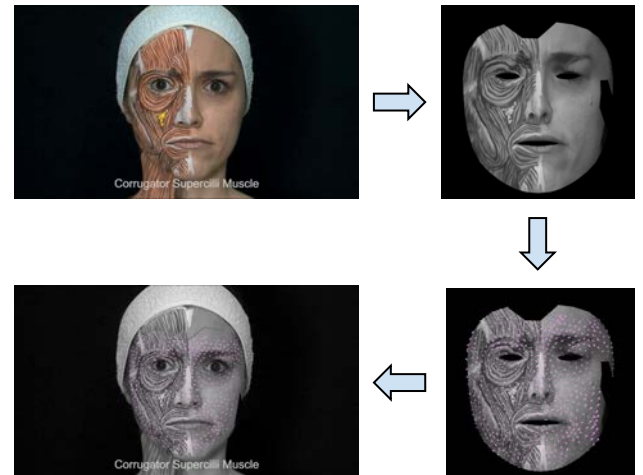


Figure 1: Canonical face and DISC transformations

¹ Lucey, P., Cohn, J. F., Kanade, T., Saragih, J., Ambadar, Z., & Matthews, I. (2010, June). The extended cohn-kanade dataset (ck+): A complete dataset for action unit and emotion-specified expression. In *2010 IEEE Computer Society Conference on Computer Vision and Pattern Recognition-Workshops* (pp. 94-101). IEEE.

² Gupta, A., D'Cunha, A., Awasthi, K., & Balasubramanian, V. (2016). Daisee: Towards user engagement recognition in the wild. arXiv preprint arXiv:1609.01885.

Session 6: TiO₂ Nanotoxicology & DNA Sequencing Chips

Chair: Shi Fu, Diya Rai-Gersappe

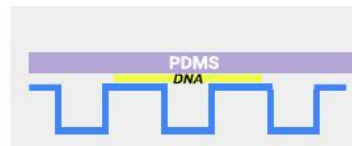
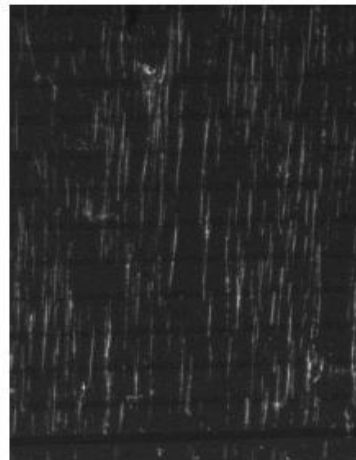
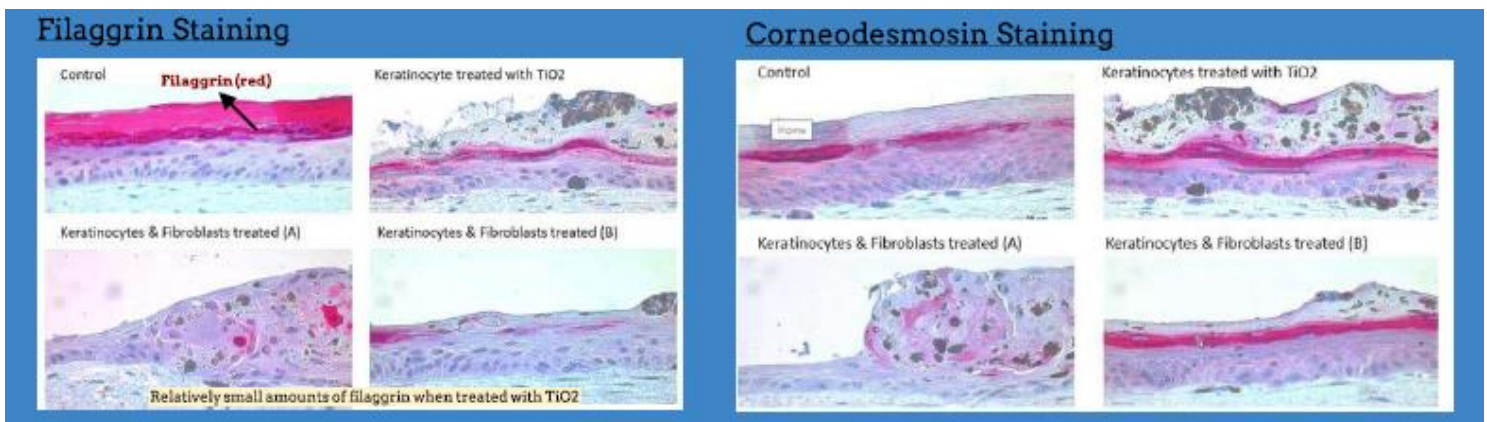


Fig 1. A diagram of the stamping mechanism

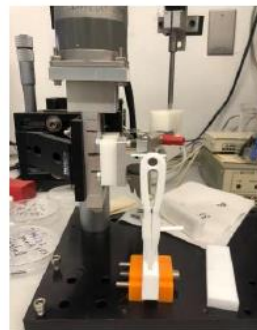


Fig 2. A photo of the dipping mechanism

Impact of Titanium Dioxide (TiO₂) Nanoparticles on Skin Dynamics in Conjunction with Analysis of Treated Skin Organotypics

Navya Gautam¹, Annie Hu², Darshini Podder³, Harsha Rajkumar⁴, Matthew Sharin⁵, Sherlyn Wu⁶, Sarah Yim⁷, Jeffery Zhang⁸, Christopher Gazis⁹, Ian Lau¹⁰, Nicole Niculescu⁹, Diya Rai-Gersappe¹¹, Noah Kim⁹, Shi Fu⁹

¹Hauppauge High School, Hauppauge, NY 11788, ²Great Oak High School, Temecula, CA 92592, ³Jericho High School, Jericho, New York 11753, ⁴Fremont Christian High School, Fremont, California 94536, ⁵Lawrence High School, Cedarhurst, NY 11516, ⁶Stuyvesant High School, New York City, New York 10282, ⁷Seoul International School, Seongnam, South Korea 13113, ⁸Shenzhen Middle School, ⁹Stony Brook University, ¹⁰Tufts University, ¹¹Vassar College

Titanium dioxide is utilized in a variety of cosmetic products due to its optical properties, including being a catalyst for UV rays. Such products have a “mean particle size”, and usually, this size is unable to penetrate the skin; however, unintentionally created nanoparticles could, thus posing a greater risk to the skin [1]. We sought to investigate the effects of TiO₂ nanoparticles on various properties of skin in order to assess the risk it poses to skin health. Skin equivalent organotypics were created using traditional pouring methods to form a dermis and epidermis (these were either treated with 0.8 mg/ml of TiO₂ or left untreated in varying combinations) [2]. Analysis showed that TiO₂ is more detrimental on keratinocytes than fibroblasts, which retained their ability to support the epidermis (**Figure 1**). A histological analysis of the constructs after filaggrin staining further demonstrated an abnormal stratum corneum, as it formed aberrant structures which were unable to be conventionally analyzed. Further staining of the corneodesmosin protein showed, however, that the stratum granulosum was not significantly altered by the treatment.

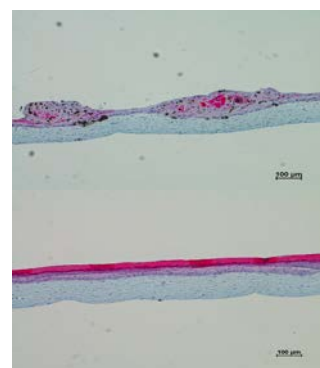


Figure 1. Filaggrin stains of sample treated in fibroblasts and keratinocytes(top) and a control sample(bottom).

We conducted a series of experiments which sought to explain these histological results at the cellular level, examining both epidermal keratinocytes and dermal fibroblasts. We determined the titanium dioxide association with keratinocytes and fibroblasts at varying concentrations using flow cytometry, showing that initial TiO₂ uptake in fibroblasts was significantly greater (almost 100% compared to 50% in keratinocytes). For fibroblasts this number remained near 100% for several days. TiO₂ impact on cell proliferation rates for fibroblasts was also evaluated using a hemocytometer and alamar blue staining over time; keratinocyte proliferation rate comparisons were done by evaluating colony formation efficiency (CFE). Results demonstrated that presence of TiO₂ nanoparticles did not significantly impact cell proliferation at the same rate as the control for either cell type. To gain further insight on whether TiO₂ impacted cell development, we performed actin & DAPI staining on fibroblasts. Visual analysis of actin and DAPI stained fibroblasts showed that actin filaments remained straight after TiO₂ treatment, remaining indicative of a healthy cytoskeleton.

We then examined skin tissue properties by measuring the contraction of collagen when exposed to TiO₂; this appeared not significantly affected. Lastly, we examined the impact of TiO₂ on cell modulus, which increased with increasing concentration, indicating increased stiffness.

Future work may include repeating the collagen contraction test and additional flow cytometry on keratinocytes to observe changes in association over several days (as was done for fibroblasts), as well as cross-validating collagen contraction results using a novel DISC method for tracking fluorescent bead displacement on tissue. We also may quantify features of the treated skin constructs.

- [1] Dréno, B., Alexis, A., Chuberre, B. and Marinovich, M. (2019), Safety of titanium dioxide nanoparticles in cosmetics. *J Eur Acad Dermatol Venereol*, 33: 34-46. <https://doi.org/10.1111/jdv.15943>
[2] Li, J, Fu, S, Lu, KW, et al. Engineering functional skin constructs: A quantitative comparison of three-dimensional bioprinting with traditional methods. *Exp Dermatol*. 2022; 31: 516– 527. <https://doi.org/10.1111/exd.14488>

Impact of Titanium Dioxide (TiO₂) Nanoparticles on Bacterial Infection Resistance of Fibroblasts and HUVEC Cells/Gene Expression

Navya Gautam¹, Annie Hu², Darshini Podder³, Harsha Rajkumar⁴, Matthew Sharin⁵, Sherlyn Wu⁶, Sarah Yim⁷, Jeffery Zhang⁸, Christopher Gazis⁹, Ian Lau¹⁰, Nicole Niculescu⁹, Diya Rai-Gersappe¹¹, Noah Kim⁹, Shi Fu⁹

¹Hauppauge High School, Hauppauge, New York 11788, ²Great Oak High School, Temecula, CA 92592, ³Jericho High School, Jericho, New York 11753, ⁴Fremont Christian High School, Fremont, California 94536, ⁵Lawrence High School, Cedarhurst, NY 11516, ⁶Stuyvesant High School, New York City, New York 10282, ⁷Seoul International School, Seongnam, South Korea 13113, ⁸Shenzhen Middle School, ⁹Stony Brook University, ¹⁰Tufts University, ¹¹Vassar College

Titanium dioxide (TiO₂) is used in cosmetic products due to its ability to perform as a UV catalyst as well as its ideal optical properties. Heightened exposure to TiO₂ nanoparticles has raised concerns regarding its effects on human skin tissue/cell abilities to carry out essential processes [1]. One such concern is whether the nanoparticle presence impacts cellular response to bacteria eminent in skin. In order to investigate this question, varying concentrations of the nanoparticles were tested on both dermal fibroblasts and HUVEC cells, grown in media infected with *Staphylococcus aureus*, a bacteria that commonly lives on human skin. *S. aureus* was sampled from infected cells, and agar plate counts of colonies formed from these samples after two days of culture revealed relative bacterial infection for each concentration. We found that bacterial infection increased significantly with respect to increasing TiO₂ concentration in fibroblasts (**Figure 1**), while the opposite trend was observed for HUVEC cells.

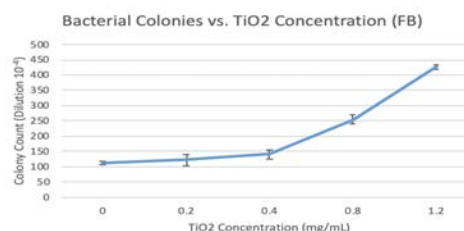


Figure 1. Fibroblast bacterial infection

In the past, a similar result has been shown in HeLa cells, where exposure to TiO₂ NPs reduces resistance to bacterial infection by *S. aureus*. This result has been tied to an increase in cholesterol outside of the cell membrane by upregulation of ABCA1 and ABCG1 genes in response to TiO₂ [2]. Cholesterol aids infection because *S. aureus* requires cholesterol for membrane attachment. Our experiment repeated a similar procedure in fibroblast cells. We hypothesized that since fibroblasts showed increased bacterial infection with TiO₂, the same genes would be upregulated in TiO₂, finding the increase to be due to cholesterol as seen in HeLa cells. The GAPDH gene was used as the reference gene for the experiment, as it would not be impacted upon regulation of gene expression. Then, the genes ABCA1 and ABCG1 were assessed for their expression using RT-PCR. However, the results showed that the genes were downregulated (**Figure 2**), suggesting that increasing cholesterol levels may not be the mechanism behind the increased infection, contrary to our hypothesis.

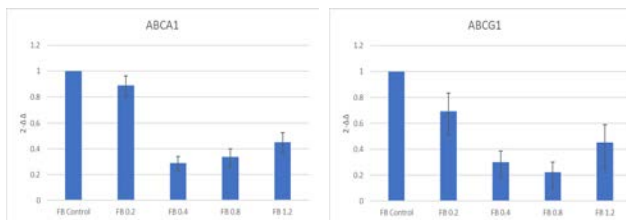


Figure 2. ABCA1 and ABCG1 RT PCR results showing downregulation

We will repeat the experiment with fibroblasts but will add a cholesterol blocker to confirm these results, as well as with HeLa cells to confirm the previous results.

[1] Dréno, B., Alexis, A., Chuberre, B. and Marinovich, M. (2019), Safety of titanium dioxide nanoparticles in cosmetics. *J Eur Acad Dermatol Venereol*, 33: 34-46. <https://doi.org/10.1111/jdv.15943>

[2] Fan Yang, Shu-Lin Liu, Yan Xu, Stephen G. Walker, Wonhwa Cho, Tatsiana Mironava, Miriam Rafailovich, The impact of TiO₂ nanoparticle exposure on transmembrane cholesterol transport and enhanced bacterial infectivity in HeLa cells, *Acta Biomaterialia*, Volume 135, 2021, Pages 606-616, ISSN 1742-7061, <https://doi.org/10.1016/j.actbio.2021.08.012>

Determining the Efficacy of Using Transposase (Tn5) to Cut DNA on PMMA Surfaces

Tanya Shukla¹, Yuhang Wu², Jonathan Sokolov³

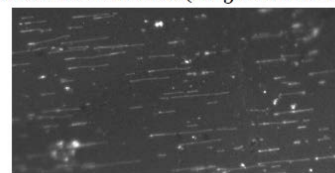
¹Ardley High School, NY, 10502, ²Worcester Academy, MA, 01604, ³Stony Brook University, NY, 11794

DNA sequencing technology has evolved rapidly in the past decade. One of the most promising sequencing technologies is the Next Generation Sequencing (NGS) which streamlines the process of DNA sequencing. Sequencing a whole chromosome at once is impossible, much less the entire genome. Therefore cutting the DNA into sequenceable portions is vital [1]. After cutting, the DNA is submerged in a buffer solution, however, its orientation is consequently lost, requiring a complex computational method for reassembly. Use of soft lithography and hydrophobic surface can be effectively used to solve the ordering problem in a cut DNA segment. The Transposase (Tn5) enzyme is commonly used to cut DNA strands. This work tests the ability of Tn5 enzyme to fragment a DNA strand on a PMMA surface.

In this work, Tn5 solution was made by mixing transposase solution, Tagmantase buffer, and water. Using diamond cutters, the silicon wafers were cut into 6 mm wide and 15 mm long samples to be spun cast with PMMA. The wafers were dipped into DNA solution and later in Tn5 solution for the DNA-cutting reaction. Using the Leica Fluorescent microscope, images of the DNA strands were taken and then used for data analysis. To test the efficacy of using SDS soap solution and Proteinase K as a Tn5 removal agent, this experimental procedure was repeated for different concentrations of Tn5 solutions (5 μ L, 10 μ L, and 20 μ L) for both SDS and Proteinase K reactions. Additionally, Proteinase K reactions were repeated at both room temperature as well as 55°C.

The results indicate that after Proteinase K removed Tn5, DNA strands were cut into smaller and linear segments that were easily sequenceable; while with SDS, the DNA strands were curled up and in disorder. The trials with Proteinase K were analyzed using ImageJ. It was found that DNA strands were shorter after the Tn5 reaction, meaning that Tn5 had cut the strands to a fewer number of base pairs. The average length of DNA strands decreased greatly after Tn5 was applied. This indicates that Tn5 can effectively separate DNA into small segments to be more easily sequenced, which is useful for more complete and efficient sequencing genomes. It was also found that the Proteinase K removal method works equally well at both room temperature and at 55°C.

Before Proteinase K (Tn 5 still attached)



After Proteinase K (Tn 5 removed)

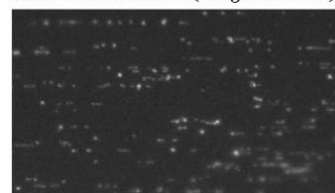


Figure 1. Visual Comparison of DNA Strands before and after Tn5 reaction

Average Length of DNA Strands (microns) After Tn5 Reaction

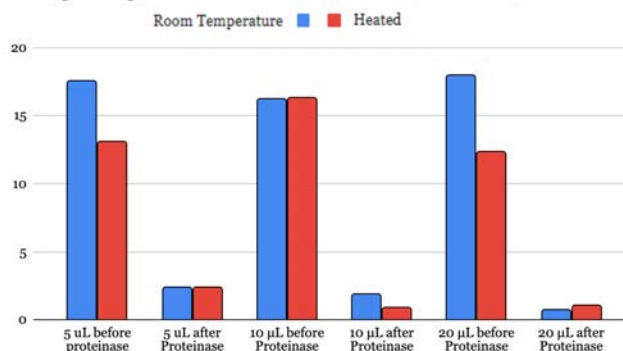


Figure 2. Average Length of DNA Strands in various Tn5 solutions

[1] Goodwin, S., McPherson, J. D., & McCombie, W. R. (2016). Coming of age: Ten Years of next-generation Sequencing Technologies. *Nature Reviews Genetics*, 17(6), 333–351. <https://doi.org/10.1038/nrg.2016.49>

[2] Cho, N. H., Goodwin, S., Budassi, J., Zhu, K., McCombie, W. R., & Sokolov, J. (2017). Fragmentation of surface adsorbed and aligned DNA molecules using soft lithography for next-generation sequencing. *Journal of Biosensors & Bioelectronics*, 08(04). <https://doi.org/10.4172/2155-6210.1000247>

Determining the Extent to Which Sodium Dodecyl Sulfate Could Desorb DNA from Flat Surfaces

Derek Days¹, Ohm Patel², Jonathan Sokolov³

¹Noble and Greenough School, Dedham, MA, 02026, ²Patchogue-Medford High School, Medford, NY, 11763,

³Stony Brook University, Stony Brook, NY, 11794

The use of Tn5 transposases is essential to Next Generation Sequencing (NGS) as it is required to both cut DNA into shorter and more manageable lengths while also labeling the shortened strands to be later rearranged into the original sequence.¹ However, Tn5 transposases have to wrap around DNA in order to cut, posing an issue for surface-adsorbed DNA samples.² In recent transposon experiments, evidence to suggest that sodium dodecyl sulfate (SDS), which is already used to remove the Tn5 transposases from DNA molecules after cutting is complete, could desorb the DNA from a flat surface specifically polymethyl methacrylate (PMMA) spun-cast on silicon. Finding a method of desorbing DNA from a flat surface remains important because it provides an opportunity to increase the efficiency and decrease the cost of NGS in fields such as medical diagnoses and forensic science. Although there are already existing methods of desorbing DNA, they are cumbersome and time consuming. In this study, we aimed to investigate whether or not SDS could desorb surface-adsorbed DNA. To do this, 0.286% DNA in DNase buffer dyed with SYBR Gold was prepared and machine-dipped onto PMMA spun-cast onto silicon. After doing so, the DNA sample was imaged under a fluorescence microscope under 63x magnification to determine the quality of the sample. Once the quality was confirmed, the sample was placed into a well containing 350 μ L of varying concentrations of SDS in water. This way, half of the wafer would have been treated with SDS while the other side would serve as a control. The wafer, still in the well, was then placed into a column heater and heated for 55°C for 20 minutes. Once finished, the wafer was once again placed under the microscope for analysis.



Figure 1. Border between SDS-treated half (dark) and non-SDS

Initially, it was thought that the SDS did in fact desorb the DNA from the surface as no DNA could be seen in the SDS-treated side. However after re-dyeing the SDS-treated side in SYBR Gold, DNA was once again shown on the surface. This implied that SDS could not desorb surface-adsorbed DNA but could remove SYBR Gold dye from DNA. Although SDS likely cannot desorb surface-adsorbed DNA, future experiments will be done on Triton X-100 instead in an effort to find an easier method of desorbing DNA from flat surfaces.

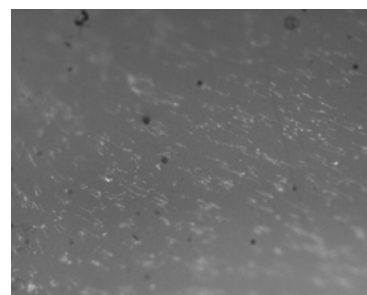


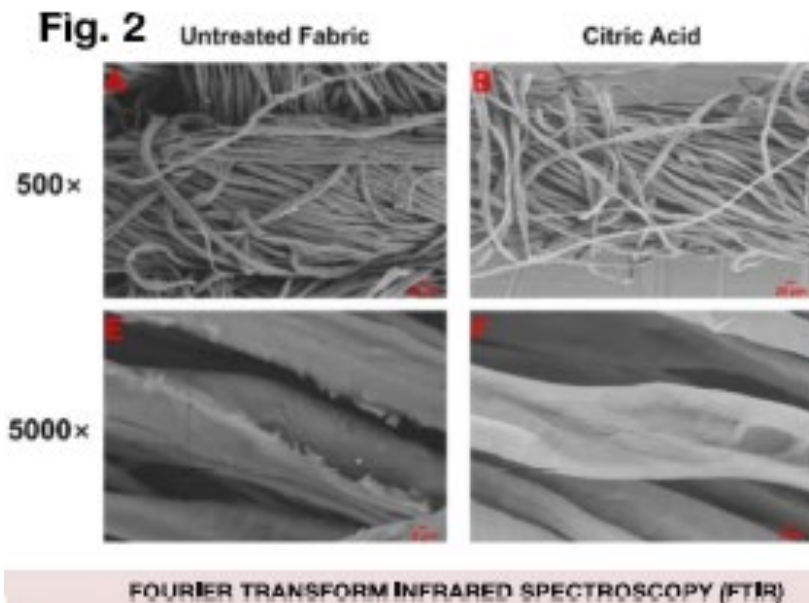
Figure 2. Border between SDS-treated half and non-SDS after re-dyeing

¹ Feng, Kuan. "Comprehensive Sequencing with Surface Tagmentation Based Technology." (2018). https://digitalrepository.unm.edu/biom_etds/188

² Cho N, Goodwin S, Budassi J, Zhu K, McCombie WR, et al. (2017) Fragmentation of Surface Adsorbed and Aligned DNA Molecules using Soft Lithography for Next-Generation Sequencing. *J Biosens Bioelectron* 8: 247. doi: 10.4172/2155-6210.1000247

Session 7: Repurposing Cellulose & Longest Living Oral Bacteria

Chairs: Dr. Michael Cuiffo, Tony Deluxe



| Strain | 310 bp | 941 bp | 404 bp |
|--------------------|--------|--------|--------|
| ladder (1 kb) | + | + | + |
| B50 PL0 D2 | + | - | + |
| B50 PL30 D3 | + | - | + |
| 13 bottom D4 | + | + | + |
| 13 top D5 | + | + | + |
| B50 PL0 D | + | + | + |
| B35 NCC D8 | + | + | + |
| B35 PCE D7 (small) | + | + | + |
| B35 PCE D7 (large) | + | + | + |

Figure 1: PCR assay selective for *E. faecalis*

Analysis of microorganisms associated with failed endodontic treatment in fifteen-year-old samples of root canals

Tony Deluxe¹, Michelle Bok², Andrew Zhang³, Shreya Tiwari⁴, Stephen Walker⁵, Miriam Rafailovich

¹College of Art and Science, New York University, NY 10003; ²Seoul International School, Seoul, South Korea;

³Del Norte High School, San Diego, CA 92127, USA; ⁴Westwood High School, Austin, TX, 78750, USA;

⁵Department of Oral Biology and Pathology, Stony Brook University, NY 11794

1. BACKGROUND

Enterococcus faecalis is a gram-positive microbe, known as the main factor causing endodontic treatment failure, that has been observed to survive for prolonged periods of nutritional deprivation under harsh conditions. This microbe is often found in the human oral cavity or gastrointestinal tract and is resistant to many common antibiotics such as vancomycin. *E. faecalis* is known for its resilience. It has been found to survive harsh conditions such as at 10°C or 45°C, acidic or basic conditions, in ethanol, in hydrogen peroxide, or under UV irradiation.¹ Previous studies found that the bacterium survived *ex vivo* for approximately 12 months²; The current study utilized samples collected from a root canal study that was conducted 16 years ago to determine if *E. faecalis* could survive after lying dormant in a desiccated state for 16 years.

2. METHODS

A. Confirming identity of Samples: Infected root canals prepared during the 2006 study were left in glass vials wrapped in parafilm that desiccated over time. Samples were rehydrated with 1 mL of BHI (Brain-Heart Infusion) broth per sample and then incubated for 2 days at 37°C. 100 µL of broth was taken from each sample, plated on KF Streptococcus agar, and then incubated for 2 days at 37°C. Plates were checked for growth: samples that showed growth were plated and incubated once more for 2 days at 37°C. A loop of growth was taken from these samples, placed in solution, and spun in a centrifuge. Samples were then frozen at -80°C.

E. faecalis was identified in samples using polymerase chain reaction (PCR)³. Four PCR procedures were carried out using supernatant from the centrifuged samples, primers, dNTPs, MgCl₂, buffer, and Taq polymerase. The first procedure used primers that amplify the 16S gene coding for 16S rRNA, which is common to all bacteria. The second procedure used primers that amplify a section of the 16S gene that is specific to *E. faecalis*. The third used primers for the *vanA* gene encoding vancomycin resistance⁴; the final procedure was carried out using primers for genes in the Entner-Doudoroff pathway.⁵

B. Biofilm Assay: Assessing strength of E. faecalis biofilms against common treatments

Another major focus in the project was comparing the durability of different dental detergent candidates against *E. faecalis*. On the microtiter plate, the 8 different strains were treated with crystal violet and the samples of Triton, solution 2 (an unknown endodontic polymer developed by the dental school), and the negative control (phosphate buffered saline). Relative absorbances were measured using spectrophotometry.

3. RESULTS

A. PCR Results

Two PCR products with sizes of ca. 310 and 404 bp resulting from amplification of portions of the 16S gene specific to *E. faecalis* and genes in the Entner-Doudoroff pathway were obtained for all six samples of *E. faecalis* from the root canal study. PCR products with sizes of ca. 941 bp resulting from amplification of portions of the *vanA* gene were observed in 4 of the 6 samples tested.

B. Biofilm Assay Results

Through the spectrophotometer, the obtained results for both sealants demonstrated a statistically significant difference between the negative control while there were minimal differences between the two types of treatments. Both the Normality Test and the Equal Variance Test were passed with P-values of 0.296 and 0.441, respectively.

4. CONCLUSIONS

Samples of *E. faecalis* collected 16 years ago in a root canal study are still able to be resurrected, demonstrating *E. faecalis* can survive under harsh conditions for very long periods of nutritional deprivation. The future direction of research is to conduct biofilm experiments to understand the mechanism that allowed such long survival.

Sequencing of the 16S gene in strains that showed the strongest biofilm formation could help assess potential causes of their long-term survival.

Citations:

1] Halkai, R., Hegde, M.N., Halkai, K. "Enterococcus faecalis can survive extreme challenges – overview." Journal of Health and Allied Sciences NU, Vol. 2, No. 3, doi: 10.1055/s-0040-1703595

2] Sedgley, C M et al. "Survival of Enterococcus faecalis in root canals ex vivo." International endodontic journal vol. 38,10 (2005): 735-42. doi:10.1111/j.1365-2591.2005.01009.x

3] Siqueira, J.F. and Rocas, I.N. "Polymerase chain reaction–based analysis of microorganisms associated with failed endodontic treatment." Oral Surg Oral Med Oral Pathol Oral Radiol Endod 2004; 97:85-94, doi: 10.1016/s1079-2104(03)00353-6

4] P., Dutka-Malen S;Evers S;Courvalin. "Detection of Glycopeptide Resistance Genotypes and Identification to the Species Level of Clinically Relevant Enterococci by PCR." Journal of Clinical Microbiology, U.S. National Library of Medicine, pubmed.ncbi.nlm.nih.gov/7699051/.

5] SG;, Peykov SZ;Aleksandrova VD;Dimov. "Rapid Identification of Enterococcus Faecalis by Species-Specific Primers Based on the Genes Involved in the Entner-Doudoroff Pathway." Molecular Biology Reports, U.S. National Library of Medicine, pubmed.ncbi.nlm.nih.gov/22307795/.

Deweaving Cotton Cloth using Non-Toxic and Environmentally-Friendly Methods

Ivan Yuan¹, Elizabeth Zhang², Hannah Tao³, Andrew Yuen⁴, Aleena Sheikh⁵, Michael Cuiffo⁶, and Miriam Rafailovich⁶

¹Shanghai High School International Division, Shanghai, China 200237; ²Massachusetts Institute of Technology, Cambridge, MA 02139;

³Academy for Information Technology, Scotch Plains, NJ 07092; ⁴Jericho High School, Jericho, NY, 11753; ⁵Department of Materials Science and Chemical Engineering, Stony Brook University, Stony Brook, NY, 11794

As the demand for cellulosic fibers increases, the amount of cotton fabric wastes produced also increases. Many methods currently available for recycling cellulose involve costly and potentially hazardous reagents such as ionic liquids and N-methylmorpholine-N-oxide [1]. Thus, we will show that mild physical and chemical treatments can deweave cotton fabric into fibers that can then be re-woven or repurposed for a variety of applications.

Diagonally-cut cotton muslin fabric pieces of around 0.25 g were deweaved using a 40 mL solution of 0.5 M citric acid, 0.5 M sodium nitrate, or a 3:1 mixture of the two aforementioned solutions, being stirred at 600 rpm and 50°C. All samples were subsequently dried. The deweaving solution was shown to successfully deweave material up to three times. However, significant decreases in solution volume and pH, and fiber bleaching imply that the solution would need to be replenished by adding fresh stock solution after each reuse.

The untreated fabric and deweaved fibers were examined using Fourier-transform infrared (FTIR) spectroscopy (**Figure 1**). FTIR analysis indicates preservation of the β -glycosidic linkage (898 cm^{-1}) in cellulose as well as other peaks characteristic of cellulose. Comparison of the peak associated with the C=O stretching vibration (1727 cm^{-1}) shows that this peak is insignificant for the untreated cotton fabric and the fibers deweaved with sodium nitrate, but is clearly seen in the fibers deweaved with the 3:1 mixture and is even higher in the fibers deweaved with citric acid, suggesting that esterification between citric acid and cellulose occurred. The total crystallinity index and the lateral order index were computed with peak heights [2], and no substantial changes were seen, suggesting minimal alteration to the arrangement of cellulose polymers.

To confirm the possibility of esterification occurring during deweaving, a back titration was performed on a dry fiber sample deweaved with citric acid by first adding sodium hydroxide and then titrating with hydrochloric acid, using a methyl red indicator. The fibers were tinted pink after each trial, indicating an acidic fiber surface, which may imply the presence of citrate groups from esterification.

Zeta potential measurements were performed on the solution after deweaving. Negative zeta potential values (-3 to -6 mV) were observed due to the microfibers suspended within the deweaving solution. Fibers were imaged with optical and scanning electron microscopy (SEM). Optical microscopy showed contaminants on the cotton scrap fabric that were removed after deweaving. SEM demonstrated that the structure of fiber bundles is mostly preserved, albeit with roughening of fiber surfaces and the increase of spacing between fibers.

Tensile strength tests were conducted on individual fibers to characterize mechanical changes after deweaving. Compared to fibers from the untreated fabric, fibers deweaved with citric acid have a lower ultimate tensile strength (175 MPa compared to 404 MPa) but a greater elongation at rupture (5.8% compared to 4.6%). However, the untreated fibers snapped upon reaching the ultimate tensile strength, while the deweaved fibers gradually disintegrated, suggesting that the decrease in strength is likely due to physical, rather than chemical, changes.

In the future, we would like to further characterize the fibers' mechanical changes and quantify the degree of esterification to clarify the chemical basis for deweaving. Experiments are currently underway to use a different cutting shape, allowing for trials to scale up the deweaving process for recycling cotton fabric on a larger scale.

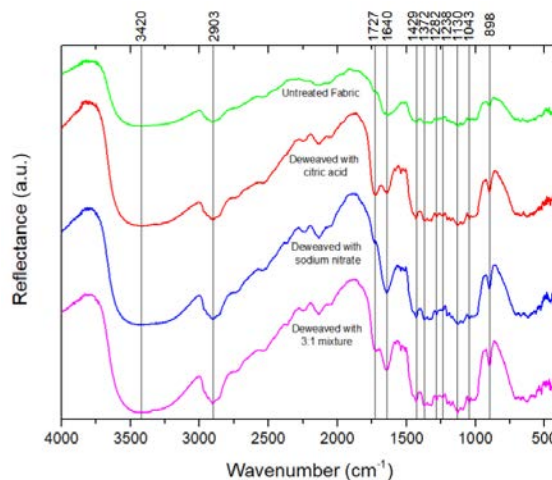


Figure 1. FTIR spectra of untreated and deweaved fibers.

[1] El Seoud, Omar A., et al. "Cellulose Regeneration and Chemical Recycling: Closing the 'Cellulose Gap' Using Environmentally Benign Solvents." *Macromolecular Materials and Engineering*, vol. 305, no. 4, Apr. 2020, p. 1900832. DOI.org (Crossref), <https://doi.org/10.1002/mame.201900832>.

[2] Nelson, Mary L., and Robert T. O'Connor. "Relation of certain infrared bands to cellulose crystallinity and crystal lattice type. Part II. A new infrared ratio for estimation of crystallinity in celluloses I and II." *Journal of Applied Polymer Science* 8.3 (1964): 1325-1341.

Repurposing Waste Fabric by Synthesizing Silver Nanoparticles on Deweaved Cotton Fibers

Ivan Yuan¹, Elizabeth Zhang², Hannah Tao³, Andrew Yuen⁴, Aleena Sheikh⁵, Michael Cuiffo⁶, and Miriam Rafailovich⁶

¹Shanghai High School International Division, Shanghai, China 200237; ²Massachusetts Institute of Technology, Cambridge, MA 02139; ³Academy for Information Technology, Scotch Plains, NJ 07092; ⁴Jericho High School, Jericho, NY, 11753; ⁵Department of Materials Science and Chemical Engineering, Stony Brook University, Stony Brook, NY, 11794

Silver nanoparticles (Ag NPs) have well-studied antimicrobial properties effective against many types of bacteria and fungi. Applications of Ag NPs in textiles have gained worldwide attention due to the importance of antimicrobial textiles for wound dressings, medical equipment and staff uniforms, bedsheets, and others. Because textiles serve as a medium for microbe growth and cross-contamination, there is a growing demand for antimicrobial textiles [1]. Ag NPs have also been experimentally found to have high conductive and catalytic activities, although frequently agglomerate during catalytic processes due to strong Van der Waals forces and high surface energy. A stabilizing agent such as cellulose fibers can prevent such agglomeration and stabilize silver nanoparticle catalysts [2]. To reduce waste, especially since the textile industry produces over 10 million tons of waste cotton cloth globally each year, this study seeks to synthesize Ag NPs on discarded cotton muslin tailoring cloth [3]. Cotton fabric can be deweaved into cellulose fibers, which act as a stabilizing agent on which silver nanoparticles can be synthesized through the reduction of silver nitrate with trace amounts of sodium borohydride.

Diagonally-cut fabric pieces of approximately 0.25 g were deweaved using a 40 mL solution of 0.5 M citric acid, being stirred at 600-800 rpm and 50-60 °C. After washing with deionized water and drying, Ag NPs were synthesized on the fibers through immersion in a 20 mL solution of 0.01 M silver nitrate and reduction through 2 to 6 drops of 0.01 M sodium borohydride. A portion of samples were ultrasonicated for 20 minutes at 40 °C, while other samples were ultrasonicated for 30 minutes at 40 °C. All samples were subsequently dried.

The Ag NP material imaged using scanning electron microscopy (SEM) to visualize size and features of the nanoparticles (Figure 1). Energy-dispersive X-ray analysis (EDX) was simultaneously performed to the existence of silver on the fabric. The fibers heated for 20 minutes in the ultrasonicator

showed more and finer nanoparticles than the samples ultrasonicated for 30 minutes. The 30-minute samples showed more agglomeration of nanoparticles and a higher silver peak in EDX. The size of the nanoparticles analyzed on both samples were below 40 nm in diameter.

Zeta potential tests were performed on the Ag NP synthesis solution (containing silver nitrate, sodium borohydride, and silver nanoparticles). The samples heated at 20 minutes showed a zeta potential of -29.32 mV, while the samples heated at 30 minutes showed a zeta potential of -27.32 mV, suggesting that the silver nanoparticles synthesized are relatively stable and would not agglomerate rapidly in solution.

In the future, further tests, such as dynamic light scattering (DLS) and transmission electron microscopy (TEM), will be performed to characterize the size of the Ag NPs formed. The catalytic properties of the silver nanoparticles formed will also be examined through electrochemical methods and organic dye degradation tests.

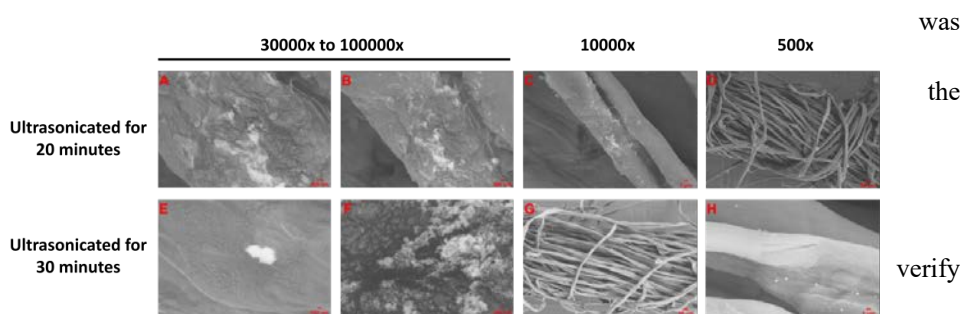


Figure 1. SEM images of fiber samples with Ag NPs synthesized (magnifications from 500x to 100000x).

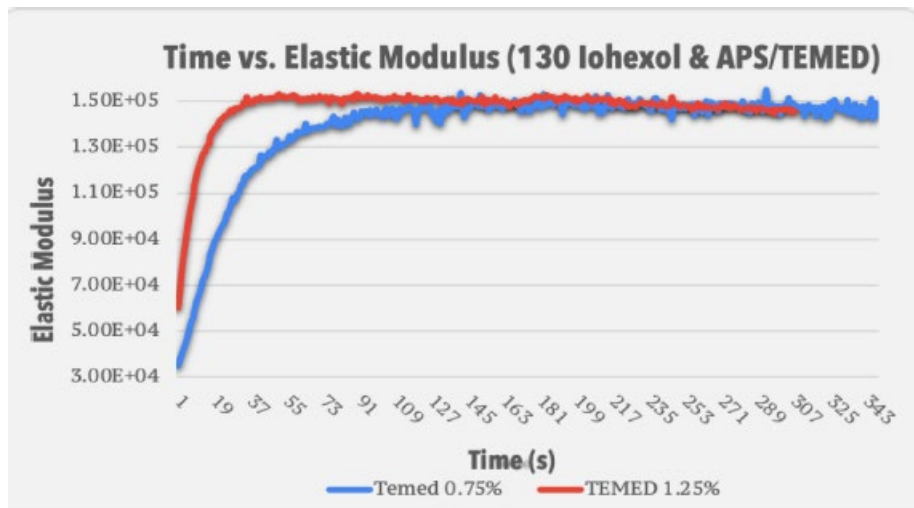
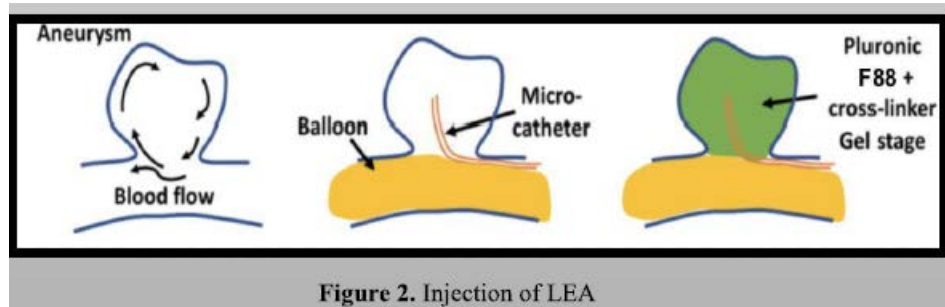
[1] Mori, Yasutaka, et al. "Antiviral activity of silver nanoparticle/chitosan composites against H1N1 influenza A virus." *Nanoscale research letters* 8.1 (2013): 1-6.

[2] Jiang, Zhong-Jie, et al. "Catalytic Properties of Silver Nanoparticles Supported on Silica Spheres." *The Journal of Physical Chemistry B*, vol. 109, no. 5, Feb. 2005, pp. 1730–35. DOI.org (Crossref), <https://doi.org/10.1021/jp046032g>.

[3] Mohamed, Siti Hajar, et al. "Recycling Waste Cotton Cloths for the Isolation of Cellulose Nanocrystals: A Sustainable Approach." *Polymers* 13.4 (2021): 626.

Session 8: Liquid Embolic Agents

Chairs: Robert Wong, Dr. Aaron Sloutski



Optimizing a Minimally Invasive Reverse Thermo-Responsive Liquid Embolic Agent Polymer Treatment for Brain Aneurysms

Noah Fensterheim¹, Elaina Heghes², Shaheer Khan³, Dohyun Kim⁴, Briana Poon⁵, Evelyn Shue⁶, Lorenzo Verona⁷, Megha Gopal⁸, Aaron Sloutski⁸, Robert Wong⁸, Chandramouli Sadasivan⁸, Miriam Rafailovich⁸

¹Ida Crown Jewish Academy, Skokie, IL 60076; ²South Side High School, Rockville Centre, NY 11570; ³Half Hollow Hills High School East, Dix Hills, NY 11746; ⁴Seoul Foreign School, Seoul, South Korea; ⁵Arlington High School, NY 12540; ⁶Richard Montgomery High School, Rockville, MD 20852; ⁷American School of Milan, Noverasco MI, Italy; ⁸Department of Materials Science and Chemical Engineering, Stony Brook University, Stony Brook, NY 11794

*Authors 1-7 contributed equally to this work

Brain aneurysms are sac-like pathological dilations of intracranial blood vessels which, if left untreated, can rupture and cause fatal brain hemorrhaging or ischemic strokes. Current treatments only yield a success rate of approximately 20-30%^[1,2] or lower. We take an innovative approach by developing a reverse-thermoresponsive, biodegradable polymer gel that conforms to the aneurysm's shape once injected. The process may be assisted with a balloon in the parent vessel to prevent the gel from seeping out of the aneurysm. The gel will promote vascular remodeling and endothelialization.

Samples of pluronic F88-DMA polymer were dissolved in deionized (DEI) water, 90 mg/mL iohexol, and 130 mg/mL iohexol to form stock gel solutions, each with a concentration of 38% F88-DMA. The stocks were further diluted with respective solvents to form intermediate stock solutions of 29.96% F88-DMA. The solutions were then mixed with ammonium persulfate (APS) and tetramethylethyldiamine (TEMED) crosslinker solutions of varying concentrations, whose solvent matched that of the intermediate solution. Each solution's elastic modulus was determined through rheometry via a Bohlin Gemini 150 HR Nano Rheometer. Results suggest that higher concentrations of TEMED caused the gel to crosslink faster (Fig. 1).

Solutions were also prepared with 3 additives: PEGDMA, tetronic 904 and tetronic 1107, diluted in DEI. Gel solutions were then crosslinked into cylinders using molds to test the viability of each solvent, additive, and respective concentration for long-term stability. Each cylinder was placed in a 0.9% saline solution and incubated at 37°C for several days. Daily rheology tests were performed on the cylinders to determine the elastic modulus of the cylinders over time. Cylinders with additives are expected to crosslink tighter due to the additives' shorter polymer chains, and thus swell less while submerged under water.

Two *in vivo* experiments were also conducted to assess injectability and stability of the gel. In the first experiment, blood was first drawn and deposited into three test tubes with different crosslinking solutions. Based on the thrombus formed within each solution, it was determined that APS/TEMED was the only non-thrombogenic crosslinker, so ensuing experimentation thus prioritized usage of the APS/TEMED crosslinker. Following the blood tests, three 1.25% TEMED/APS and F88-DMA injections were then administered so the stability of the gels injected could be assessed. The first two injections were washed away by blood flow, so the third trial thus utilized a balloon to block blood flow for ten minutes in order for the gel to crosslink inside the aneurysm. The procedure was successful but the gel crosslinked to the balloon, so experimenters were unable to assess the behavior of the gel once exposed to blood flow.

The second *in vivo* experiment involved two injections of F88-DMA: one with 1.75% TEMED, and the other with 1.25% TEMED. The first injection was unsuccessful, as the gel crosslinked within the catheter. In the second trial, the gel also crosslinked mid-injection, but a small amount was successfully injected into the rabbit. In the following weeks, the rabbit will be monitored in a survival experiment, and the vessel will ultimately be explanted to study cell growth and gel behavior.

Current *in vivo* experiments and rheology of pluronic F88-DMA polymer show promising results and identify specific areas in need of improvement. Further *in vitro* research will focus on APS/TEMED cytotoxicity, gel biodegradability, adhesivity of crosslinked gels to cells, and effects of additives on gel swelling and micropore formation to promote endothelialization.

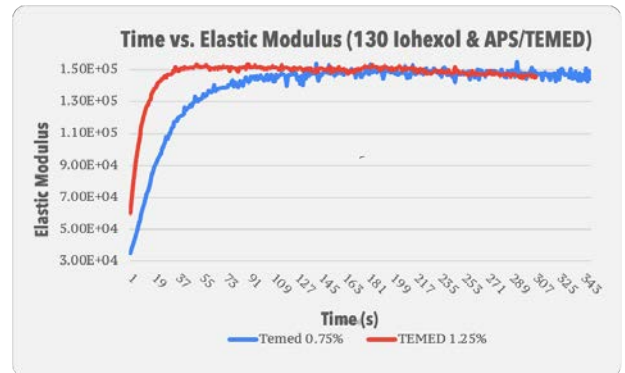


Figure 1: Time sweep and elastic modulus of 29.96% concentration F88-DMA in 130 mg/mL iohexol with varying TEMED concentrations of 0.75% and 1.25%

¹ Taschner CA, Chapot R, Costalat V, Machi P, Courtheoux P, Barreau X, et al. Second-Generation Hydrogel Coils for the Endovascular Treatment of Intracranial Aneurysms: A Randomized Controlled Trial. *Stroke*. 2018;49(3):667-74.

² Adeeb N, Moore JM, Wirtz M, Griessenauer CJ, Foreman PM, Shallwani H, et al. Predictors of Incomplete Occlusion following Pipeline Embolization of Intracranial Aneurysms: Is It Less Effective in Older Patients? *AJNR Am J Neuroradiol*. 2017;38(12):2295-300.

Cell-Adhesiveness of Poly(vinyl Alcohol) and Additives as Potential Vascular Graft Material

Caroline Brown¹, Sophia Chen², Sahana Dhama³, Emma Gao⁴, Aaron Sloutski⁵, Robert Wong⁶

¹Williamsville North High School, Williamsville, NY 14221, ²Sage Hill School, Newport Coast, CA 92657, ³The Wheatley School, Old Westbury, NY 11568 ⁴The Harker School, San Jose, CA 95129 ⁵Stony Brook University, Stony Brook, NY 11794, ⁶Stony Brook University

Failure of small-scale vascular grafts most often occurs due to thrombosis and intimal hyperplasia. Current research is investigating polymer modifications that can promote cell adhesion and reduce thrombogenicity. Polyvinyl alcohol (PVA) is a promising material, and prior research has studied the cell-adhesive properties of PVA mixed with gelatin¹ and fibrinogen. One untested additive is RDP-clay, a phosphate ester flame retardant that has been shown to promote adhesion of dental pulp stem cells and dermal fibroblasts². Adding RDP-clay to PVA may form more reliable vascular grafts.

Solutions of RDP-clay and PVA were prepared at concentrations of 1%, 2.5%, and 5% and sterilized by autoclaving at 121°C for 1 hour. Three wells of each solution and a control were filled in 24-well plates. After cross-linking with STMP and NaOH in a freeze-dry cycle and performing a media exchange 3 times, GFP-modified fibroblasts were plated on the gels.

On Days 1, 3, and 6, the cells in one well plate were fixed and stained with DAPI. The cell structure, visualized by GFP, and cell nuclei, visualized by DAPI, were studied using EVOS microscopy. The results were consistent across all 3 days, and images in **Figure 1** are from day 1.

Solution thrombogenicity was tested by spin-casting PVA and RDP-clay solutions onto square centimeter Si wafers with a polystyrene solution as a positive control. A fibrinogen solution was added onto half of the wafers. Fibers formed on the polystyrene but not on the RDP-clay wafers, indicating that RDP-clay does not promote thrombogenicity. In addition, rheology tests showed that the elastic modulus of the crosslinked gels increased with the clay concentration, and the elastic moduli of the gelatin gel and 1% RDP-clay gel were similar, as seen in Figure 1.

The gels with RDP-clay mixed in had non-significant cell growth due to clay particles sinking to the bottom, so further directions include sifting RDP-clay onto the gel, which may reduce clumping.

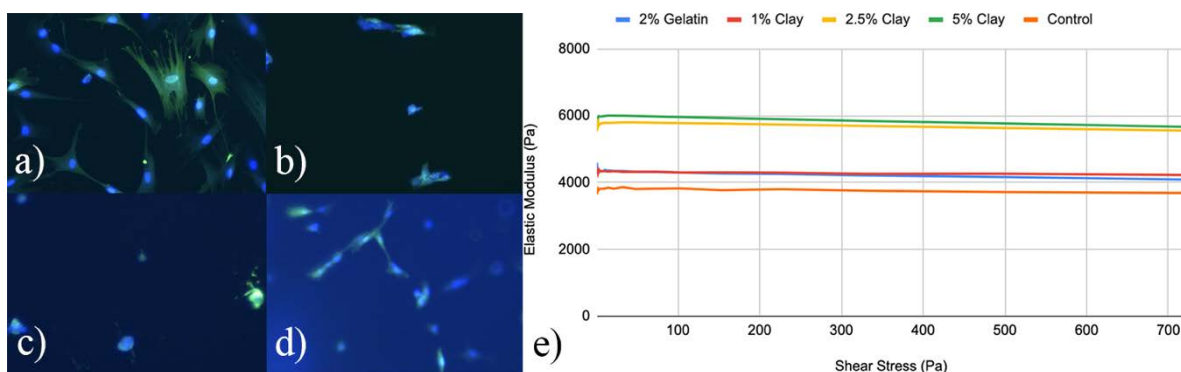


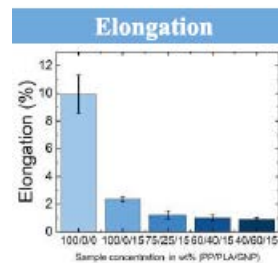
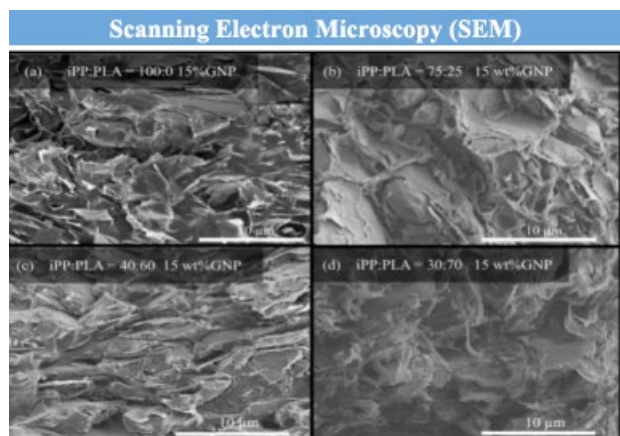
Figure 1. a) No gel - high density, many cell connections. b) Pure PVA gel - lower density, few cell connections. c) 2% gelatin gel - insignificantly different from pure PVA gel. d) Fibrinogen gel - higher density, longer cell connections. e) Elastic modulus vs. shear stress from rheology on all gels

¹ Rizwan M, Yao Y, Gorbet MB, Tse J, Anderson DEJ, Hinds MT, Yim EKF. One-Pot Covalent Grafting of Gelatin on Poly(Vinyl Alcohol) Hydrogel to Enhance Endothelialization and Hemocompatibility for Synthetic Vascular Graft Applications. *ACS Appl Bio Mater.* 2020;3(1):693-703. Epub 2020/07/14. doi: 10.1021/acsabm.9b01026. PubMed PMID: 32656504; PMCID: PMC7351135.

² Feng K-C, Ho E, Murthy B, Patel R, Deluxe A, Wen-qi, Zhao, Chang B, Zumba N, Chang C-C, Simon M, Rafailovich MH, editors. Investigating the Effects of Different Spun-Cast and Molded Polylactic Acid (PLA) and Polystyrene (PS) Composites on the Proliferation, Differentiation and Biomineralization of Dental Pulp Stem Cells. *Materials Research Society Fall Meeting*; 2018 Nov 25-30; Boston, USA.

Session 9: Polymer Blends

Chairs: Yu-Chung Lin, Yiwei Fang



- Elongation data indicates brittleness of GNP; major challenge in manufacturing
 - FLIR thermal imaging showcases relative heat conductivity of nanocomposite

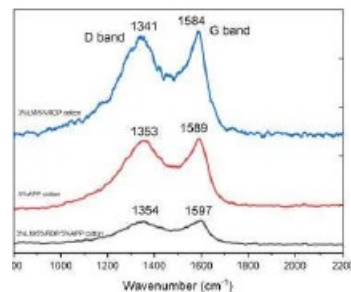
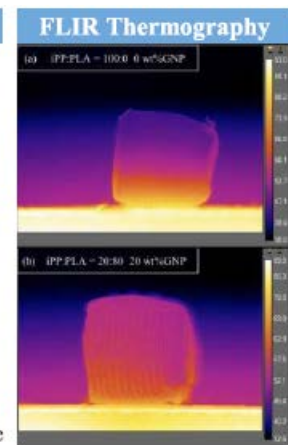


Figure 3: Raman Saturated Cotton

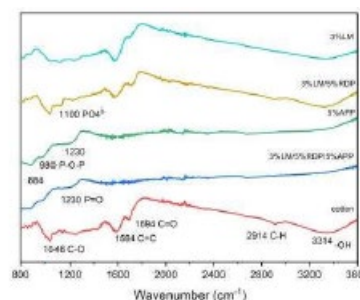


Figure 4: FT-IR Saturated Cotton

Optimizing Conductivity and Strength of Biodegradable Polymer Graphene Nanoplatelet Nanocomposites via 3D-Printing

Tavan Bhatia¹, Haaris Alam², Ruijia Zhang³, Gavin Onghai⁴, Yu-Chung Lin, Miriam Rafailovich

¹Staples High School, Westport, CT 06880, ²Portola High School, Irvine, CA 92618, ³Ed W. Clark High School, Las Vegas, NV 89102, ⁴Earl L. Vandermeulen High School, Port Jefferson, NY 11777

Electronic waste is a major cause of environmental pollution, releasing toxic chemicals such as lead, copper, and zinc into the environment. Thus, the engineering of a biodegradable and processable component of electronic systems is of great urgency. Graphene poses to be a promising candidate in replacing electrical components which are harmful to the environment. Graphene is an allotrope of carbon with distinct properties, such as incredible thermal and electrical conductivity as well as tensile strength. However, graphene is extremely difficult to isolate due to the limited and inefficient techniques there are to separate graphene sheets; graphene nano-platelets (GNP) are more accessible and can be used in place. By blending the strong and conductive GNP with biodegradable and non-corrosive polymers, these properties can be optimized. By adding polymers to GNP, ductility and ease of processing also improves. Previous research conducted by the Department of Material Science and Chemical Engineering at Stony Brook University has proven the effectiveness and capability of polymer graphene nanocomposites (PBAT-PLA-GNP) as a biodegradable replacement of convention environmentally harmful polymers, thermosets, and composites in the electronic industry.

This experiment aims to explore the possibility of using other polymer nanocomposite blends to achieve similar results with the additional 3D printable capabilities in further potential applications. Isostatic polypropylene (iPP) and polylactic acid (PLA) were used as polymers in this experiment. Due to the greater affinity between the GNP and the iPP as compared to the GNP and the PLA, bi-continuous pathways for GNP formed within iPP as areas of PLA repelled the GNP. In these composites, the GNP formed a bi-continuous structure as it was repelled by the PLA and drawn in by the iPP. The GNP % mass and iPP/PLA concentration ratio were modified to see their respective effects.

The ratios of iPP to PLA tested were 100/0, 85/15, 60/40, 50/50, 40/60, 30/70 and 20/80, and 15% and 20% mass percentages of GNP were tested as well. After blending and processing the samples, they were thermal pressed into rectangular prisms and extruded into a filament. This filament was 3D printed into small cubes to measure thermal conductivity as well as dog bone shapes to measure tensile strength, and the prisms were used to measure electrical conductivity.

Increasing GNP concentration directly correlated with increasing electrical and thermal conductivity. However, the samples were also more brittle and more difficult to 3D print and process. Current electrical conductivity data shows that the polymer blends have comparable conductivities to materials like silicon (Si) and gallium arsenide (GaAs) (Figure 1). SEM imaging has highlighted the bicontinuous GNP pathways as well as PLA domains that they are repelled from (Figure 2). FLIR thermal camera imaging has provided a relative effect of GNP on thermal efficiency (Figure 3). Tensile data reaffirms that GNP % is directly linked to brittleness, and future data will quantify and indicate the role that each material has on the mechanical properties of the system, Future research will consist of altering the iPP/PLA concentration ratio to explore the trend between the two polymers on electrical conductivity; specific thermal conductivities will be determined to find comparable mediums as well as quantify the effect of GNP %.

There are numerous applications of the creation of a 3D printable polymer blend which can be used in place of many electronic components, avoiding dire environmental consequences. Current data indicates a similarity in the properties of polymer blend to the properties of expensive elements of semiconductors. Optimizing the environmentally beneficial and durable properties of the polymers with the electrically and thermally efficient ones of the GNP yields exciting prospects for more sustainable technology and electronic systems.

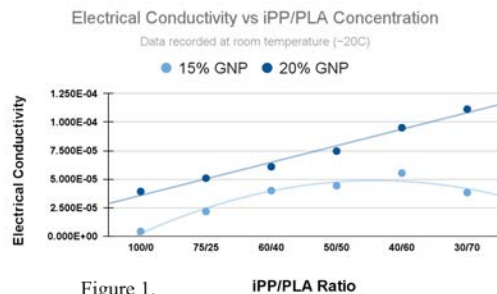


Figure 1. iPP/PLA Ratio

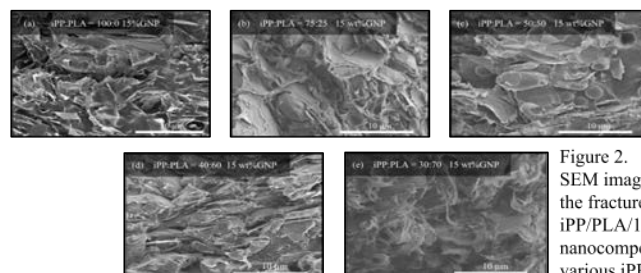


Figure 2. SEM image taken on the fracture surfaces of iPP/PLA/15wt%GNP nanocomposites at various iPP/PLA concentrations

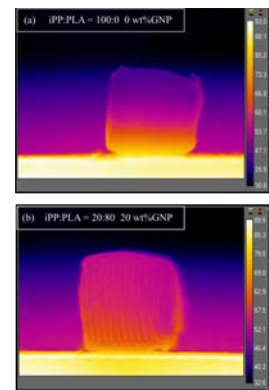


Figure 3. FLIR thermography of 3D printed iPP/PLA/15wt%GNP nanocomposites cubes, showing thermal conductivity.

Flame Retardant Polymer Blends Using Biopolymers

Minsik Shin¹, Christian Apostol², Allen Bethancourt², Yiwei Fang², Miriam Rafailovich²

¹ Seoul International School, South Korea, ² Stony Brook University, Stony Brook, NY 11794

Polymers such as Polylactic Acid (PLA), Ammonium Phosphate (APP), Resorcinol Bis (diphenyl Phosphate) (RDP), Biopolymer, and RDP-Cellulose display flame retardance when blended in tangent with various combinations of different polymers. APP and RDP have shown to increase flame retardancy from previous works, albeit with different combinations of polymers^[1,2],

| Sample | Mass (g) | Mass Composition (%) | Notes | Grade |
|---|------------|----------------------|--|-------|
| PLA/RDP | 46/4 | 92/8 | Both trials polymer melted, cotton ignited | V-2 |
| PLA/RDP | 45/5 | 90/10 | Both trials polymer melted, cotton ignited | V-2 |
| PLA/RDP/Biopolymer | 46.5/3/0.5 | 93/6/1 | First trial no cotton ignited, second trial cotton ignited | V-2 |
| PLA/RDP/Biopolymer | 46/3/1 | 92/6/2 | First trial no cotton ignited, second trial cotton ignited | V-2 |
| PLA | 50 | 100 | Both trials polymer melted, cotton ignited | V-2 |
| PLA/APP | 45/5 | 90/10 | First trial no cotton ignited, second trial cotton ignited | V-2 |
| PLA/RDP-Cellulose | 45/5 | 90/10 | First trial no cotton ignited, second trial cotton ignited | V-2 |
| PLA/RDP-Cellulose/APP | 43/4/3 | 86/8/6 | Both trials cotton did not ignite | V-0 |
| Distilled Water/Lactide Monomer/APP/RDP | 100/3/5/5 | 88.5/2.7/4.4/4.4 | Cotton charred | N/A |
| Distilled Water/Lactide Monomer/APP | 100/3/5 | 92.6/2.8/4.6 | Cotton charred | N/A |
| Distilled Water/Lactide Monomer | 100/3 | 97.1/2.9 | Cotton ignited | N/A |

Figure 1: Flame test results of different polymer blends and saturated cotton balls.

the

similar. Looking at the modulus of each polymer blend resulted in PLA having the highest modulus of elasticity. Cotton balls are saturated with different amounts of lactide monomer, distilled water, APP, and RDP to create a solution that makes the cotton flame retardant by creating char on the surface layer of the burn. Cotton samples with distilled water, RDP, APP, and lactide monomer resulted in creating a char surface on the cotton as it was burned, making the cotton visibly non-flammable.

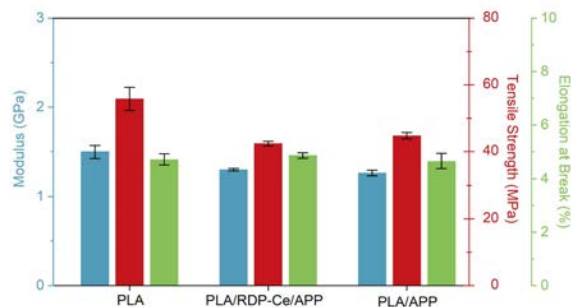


Figure 2: Physical Characteristics of polymer blends.

so optimizing the concentrations of RDP and APP is important for this study. Such combinations are subject to the UL-94 flame test, in which each polymer blend is burned over a cotton ball to see if the melted polymer blend will ignite the cotton ball. UL-94 flame test categorizes with flammability ratings such as V-0, V-1, and V-2. Polymer blend with a composition of 6g (12%) APP and 44g (88%) PLA have a rating of V-0, polymer melted with no ignition of the cotton ball. Testing the physical stress and strain of each polymer blend resulted in PLA having highest tensile strength. All other characteristics between polymers are

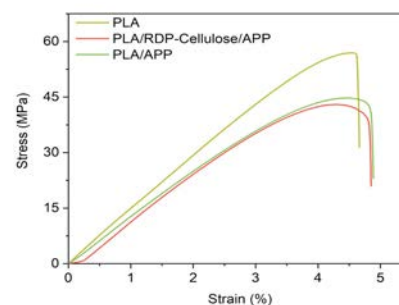


Figure 3: Modulus of polymer blends.

[1] Song, Y.-P., Wang, D.-Y., Wang, X.-L., Lin, L. and Wang, Y.-Z. (2011), A method for simultaneously improving the flame retardancy and toughness of PLA. *Polym. Adv. Technol.*, 22: 2295-2301. <https://doi.org/10.1002/pat.1760>

[2] Liu, S., Jiang, L., Jiang, Z., Zhao, J. and Fu, Y. (2011), The impact of resorcinol bis(diphenyl phosphate) and poly(phenylene ether) on flame retardancy of PC/PBT blends. *Polym. Adv. Technol.*, 22: 2392-2402. <https://doi.org/10.1002/pat.1775>

Session 10: Spin-Casting Polymer Thin Films

Chair: Rebecca Isseroff



Figure 1: DSC demonstration

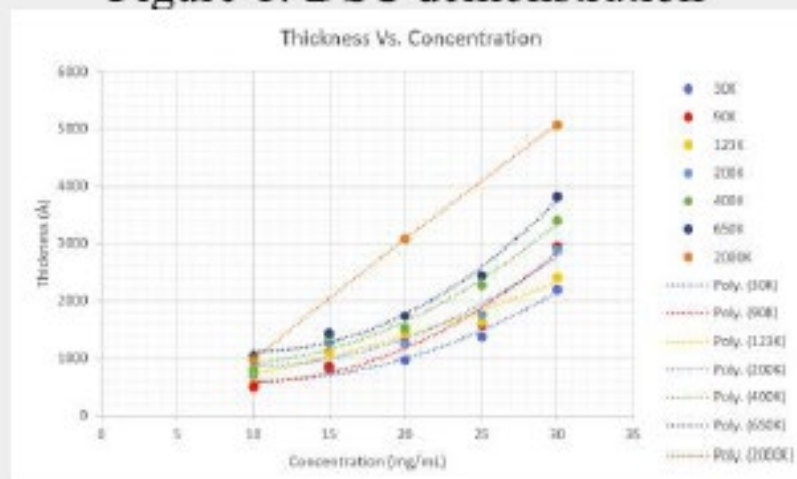


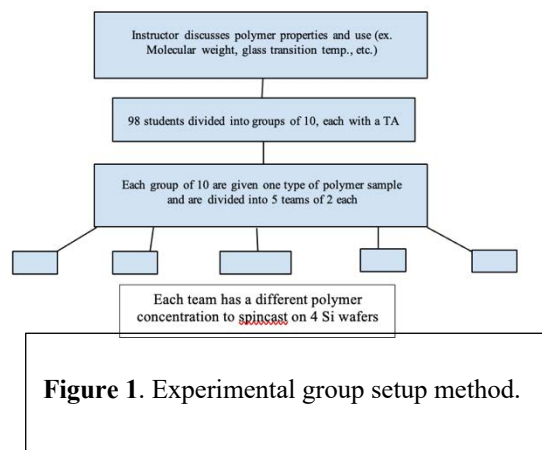
Figure 2: Data from verification

Spincasting to Determine Molecular Weights of Polystyrene Samples

Sean Fang¹, Alex Wang², Justin Kim³, Arkajyoti Sinha⁴, Sahil Sood⁵, Thomas Luong⁶, John Jerome⁷, Miriam Rafailovich⁸

¹Maggie L. Walker Governor's School, Richmond, VA 24502, ²Sewickley Academy Senior School, Sewickley, PA 15143, ³Jefferson Forest High School, Forest, VA 24551, ⁴Lexington High School, Lexington, MA 02421, ⁵Lambert High School, Suwanee, GA 30097, ⁶Plano West Senior High School, Plano, TX 75093, ⁷Department of Mathematics, Suffolk Community College, Selden, NY 11784, ⁸Department of Materials Science and Chemical Engineering, Stony Brook University, Stony Brook, NY 11794

Hands-on learning is a staple in high school education, as students understand topics quicker learning hands-on compared to learning through multimedia [1]. Hands-on learning also provides experiences and field competency that cannot be challenged by that of other types of learning [2]. In this project, 94 high school students between the ages of 16-18 participated in experiments regarding determining the molecular weights of various polystyrene (PS) samples. Determination of a PS sample's molecular weight has significant implications on polymer recyclability, as maximum capacity can be determined. Using the various methods, students determined the molecular weight and properties of certain PS samples, such as raman cup and coffee cup shreds. Through these methods, students got to experience university setting laboratory procedures.



Group 1 was to use 35K mW PS from Aldrich, Group 2 280K mW PS from Aldrich, Group 3 PS coffee cups from campus dining, Group 4 PS ramen cups from Nissin, and Group 5 PS bowls from campus dining.

Once experimentation began, students, under-supervision of qualified adults such as graduate students, carried out the procedures. Molecular characteristics testing, such as FTIR and DSC were first performed on PS samples (FIG 2). Each group created PS-toluene solutions of concentrations between 2.5 mg/mL and 25 mg/mL were created. Students pipetted 3 mL of toluene into their vials and then weighed enough PS sample to create their designated concentrations. Next, students dissolved the weighed amount of PS into their toluene solutions. Students then cleaved 4 111 miller indice silicon wafers for each concentration, air blew these wafers with compressed air, and then spin casted a thin film of PS onto the wafers at 2500 rpm for 30 seconds. Hydrophobicity of the PS coated wafer was determined on the goniometer through play placing a droplet of water on both an uncoated silicon wafer sample and PS coated samples. Throughout all samples, pure silicon wafers displayed contact angle readings of less than 60 degrees, indicating hydrophilicity. However, the PS coated wafers all displayed contact angle readings of more than 90 degrees, indicating hyperhydrophobicity. Following contact angle readings, using an ellipsometer, students determined thickness of each coated wafer, and an average was calculated to be used in creating a concentration vs thickness plot. This plot allowed students to extrapolate for critical concentration required to reach 3000 angstrom thickness, which is essential for calculating molecular weight. Students identified possible sources of error and added error bars.

Environmental health and safety concerns were addressed to students through a pre-experimental chemical safety training slideshow. In this slideshow, concepts such as PPE, fume hoods, safety data sheets, and chemical waste were covered. Additionally, students were given example demonstrations of the equipment that would be used during the experiment, such as the spin caster and FTIR machine. Following the facilities tour, students were divided into 5 experimental groups, each testing their own type of sample (FIG 1).

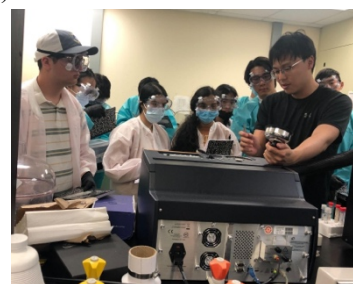


Figure 2. Students Operating DSC with Graduate Student Supervision

[1] Norman, K., Combs-Richardson, R. Emotional intelligence and social skills: Necessary components of hands-on learning in science classes. *J Elem Sci Edu* 13, 1 (2001). <https://doi.org/10.1007/BF03176215>.

[2] Davidson, Zoe E., and Claire Palermo. "Developing Research Competence in Undergraduate Students through Hands on Learning." *Journal of Biomedical Education*, 5 Aug. 2015. Hindawi, <https://doi.org/10.1155/2015/306380>. Accessed 7 Aug. 2022.

An Inexpensive Method for Determining Molecular Weight

Arkajyoti Sinha¹, Sean Fang², Alex Wang³, Justin Kim⁴, Sahil Sood⁵, Thomas Luong⁶, John Jerome⁷, Miriam Rafailovich⁸

¹Lexington High School, Lexington, MA 02421, ²Maggie L. Walker Governor's School, Richmond, VA 24502, ³Sewickley Academy Senior School, Sewickley, PA 15143, ⁴Jefferson Forest High School, Forest, VA 24551, ⁵Lambert High School, Suwanee, GA 30097, ⁶Plano West Senior High School, Plano, TX 75093, ⁷Department of Mathematics, Suffolk Community College, Selden, NY 11784, ⁸Department of Materials Science and Chemical Engineering, Stony Brook University, Stony Brook, NY 11794

Widespread plastic pollution is a pressing issue that contributes to the current climate change crisis. The accumulation of synthetic plastic products in rivers, oceans, and lakes amount to over 10 million metric tons, accounting for over 80 percent of marine pollution worldwide and 3.4 percent of global greenhouse gas emissions [1]. The vast majority of plastic pollution can be attributed to polystyrene [2]. Polystyrene is particularly dangerous due to the fact that it's not easily degradable and releases dangerous toxins into the environment [2]. The majority of polystyrene that is used for industry and commercial purposes is made up of a blend of different molecular weights. In other words, it is polydispersed. As a result, it is pertinent to understand the theory behind polydispersed polymers and their molecular weights to better address and mitigate the effect of anthropogenic emissions due to plastic waste.

In order to demonstrate the effect of polydispersity on molecular weight, we must first explore monodispersed polymers. Seven different molecular weights of polystyrene were utilized in our experiment: 30K, 90K, 123K, 200K, 400K, 650K, and 2000K. Each molecular weight was then spincasted at the concentrations of 10 mg/mL, 15mg/mL, 20mg/mL, 25 mg/mL, and 30 mg/mL onto a 1x1 in. silicon wafer. An ellipsometer was then used on each of the silicon wafers to determine the thickness of the polymer coating. The data along with lines of best fit are shown below in Figure 1. We then extrapolated the lines of best fit to 2000Å and 3000Å. Given the extrapolated concentrations that correlate with the aforementioned thicknesses, we plan on producing generalizable equations that constitute a universal curve for monodispersed polystyrene relating concentration to molecular weight at 2000Å and 3000Å.

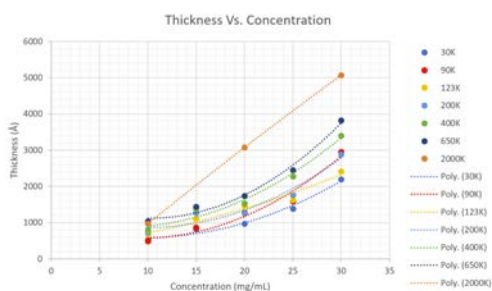


Figure 1: Lines of best fit for concentration vs thickness of monodispersed polystyrene

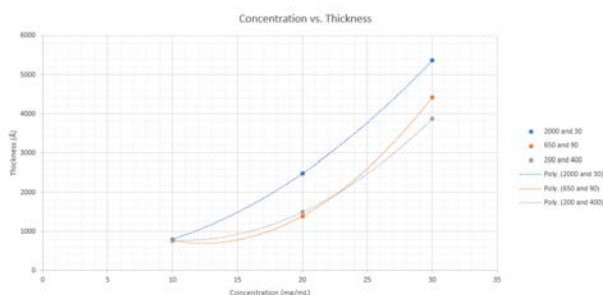


Figure 2: Lines of best fit for concentration vs thickness of polydispersed blends

When investigating polydispersity and its implications on molecular weight, we created three blends (200k and 400k, 90k and 650k, 30k and 2000k) of polystyrene with different molecular weights. The process detailed above for monodispersed molecular weights was repeated except these blends were spincasted at concentrations of 10 mg/mL, 20 mg/mL, and 30 mg/mL. The data is graphed above incorporating lines of best fit (FIG 2).

Initial data analysis shows that for molecular weights closer to zero, their polydispersed blends seem to exhibit thicknesses that are greater than each of the monodispersed molecular weights that make up the respective blend. However, as the weights of the monodispersed components of the polydispersed blend increase in weight, the thickness seems to approach that of the heavier monodispersed molecular weight.

These preliminary results suggest that polydispersed blends of polymers exhibit behavior that is different from their monodispersed components. Establishing a concrete grasp of the theory behind polydispersed polymers and their deviations from monodispersed polymers will have exciting applications in recycling and our fight against pollution.

1. Landrigan, Philip J et al. "Human Health and Ocean Pollution." *Annals of global health* vol. 86,1 151. 3 Dec. 2020, doi:10.5334/aogh.2831. Accessed 9 Aug. 2022.
2. Hwang, Jangsun, et al. "Potential toxicity of polystyrene microplastic particles." *Nature*, 30 Apr. 2020. Scientific Reports, <https://doi.org/10.1038/s41598-020-64464-9>. Accessed 8 Aug. 2022.



Siri Reddy



Tanya Shukla



Nikhita Srinivas

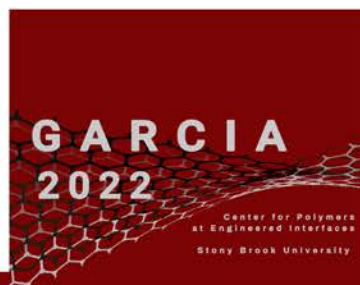


Leann Tai



Garcia
2022

Arka Sahil



Sophia Chen



Evelyn Shue

Amy Zhang
 Andrew Shih delan
 Dohyun Kim
 Anshu Anand
 Vincent Wei
 Soory Shah
 Anthony Zhu
 Tavan
 Anshu Anand
 Maytal Chelyt
 Helec Shukla
 Derek Danz
 Dongli Tian
 Gavin Onghai
 Noah Tenenbaum
 Ming Qi
 Ben Wen
 M
 Steve Tang
 Eric Chen
 Shaheer Ullan
 Siri Reddy
 Rommy Sasson
 Lorenzo Verona
 Evan Lee
 Haazim Alam
 Gabe Rothman
 Eulgi
 Eri
 Sean Feng
 Judah Rosenthal
 Anya Vaish
 Eliana Samuels
 Edén Hen
 Thomas Luong
 NIKHITA SRINIVAS
 Tanya Shukla
 Shaoxi Zhang
 Yuan
 Van
 Justin
 Ekam Singh
 I ❤️ Justin
 - Edward Sun
 I M Edward MORE
 - Justin Kim
 Ewiz Mule
 Nick Diulescu
 Joelle Gregoire Lincoln
 Jani Kim
 Quinton Geller
 Hannah Saks
 Rachel Na
 Christian Apostol
 Deryn O'Leary
 SUREHA TIWARI
 Emma Gao
 Sarah Yim
 Sahana Dharma
 Navya Gautam
 Mayao Li
 Konnie Duan
 Zixuan Lin
 Rebecca Sullivan
 Hush Rosshirt
 Laura Wang
 Ohm Patel
 Annie Wu
 Bareshani Poddar
 Elaina Heghes
 Tony Deluxe
 Leo Zeng
 Matt Sharin
 Sherlyn Wu
 AMIT SAHA
 Allen Bethancourt
 Christopher
 Anna A Cho

Garcia 2022

Thanks for a great summer!